Climate change and fire regimes in Limpopo grasslands

Mukovhe V Singo

11624426

A dissertation submitted in partial fulfilment of the requirements for the

Master of Environmental Sciences degree

Department of Geography and Environmental Sciences

Faculty of Science, Engineering and Agriculture

UNIVERSITY OF VENDA

November 2021

Declaration

I, Mukovhe V. Singo, hereby declare that “this dissertation submitted for Master of Environmental Sciences Degree at the University of Venda by me, has not been previously submitted for any degree at this or any other university. It is my work in design and execution and all reference materials contained have been duly acknowledged”.

25/02/2022

…… ……

Signature Date

Acknowledgements

Special thanks to God for the gracious knowledge I have gained during writing this dissertation.

I acknowledge Prof. Hector Chikoore and Prof. Francois Engelbrecht for the supervision, guidance and data provided. Dr Florence Murungweni co-supervised this work.

I extend a special thank you to Dr Sarah Roffe, Percy Muofhe, and Prof. Sally Archibald for sharing insightful information when I asked for help.

Finally, I acknowledge the Global Climate Institute (GCI) and the National Research Foundation for this opportunity and funding my research to its completion.

Abstract

Wildfires are becoming more frequent due to increased fuel load, human activities and climate change and are some of the major hazards in the southern Africa region. The delay in the onset of the rainy season coupled with rising surface air temperatures have increased fire risk in the region. This study investigates the interactions between climate change and fire regimes in the grasslands of Limpopo, a region in northern South Africa. The study seeks to understand how the Conformal Cubic Atmospheric Model (CCAM) simulates the present-day fire season. The frequency of high fire risk days in the "present-day climate" and the future of fire risk under climate change are analysed using a fire danger index. The study employs the "McArthur Forest Fire Danger Index" which links rainfall, temperature and wind to fire danger. The CCAM model at a horizontal resolution of 8 km is forced with an ensemble of six "General Circulation Models" (GCMs) from phase 6 of the "Coupled Model Intercomparison Project" (CMIP6) to simulate climate change projections for the period 2021-2040, 2041-2060 and 2080-2099 against a historical baseline from 1961 to 1980. The models were validated using observational data comprising CRU ts4 gridded weather station data with spatial resolution of 0.5° × 0.5° and ARC-SA weather station data. Taylor diagram was used for model verification integrating standard deviation, correlation coefficient, and Root Mean Square Errors (RMSE). Future climate projections were analysed with focus on the 50th percentile. The models' verification showed close variability, least RMSE and high correlation (>r=0.9) compared with CRU ts4. The 50th percentile future simulations projected extreme hot and dry conditions over much of the study area. Projected mean annual high fire danger days from near future (2021–2040) reached a peak (> 10–15 days) south of the grasslands, whilst the west region peaked (15–20 days) during September and October. During mid future (2041—2060), high fire danger days increased by a peak of 5 days and a further 5 days into the far future (2080–2099) during September and October. Results of this study contribute to an understanding of changing fire regimes in response to recent unprecedented temperature increases coupled with repeated heat waves, which appear to be modulating fire intensity in the study area.

Keywords: Climate change, fire regimes, fire danger, grasslands, "McArthur Forest Fire Index", CCAM.

Table of Contents

List of Figures

List of Tables

List of Acronyms and Abbreviations

ACCESS-CM	"Australian Community Climate and Earth System Simulator Coupled Model"
AR6	Sixth Assessment Report
ARC	South African Agricultural Research Council
BI	Burning Index
CAWCR	"Centre for Australian Weather and Climate Research"
CCAM	"Conformal Cubic Atmospheric Model"
CCSM	"Community Climate System Model"
CDO	Climate Data Operator
CH4	Methane
CMIP5	"Coupled Model Intercomparison Project Phase 5"
CMIP6	"Coupled Model Intercomparison Project Phase 6"
CNRM-CM	"Centre National de Recherches Meteorologiques Coupled Model"
CO	Carbon monoxide
CO2	Carbon dioxide
CRU	Climate Research Unit
CSIRO	"Commonwealth Scientific and Industrial Research Organisation"
ENSO	"El Nino Southern Oscillation"
ESM	Earth System Model
FDI	"Fire Danger Index"
FDR	"Fire Danger Rating"
FFDI	"Forest Fire Danger Index"
FPA	Fire Protection Association

FWI	Canadian Forest Fire Weather Index
GCMs	General circulation models
GFDI	“Grassland Fire Danger Index”
GFDL-ESM	“Geophysical Fluid Dynamics Laboratory Earth System Models”
GHGs	Greenhouse gases
GIS	Geographic Information System
GrADS	Grid Analysis and Display System
IPCC	“Intergovernmental Panel on Climate Change”
ITCZ	“Intertropical Convergence Zone”
KBDI	“Keetch-Byram Drought Index”
LFDI	“Lowveld Fire Danger Index”
MPI-ESM	“Max Planck Institute Earth System Model”
N2O	Nitrous Oxide
NCAR	“National Center for Atmospheric Research”
NFDRS	National Fire Danger Ratings System
NorESM	Norwegian Earth System Model
NOx	Nitric Oxide
NVFFA	“National Veld and Forest Fire Act, No. 101 of 1998”
PM	Particulate matter
r	Correlation coefficient
RCF	Rain Correction Factor
RCM	“Regional Climate Model”
RCPs	“Representative Concentration Pathways”
RH	Relative humidity

RMSE	“Root Mean Square Error”
SRES	“Special Report on Emission Scenarios”
SRZ	Summer Rainfall Zone
SSPs	Shared Socioeconomic Pathways
SST	Sea Surface Temperature
TS	Time-series data
TTTs	Tropical-temperate troughs
UN	United Nations
WG	Working Group
WRZ	“Winter Rainfall Zone”
YRZ	“Year-round Rainfall Zone”

Chapter 1: Introduction

1.1 Background

African savannas are fire prone ecosystems, with most wildfires occurring during the dry season (Laris et al. 2020). Dry and wet seasonality directly affects fuel moisture, fuel load and fire intensity, which vary from season to season (Platt et al., 2015). Most large fires that occur around the globe are influenced by weather conditions prevailing (Duane and Brotons, 2018). Weather conditions have a more direct effect on vegetation moisture content and fire behavior which becomes extreme under high-temperature, low humidity and windy conditions (Piñol et al. 1998). Large proportion of burned areas and biomass emissions around the globe are identified in African savannas (Platt et al., 2015). Climate is one of the contributing factors that define fire regimes with the interaction of topography and fuel available (Countryman, 1972; Kasischke and Hoy, 2012). Since about 400 million years ago, the frequent occurrence of wildfires maintained bush encroachment into the grasslands (Scott, 2000). Using proxies such as pollen spectra and micro-charcoal adopted as phenomena to explain frequent occurrence of wildfires since the last glacial maximum (Flannigan et al. 2009; Cordova et al. 2019).

Biomass burning is a significant source of atmospheric pollutants, both gasses and particulates, at regional and global scales (Crutzen et al, 1979). Atmospheric gases such as carbon monoxide (CO), carbon dioxide (CO2), methane (CH4), volatile and semi-volatile organic compounds, aldehyde, organic acid and inorganic elements and particulate matter (PM) are released when burning biomass materials (Yadav and Devi, 2019). The continuous emission of CO2 to the atmosphere stimulates growth of vegetation biomass (Hovenden et al, 2019). Since rising CO2 levels in the atmosphere directly affect the climate and stimulate growth of woody vegetation, fire frequency and intensity in the grassland's ecosystem have also changed while posing significant threats (Ratajczak et al, 2014). Thus, sub-tropical and tropical grassland ecosystems require frequent fire to curb the woody plant encroachment because fire exerts significance on the structure, composition, and dynamics of areas (Gordijn et al, 2018).

Grassland and savanna fires occur frequently, mostly in tropical regions, but also in temperate latitudes (Flannigan et al, 2009; Petermann and Buzhdygan 2021). Southern Africa is largely a semi-arid region with strong warming induced by the increase of an albedo due to suppressed precipitation and desertification which influence radiative cooling at the land surface (Wang, 2004; Kruger and Shongwe, 2004). The accumulated dead biomass and other fine flammable fuels ease ignition under strong winds while inducing high intensity fires (de Groot et al, 2010). Wildfires

spread widely in grassland around the world and number of fires that occur in grasslands is shown in Figure 1.1 (Leys et al, 2018).

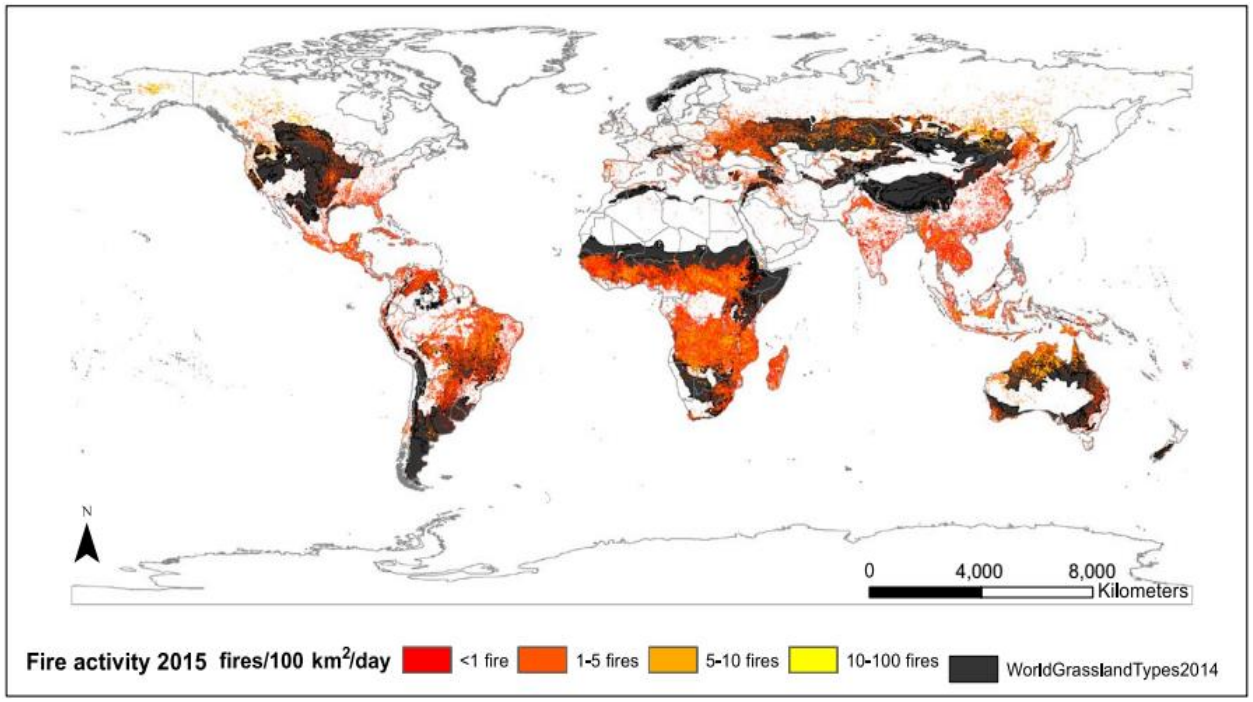

Figure 1.1 Fire activity for the year 2015 over Global Grassland Types. Colour ranges represent a number of fires over 100 km^2 per day; from low fire activity in the red to high fires in yellow. Black areas represent grassland (source: Leys et al, 2018).

The main synoptic weather system that affects fire regimes over the southern Africa region is the subtropical high-pressure belt which is divided by the continent to become the Atlantic Ocean High and the Indian Ocean High (Dyson and van Heerden, 2002). During the austral summer, easterlies draw moisture from the southwest Indian Ocean and warm Agulhas Current, which is a major moisture source region (Rapolaki et al, 2019). The winter season corresponds with the dry season over much of the subcontinent and the airflow is predominantly anticyclonic and subsiding (Tyson and Preston-Whyte, 2000). Strong drainage winds locally known as Berg winds are associated with most large fires that occur in South Africa. This occurs when a continental high situated over the interior and coastal lows develop resulting in descending air down the escarpment which warms adiabatically (Tyson and Preston-Whyte, 2000).

Several studies have determined the significant role of climate and weather in wildfire activity (e.g., Kraaij et al, 2018; Engelbrecht et al, 2015; Keeley et al, 2016). Thus, Global Climate Models' (GCMs) ability to simulate the past and future climate under different greenhouse gases emission

scenarios aids the understanding of present and future fire regimes (Fried, et al, 2008). Fire frequency and fire severity have been projected to increase by most GCM simulations in the western United States (Liu and Wimberly, 2016). These projections are based on links between fire activity, annual temperature, and the literature connecting fire activity with annual climate variability, and often at varying spatial scales (Liu and Wimberly, 2016).

1.2 Dry and wet seasonality

Seasons are determined by the rotation of earth around the sun and intensity of sunrays that a certain area receives at a given time of the year (De Paor et al, 2017). Due to the earth's tilted axis at an angle of 23.5°, seasons are established on different parts of earth (Milutin, 1941). The mid-latitude climate is distinguished by four seasonal cycles consisting of summer, winter, spring and autumn, whereas the tropical climate is mainly characterized by a dry season and a wet season (Perry, 1987).

The expansion of the Hadley cell poleward is distinguished by upwards lifting of convergent winds in the tropics which then sink along the subtropical regions in a high-pressure zone (Reichler, 2016). However, where the Hadley cell converges upwards, the Intertropical Convergence Zone (ITCZ) is established (Yan, 2005). The north-south movement of the tropical rain belts and the ITCZ is a major cause of dry and wet seasonality (Yan, 2005). Shifting of ITCZ over Africa brings more summer rainfall towards the subtropical regions of either the Southern or Northern Hemisphere (Nicholson, 2018). Dry and wet seasonality in southern Africa is influenced by various factors including topography, Pacific El Niño Southern Oscillation (ENSO), Indian Ocean dipole and seasonality of weather systems (Ogwang et al, 2020). It is also driven by several synoptic weather systems (Rapolaki et al, 2019). Rainfall producing systems include cloud bands, cut off-lows, subtropical ridging high pressure systems, tropical cyclones and tropical lows most of which tend to occur at certain times of the year (Muofhe et al, 2020; Chikoore et al, 2021; Ndarana et al, 2022).

The wet season over southern Africa is influenced by tropical-extratropical cloud band or Tropical-temperate troughs (TTTs) that contribute nearly half of the regional summer rainfall (Harrison, 1984; Hart et al 2010; Hart et al, 2013). A complex topography also contributes to more summer rain through orographic lifting over the escarpment (Chikoore, 2017). Nonetheless, the onset of the rainy season is projected delay considerably by 2070 – 2099 across southern Africa (Wainwright et al., 2021). Interannual variability of mid-tropospheric Botswana High advances the formation of TTTs when it is anomalously weak. Dry spells are becoming more intense due to mid

tropospheric anticyclone that develops over Namibia and ocean warming east of Madagascar that drives atmospheric moisture away from the continental interior (Ndarana et al. 2022). The Botswana High is found to have strong positive correlation with dry spell frequency and extreme temperature days during summer over southern Africa (Driver and Reason, 2017). Extreme drought conditions occur over southern Africa under strong Pacific El Niño conditions, a strengthened westerly jet stream and a positive Indian Ocean Dipole mode (Chikoore and Jury, 2021).

1.3 African Savanna

African savannas supply valuable ecological services including water, grazing and browsing land, food, fuel and habitat for a large proportion of African people, and incomparable biodiversity that sustain wildlife tourism (Osborne et al, 2018). Savannas are distinguished by trees and grasses co-occurring in the seasonal tropics between the rainforests along the equator and mid-latitude desert ecosystems (Hutley and Setterfield, 2008). The structure and function of savannas are complex as shown in Figure 1.2, with interactions between various environmental determinants which include fire activities, herbivory, available nutrients and moisture to be effective (Hutley and Setterfield, 2008).

African savannas transverse over a range of soil types and receive annual rainfall within a large range of 200 – 1800 mm (Mishra and Young, 2020). The largest savanna in Africa is the Miombo extending across central and southern Africa with area coverage of 2.7 million km^2 which is distinguished by tall deciduous species with canopy height of less than 12 m and herbaceous layer of tall grasses (Frost, 1996; Muvengwi et al, 2020; Sikuzani et al, 2020). In southern Africa, savannas that spread on fertile soil are distinguished by fine leaves which help them to save water and thrive in the semi-arid areas which are dominated by *Senegalia* and *Vechelia* species whilst weathered and infertile soils are dominated by Broadleaved savannas, such as *Combretum* species (Hutley and Setterfield, 2008; Hassan and Hamdy, 2021). In northern Africa, deciduous trees and xerophytic grasslands have dominated the Sudanian savannas which in turn act as transitional zone for the drier Sahelian savannas north and wetter Guinea type savannas on the south (Fayolle et al, 2019). The east African savannas expand on arid and semiarid environments, as they are dominated by grasslands with scattered shrubs and trees (Hutley and Setterfield, 2008; Utaile et al, 2021).

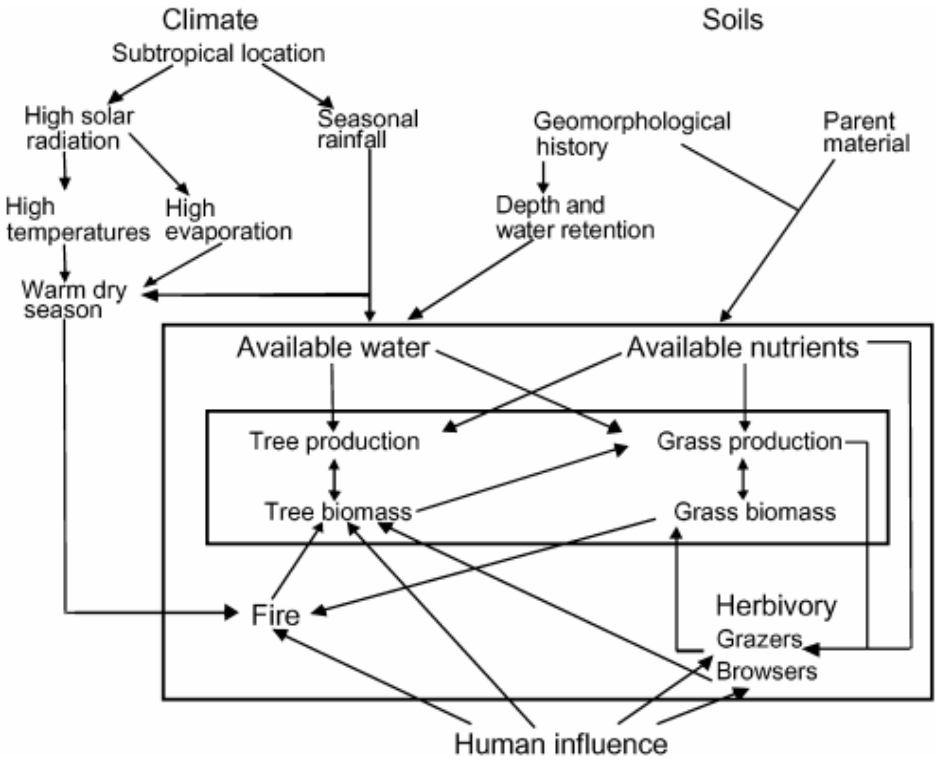

Figure 1.2 Interactions between factors influencing the savanna structure. The biomass on the savannas is determined by water availability, nutrients, and fires. Climate and soil types regulate these factors for any given location (Source: House et al, 2003)

The savanna biome in Africa is estimated to have existed at different ages. Subtropical savannas are estimated to date between 10 and 15 million years ago, while the savanna that is found farther south is estimated to be less than 3 – 4 million years old (Hutley and Setterfield, 2008). Evidence has shown grasslands to date between 15 and 17.5 million years ago in East Africa with dominant transition to C4 grassland from 10 million years ago (Retallack, 1992; Linder, 2017). C3 photosynthetic pathway grasses are more nutritious than C4 but their nutritional quality is affected by elevated atmospheric CO2 (Barbehenn et al, 2004; Jobe et al, 2020). Temperature and rainfall also determine distribution of C3 and C4 grasses, whereby C4 grasses commonly grow in areas that are warm and wet, while C3 grows in drier and cold areas (Sinclair, 2002; Mahdavi et al, 2018; Pardo and VanBuren et al, 2021). Nonetheless, C4 grasslands are presently well established in East and southern Africa due general transition towards an increasing magnitude of C4 to C3 grasses and their patches may have existed before 10 million years ago (Uno et al, 2011).

1.4 Fire on the Savanna

Annually, up to 80% of landscape in African savannas are burnt by wildfires and this is driven by the availability of finer fuels and variable rainfall patterns (Archibald et al., 2010; Laris et al, 2020; de Dios, 2020; Harrison et al, 2021). Naturally occurring wildfires are common during the dry season on the African savannas and play a significant role in maintaining the arrangement and structure of these ecosystems (Bond, 2019). In southern Africa, savanna is a fire-prone ecosystem due to climate variability and vegetation types over the region (Maurin et al, 2014). Miombo woodlands and Dambo grasslands are the most dominant savanna ecosystems in southern Africa. During dry season in the year 2000, over one-third of the total burned area in southern Africa was recorded from this savanna ecosystem (Sinha et al, 2003).

Increasing inter-annual variability of rainfall and emission of greenhouse gases have significant impacts on the savanna and fire regimes (Synodinos et al, 2018; Devine et al. 2017). Savanna ecosystems are highly vulnerable to woody encroachment due to rising levels of atmospheric CO2 and improper land management, with significant consequences on grazing systems, fire regimes and symbolic wildfires (Smit and Prins, 2015). Natural fires or prescribed burning help maintain vegetation composition and structure of the savannas, such that herbaceous and woody plants coexist (Archibald et al, 2017). Prescribed burning refers to controlled fires conducted in fire management on protected African savannas. The goal is to remove moribund and unpalatable grass by burning at given time to supress uncontrolled/unplanned fires which may rise during the dry season (Nieman et al, 2021).

1.5 Climate Change in the Savanna

Climate change disturbances to the ecosystem are expected to intensify in future with catastrophic events such as longer droughts affecting the tropical savannas (Sankaram, 2019). Furthermore, tropical savanna climate will become more vulnerable to extreme heatwaves, high fire frequencies, and loss of vegetation cover (Hoffmann et al, 2002). When the climate gets warmer, precipitation becomes more intense but less frequent. Precipitation intensity directly affects soil water availability from surface to deep soil, an increase in precipitation intensity increases deep soil water availability which in turn support rapid growth of woody plants that has deep roots system resulting into bush encroachment in savanna ecosystems (Engelbrecht et al, 2016; Berry and Kulmatiski, 2017).

Köppen-Geiger climate zones are projected to change when global temperatures increase by 3°C (Engelbrecht and Engelbrecht, 2016). High-resolution regional climate models showed south-

westwards expansion of tropical savanna zone to South African east coast and invasion of woody cover into grasslands (Engelbrecht and Engelbrecht, 2016). The semi-arid region is observed to have shifted hundreds of kilometres eastwards across South Africa (Jury, 2021). Furthermore, there are large uncertainties in future projections of biomes across Africa due to climate and CO2 changes but using high resolution improve model simulation of these impacts may provide adaptable strategies that are highly flexible (Martens, 2020).

1.6 Research questions

1.6.1 How do models simulations compare with observations?

1.6.2 To what extent has climate change altered fire season characteristics over the Limpopo grasslands?

1.6.3 How are high fire risk days projected to change between the current and future fire regimes?

1.7 Aim and specific research objectives

1.7.1 Aim

The aim of this study is to investigate impacts of climate change on fire regimes on Limpopo grasslands using historical observations and downscaled climate change projections

1.7.2 Specific research objectives

(a) To determine models' performance against observations (1961-1980)

(b) To simulate future changes in the climate of the grasslands under the RCP8.5 emission scenario

(c) To investigate changes in the future high fire risk days using the McArthur Forest Fire Danger Index under RCP8.5 scenario

1.8 Dissertation structure

This research is divided into six chapters: Chapter 1 provides the background of the study, research questions, study aim and specific research objectives. The literature review is detailed in Chapter 2, focusing on studies of grasslands and aspects that influence fire behaviour at different temporal and spatial scales. This chapter explains the link between climate conditions and the occurrence of wildfires. Chapter 3 details the datasets, models, methods of analysis and instruments employed in this study. The delineation of the research and study area have been also covered in this chapter. Results of this study are presented in Chapter 4 and 5. Chapter 4 focuses on the historical baseline climatology of the Limpopo Grasslands: 1961 – 1980 through

analysing several climate variables important for fire risk. Projections of high fire risk days on the grasslands for the near-term, medium-term and the far future are presented in Chapter 5. The conclusions and recommendations of this study are offered in Chapter 6.

Chapter 2: Literature Review

2.1 Introduction

Understanding dynamics in drivers that shaped present-day fire regimes helps to predict changes to fire regimes in future (Rogers et al, 2020). Drivers of fire regimes include the climate, land cover, and human activity via ignition and suppression (Rogers et al, 2020). Climate variability is a significant role in global fire activities, hence human activities interfere with an interaction between climate and fire (Abatzoglou et al, 2018). “General Circulation Models” (GCM) have simulated future climate induced by human activity to be composed of more severe fire weather, longer fire seasons, more fire ignitions and more area burned (Flannigan et al, 2006; Restaino and Safford, 2018). Fire activities are increasing in many regions around the world because of climate change (Barros et al, 2021). High temperatures associated with drought and prolonged dry periods and drought are major drivers of increased wildfire activities experienced in recent decades (Vose et al, 2021).

This chapter reviews and acknowledges the refereed literature on climate change and fire regimes, with a focus on those that have used climate model simulations and meteorological observations.

2.2 Climate Change

Climate change results from the variability of the climate system that includes the atmosphere, land, ice, biogeochemical cycles, living and non-living components of the planet earth because of rising temperatures induced by human activities (Ahmed, 2020). A significant consequence of climate change is global warming, which emerged by excessive emission of greenhouse gases such as CO2, N2O, and CH4 (Fawzy et al, 2020; Ahmed, 2020). Human activities since the industrial revolution have contributed about 1°C of global warming and are still expected to have risen by 1.5°C in the early 2030s (Fawzy et al, 2020). Global warming of 1.5°C projected high climate variability because of climate change as the most concerning issue that requires new knowledge of adaptation and mitigation.

Climate models from “Phase 6 of the Coupled Model Intercomparison Project” (CMIP6) are ensembled to project future greenhouse gas emission and climate change milestone through illustrative emission scenarios referred to as “Shared Socioeconomic Pathways” (SSPs) and Representative Concentration Pathways (RCPs) (Su et al, 2021). Climate change research community pioneers’ emission scenarios to ease the evaluation of the future climate, including mitigation, vulnerability and adaptation (Raihi et al, 2017; O’Neil et al, 2017). The Sixth

"Assessment Report" (AR6) prepared by the "Intergovernmental Panel on Climate Change" (IPCC) which comprises three working groups (WG) incorporating developments in climate science to project scenarios that are pivotal to climate change and policy makers (Burgess et al, 2020; Eyring et al, 2021).

SSPs scenarios in AR6 WG1 report illustrated future greenhouse gas scenarios ranging from best effort mitigation scenarios SSP1-1.9 to the succeeding high mitigation SSP2-2.7 then low SSP3-7.0 and SSP5-8.5 mitigation (IPCC, 2021; Engelbrecht and Monteiro, 2021). Climate change projected under SSP5-8.5 low mitigation at 1.5°C, 2°C, 3°C, and 4°C global warming is considered 'code red for' humankind by the United Nations (UN) Secretary - General (van der Linden et al, 2021; Engelbrecht and Monteiro, 2021). The statement complements the Paris Agreement on Climate Change about global warming at 1.5°C and 2°C defined as 'dangerous climate change' (van der Linden et al, 2021; Engelbrecht and Monteiro, 2021).

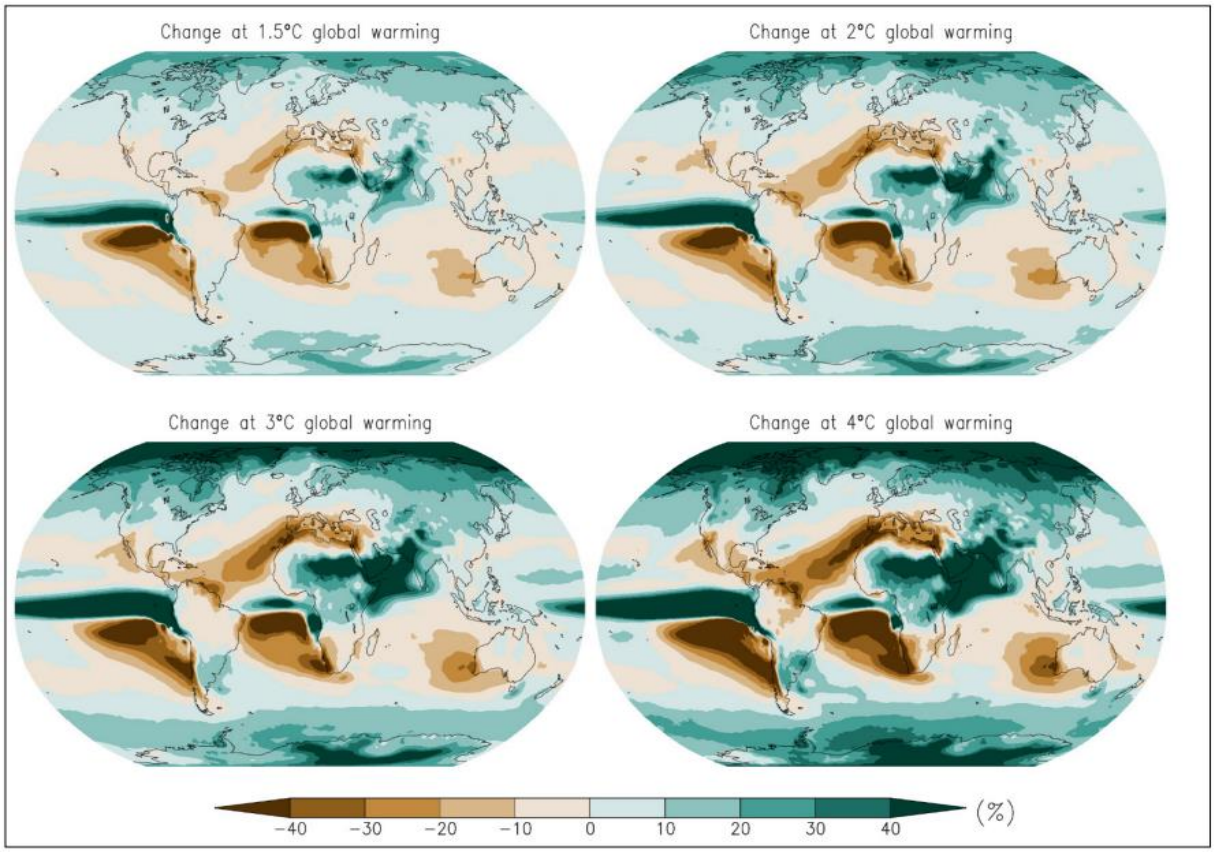

Figure 2.1 Near term (2021 -2040) projection of change in annual precipitation under SSP5-8.5 global warming level 1.5°C, 2°C, 3°C, and 4°C using historical baseline of 1850 -1900 (Source: Engelbrecht and Monteiro, 2021)

Projections of change in annual precipitation may be derived from an ensemble of 30 global circulation models that contributed to the CMIP6 as shown on Figure 2.1 (Engelbrecht and Monteiro, 2021). Annual precipitation over southern Africa is projected to decline and the region becoming very dry moving from global warming level 1.5°C, 2°C, 3°C, and 4°C (Engelbrecht and Monteiro, 2021). The southern Africa region, particularly South Africa, Namibia and Botswana will encounter outstanding significant warming during SON (September-October-November) season (Maure et al, 2018). Reduced precipitation is projected in regions such as the Limpopo River Basin, Zambezi River Basin and parts of South Africa's Western Cape (Maure et al, 2018). Projected changes in mean annual rainfall and length of dry – wet period over southern Africa exert significant threats to fragile ecosystems and agriculture (Kluste et al, 2018).

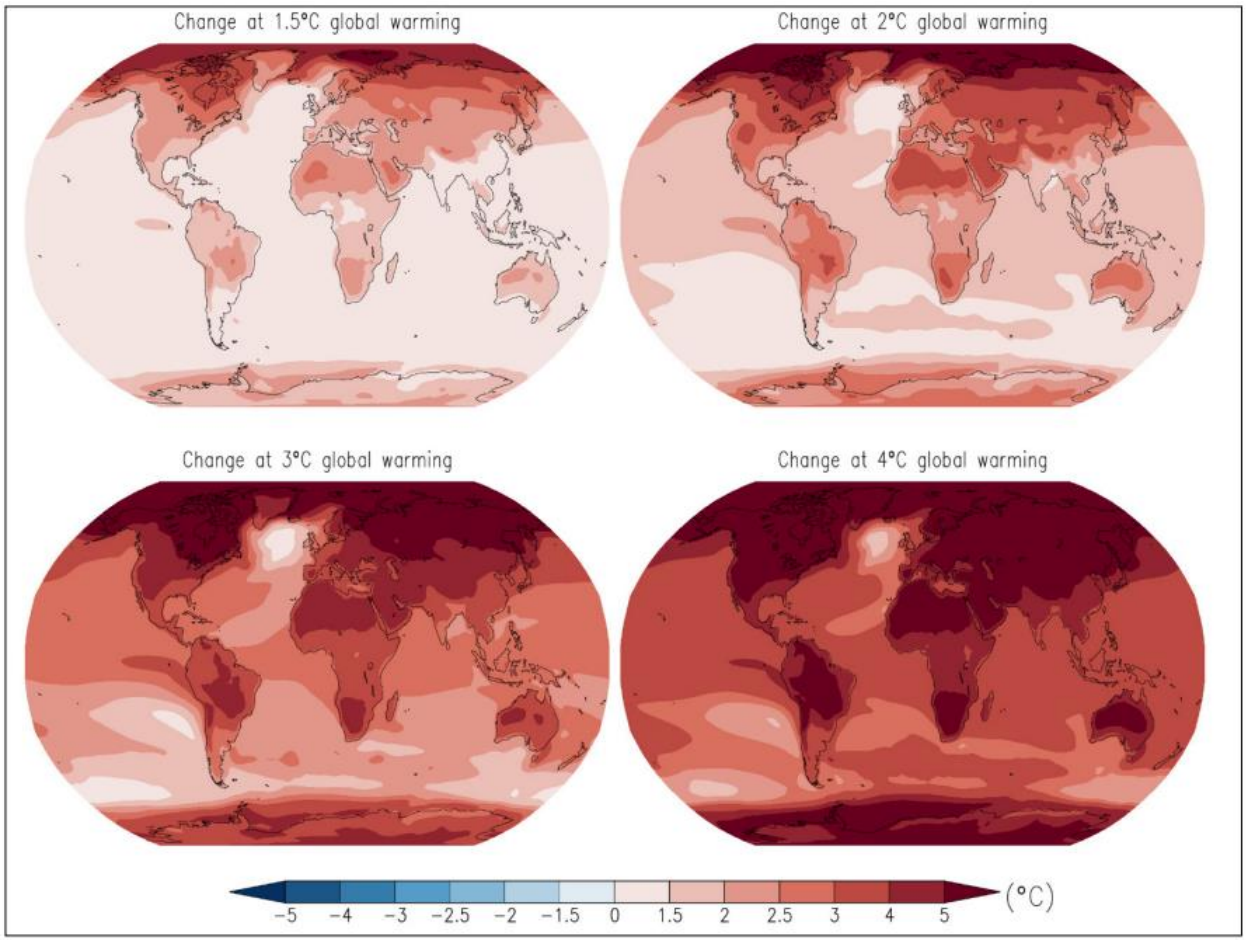

Figure 2.2 Near term (2021 -2040) projections of change in surface temperature (°C) under SSP5-8.5 at global warming level 1.5°C, 2°C, 3°C, and 4°C using historical baseline of 1850 -1900 (Source: Engelbrecht and Monteiro, 2021)

Temperatures are projected to increase drastically across the north pole, continental Europe, North America, southern Africa and Australia as shown on Figure 2.2 (Engelbrecht and Monteiro, 2021). The projections under SSP5-8.5 at global warming level 2°C show temperature to increase by 4°C in the middle of 2021 – 2040 over the northern latitudes (Carvalho, 2021). The Paris Agreement and IPCC aim to limit mean global warming to below 2°C throughout the 21st century and to encourage even warming below 1.5°C aiming to reduce Arctic ice melting (Ming et al, 2021; DeConto et al, 2021).

2.3 Climate Change in South Africa

South Africa is highly vulnerable to impacts of extreme temperature events, including frequent heat waves, warm spells, cold waves and cold spells (Mbokodo et al, 2020; van Der Walt and Fitchett, 2021). Over the past five decades, temperature is increasing over southern Africa at more than twice the global levels of temperature increase (Engelbrecht et al, 2015). The main consequence of climate change is increasing the frequency of extreme weather and climate events such as drought all over the world (Dube et al, 2020). Global Climate Models (GCM) have projected much of South Africa to become warmer and drier at global warming level of 1.5°C in the middle of near future term 2021 to 2040 (Englebrecht and Monteiro, 2021).

The location of South Africa in the subtropics makes it more vulnerable to extreme climatic events (Smith & Sheridan, 2020). Climate – induced drought often leads to food insecurity, water scarcity, and threatens tourism (Zwane 2019; Muringai et al, 2021; Nyoni et al, 2021; Verschuur et al, 2021). The drought episode commonly known as the “Day Zero” phenomenon during early 2018 in the City of Cape Town (3.7 million population) was among the first major urban settlements areas to run low on water (Burls et al, 2019). Water shortages in Cape Town were significantly influenced by decreasing winter rainfall days and intensity over a long period (Burls et al, 2019). Most of South Africa receives summer rainfall while Cape Town and neighbouring south western Cape regions receive winter rainfall mostly from cold fronts linked to extratropical cyclones which propagate east across the South Atlantic (Reason et al, 2002).

Drought is persistent in the Northern Cape Province in South Africa because of climate change (Ramafoko et al, 2021), even though the concept of drought is debatable in arid regions. Unprecedented extreme drought events induced water supply deficiency affecting agricultural sector in different parts of South Africa including Eastern Cape (Archer et al, 2022), Free State, KwaZulu-Natal, North West and Limpopo Province during the past decades (Masemola, 2021). Meanwhile, drought led to a reduction of tourists from the Western Cape because of water supply

shortage (Dube et al, 2020). Extreme wildfire events have occurred in southwestern Cape Coast in the last decade due to climate change and global warming (Kganyago et al, 2021). The recent Knysna fire was a catastrophic event in the Western Cape triggered by unprecedented drought, high fire danger conditions and land use change (Kraaik et al, 2018).

In addition to increased risk of drought and wildfire activity over South Africa due to climate change, heavy rainfall events have also become more frequent. The annual risk of flooding in South Africa is forecasted to be above 80% because of anomalous rise in global temperatures triggered by socio-economic activities (Munyai et al, 2019). Warming will most like result in more frequent tropical cyclones over the warm Indian Ocean resulting in flooding over the coastal areas (Kusanganya et al, 2014). Flooding may affect the vegetation and fuel load and fire regimes. Understanding vulnerabilities and risks due to climate change will help to develop adaptation strategies and finding solutions towards natural disaster risk reduction (Masipa, 2017; Ofuegbu et al, 2017).

2.4 Understanding wildfire

2.4.1 Drivers of fire

Fire has a significant role in the earth system, regardless that some terrestrial ecosystems are fire sensitive, wildfires are not foreign ecological disturbances (Cochrane et al, 2021; Bowman et al, 2020). Wildfires occur in ecosystems as a function of climate, human activities, and vegetation types (Cochrane et al, 2021). Humans affected factors that shape fire regimes by changing timing of ignitions, climate and fuels (Rogers et al, 2020; Archibald 2016). Factors that shape fire regimes include fire frequency, severity, intensity, type, seasonality and spatial scale (Cochrane et al, 2021).

Wildfire occurrence and behavior have been changing during recent decades in several regions worldwide (Keely and Syphard, 2021). Land use change and associated climate related stress factors induced extreme events such as drought which influence occurrence of wildfires (Roces-Diaz et al, 2021). By far, the majority of wildfires are ignited by human interactions with landscapes which influence flammability (Viedma et al, 2018). Impacts of human factors on wildfires override the role which climate plays and it is difficult to understand due to the varying nature of factors (Viedma et al, 2018). Variation caused by human factors involves decreasing fires through enforcing suppression policy or increasing fire activities due to Land Use/Land Cover (Bajocco et al, 2019; Schmidt and Eloy, 2020).

2.4.2 Fire seasonality and frequency

Fire frequency may be defined as the rate at which fires occur within a specific region over a precise period of time (Curt, 2018). Factors affecting fire frequency consist of natural (weather conditions, dead biomass level and topography) and anthropogenic (human) factors (Kavhu and Ndaimani, 2021). The composition and structure of plant communities determine their fire frequency (Gallagher et al, 2021). The savanna is a fire-prone biome that requires fire to maintain their structure and composition but high fire frequency causes high mortality of other plant species (Gallagher et al, 2021). Fire frequency is also determined by the preceding extreme rainfall events which influences high fire frequency of large fires in the succeeding years (Verhoeven et al, 2020).

Fire season refers to the period throughout the year when the ignition and spread of wildfires is most likely, burning dry fuel while affecting resources (Zhao et al, 2020). The fire season is associated with high fire frequency and intensity (Govender et al, 2006). The length of a fire season is determined by climate conditions: high temperatures, low humidity, no rain or days with little rain, and high winds that influence fire to spread (Wotton and Flannigan, 1993; Flannigan et al, 2013; Zhao et al, 2020). Fire frequency is a critical component of defining a fire regime, which is integrated with the intensity of wildfires to determine fire seasonality over a region (Pyne et al, 1996a; Pyke et al, 2010; Gao et al, 2021)

2.4.3 Fire Intensity and Severity

Fire intensity is linked to the amount of heat released by an active fire per unit area and time (Rossi et al, 2019). It is used to measure energy output, but it is confused with fireline intensity by some authors (Keeley, 2009). Fire records comprise fire intensity measured as an attribute, making it a significant key element of a fire regime (Govender et al, 2006). Fire intensity plays a significant role in understanding fire behaviour in forests measuring energy released at different stages of a fire (Keeley, 2009). Fire intensity is defined as the most commonly used factor to describe fire behaviour among others, including fire direction and rate of spread (Byram, 1959; Ruecker, 2021). High fire intensity induces high mortality and loss of species with profound destructive impacts on vegetation composition and structure (Trouve et al, 2021).

Fire severity refers to destructive impacts, such as tree mortality or loss of biodiversity that fire has on the ecosystem (Keeley, 2009). Factors influencing fire severity include forest type, aspect, slope, fire weather and period since previous major disturbance (Lindenmayer 2021). Vegetation composition influences high fire severity in previously long-time unburned areas (Cansler et al, 2022). Invasive non-native grasses drive high fire intensity and promote mortality of heat-sensitive

seeds and buds within native vegetation communities (Tomat-Kelly, 2021). Since the savanna is made up of trees, shrubs and grasses, expansion of woody savanna jeopardizes grass cover hence increasing fuel load, fire intensity and fire severity (Johansson et al, 2021).

2.4.4 Fire duration and size

Fire duration and size are correlated key outcome when assessing fire behaviour and the area burnt over a specific time certain period (Xi et al, 2021). The size of wildfires, whether small or large and the time during which wildfires continue burning play's critical role in understanding fire behaviour (Calkin et al, 2021; Santos et al, 2021). Fire duration and fire size are correlated due to dominant variability in extreme magnitude (Xi et al, 2021). Rate coefficients have indicated rapid increase in fire size as the number of spread days increases (Wang et al, 2020). Large and long duration fires are influenced by weather and vegetation conditions, resulting in a large extent of burned area (Chuvieco, 2008; Wang et al, 2020; Potter and McEvoy, 2021).

2.4.5 Fire weather

2.4.5.1 Wind

Understanding wind components in fire weather forecasting and prediction is crucial for foresters, wildfire risk management and public (Vancil et al, 2020). Wind is the most influential weather variable to fire behaviour due to the unpredictable variability of wind speed and wind direction over time and space (Payne et al, 1996). Wind speed and direction are important variables in predicting the occurrence and spread rate of wildfires (Cruz et al, 2020; Vancil et al 2020). Most large wildfires in an area with less fuel load are wind driven (Prichard et al, 2020). Dangerous wildfire conditions are frequently rendered by extreme downslope mountain winds (Zigner et al, 2020). Wind direction over uphill, sidehill and downhill the slope influences smouldering of wildfires (Christensen et al, 2021). Since wildfires affect air quality, both wind speed and direction contributed to accurate prediction of biomass burning emission pathways within or above the planetary boundary layer (Friberg et al, 2021).

2.4.5.2 Temperature

Temperature distributes heat required for the ignition and combustion process (Cardil et al, 2021). The warming of the earth's climate is fuelling the frequent occurrence of extreme wildfire hence affecting fire behaviour (Shi et al, 2021). When temperatures are extremely high, soil and fuel moisture content decreases with chances of ignition and fire spread becoming high (Cardil et al, 2021; Marques et al, 2021; Turco et al, 2019; Wei et al, 2020). Temperature is a critical factor that

determines fuel moisture and dryness of fuel (Countryman, 1972; Rani, 2021; Ma et al, 2021). Change of state from lower to higher temperatures increases fuel flammability and incidence of wildfires (Agovino et al, 2021).

2.4.5.3 Relative Humidity

Relative humidity (RH) is the ratio of moisture content in the atmosphere to the amount of moisture necessary to saturate the atmosphere at the same temperature and pressure (Yahia, 2019). RH directly affects moisture content of dead biomass due to exchanging moisture with air. When RH is low, moisture is withdrawn from the fuels, whereas when the RH is high fuels take moisture from the air (Barik and Baidya, 2020). Finer fuels are quick to gain and lose moisture content when relative humidity changes (Castillo et al, 202). Decreasing RH influences an increase in fire behaviour because of rapid dryness of fine fuels (Rodrigues and Torres, 2020; Biswell, 2020). Heavy fuel reaction to change in humidity is slower and usually requires significant moisture from rainfall (Rodrigues and Torres, 2020; Biswell, 2020).

2.4.5.4 Precipitation

Changes in precipitation affects the flammability of fuels and the frequency of ignition (Ziel et al, 2015; Pickell et al, 2017; Gowan and Horel, 2020). Precipitation increases moisture content of surface fuel, resulting in suppression of wildfires during the wet season (Kharuk et al, 2021; Tang et al, 2021). Significant precipitation during the rainfall season enhances growth in vegetation cover, resulting in more fuel available for the upcoming dry or fire season (Lui et al, 2021). Precipitation deficiency has led to rapid development of drought conditions with extreme fire behaviour because of high ignition rate and rapid spread of wildfires (Miller, 2020; Lui et al, 2021; Ma et al, 2021; Kennedy et al, 2021). Dry or drought seasons are often associated with very hot weather and heat wave conditions over southern Africa (Lyon, 2009; Chikoore, 2016; Chikoore and Jury, 2021)

2.4.6 Fuel load

Fuel load is referred to as the quantity of dead and live biomass available to burn (Rodrigues et al, 2021). The overall forest fuels are determined by fuel on both grasses and forest surface and ground layer only excluding the crown fuel even if they are likely to catch flame during a fire event (Stefandou et al, 2020). Fuel load estimation only takes into consideration any fuel with a diameter less than 6 mm, including leaves, twigs and barks that are classified as fine fuel, whereas woody fuel such as logs, larger twigs, large shrubs and fallen branches are coarse fuels (Matthews, 2014; Sullivan et al, 2018; Price et al, 2022). Coarse fuels with diameter greater than 6 mm are

not considered when modelling the rate of fire spread (Sullivan et al, 2018). However, fine “dead fuel moisture” content is significant in understanding extreme wildfire behaviour when interacting with other factors, including weather, topography, and live fuel (Matthews, 2014).

Predicting wildfire behaviour requires understanding interactions between fuel load and fuel type (Prior et al, 2018; McLauchlan, 2020). Fuel types comprise ground, surface, ladder and crown fuels, as shown in Figure 2.3. (Vora, 2016). Ground fuels are forest duff and other organic material, rotten roots, tree base, logs, and other decomposed woody debris (Reardon, 2020). They burn slowly while producing a large quantity of smoke (Reardon et al, 2007). Surface fuel refers to fuel lying on or near the ground surface, including litter, rotten logs, grass, herbs, and small shrubs (Keane, 2015). Ladder fuels transport fire from the surface to the canopy, including small trees, low-lying branches on medium to large trees (Pyne et al, 1996; Menning and Stephens, 2007). Crown fuels refer to the biomass that composes forest canopy, including snags, lichen, tree needles, mosses and small branches (Keane et al, 2001; Affleck, et al, 2013).

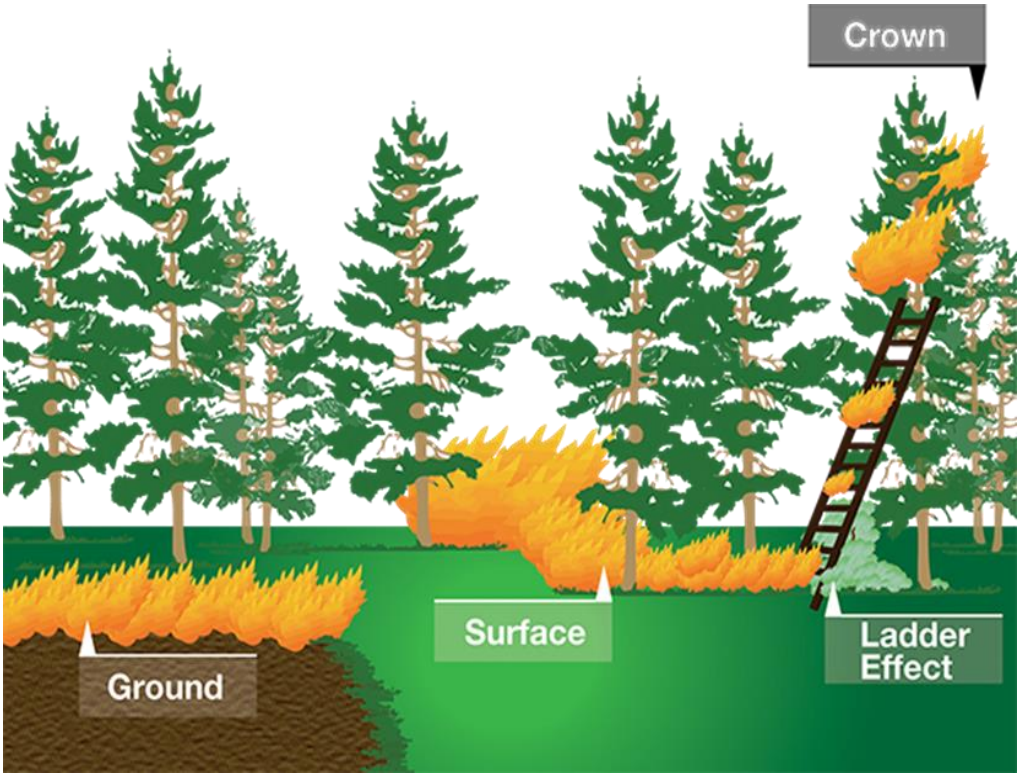

Figure 2.3 Categories of fuels in the fire environment (source: Vora, 2016)

2.4.7 Topography

Topography is a stable variable in the triangle of fire behaviour (Pyne et al, 1996). Since topography influences the formation of local weather and distribution of dead or live biomass over

a certain region, topographic factors including slope, aspect, and elevation influence the fire spread rate or burn severity (Birch, et al, 2015). For example, fire spreads faster up-slope than downslope because flames of fire-head preheat fuels lying in front (Biswell, 2020). Aspect regulates insolation and also the vegetation type on-site. In southern hemisphere north-facing slopes comprises of drier vegetation and high intensity fires frequently occurs (van Breda Weaver, 1991).

Elevation directly affects fire behaviour due to change in temperature from low to high elevation, orographic lift of prevailing winds and adiabatic lapse rate (Estes et al, 2017). Fuels at lower elevation dry quicker because of high temperatures and low rainfall, unlike at higher elevations whereby orographic lift of prevailing winds and adiabatic lapse rate had resulted in condensation causing more rainfall (Estes et al, 2017). Fuel may be abundant at higher elevation but at extremely high elevations, there may be no fuel (San-Miguel et al, 2020). Fires at high elevation occur frequently because of extensive lightning strikes that occur at those levels (Vaughan et al, 2021). Landscape features also play a critical role in fire behaviour, whereby canyons and ridges change prevailing wind patterns whilst intensifying fire behaviour (McBride, 2019). Other landscape features that affect fire behaviour include water bodies, roads and rock outcroppings, act as barriers that curb fire spread (Rothermel, 1972; McBride, 2019).

2.5 Impacts of wildfire

Fire has a significant role on earth system processes, but has profound adverse effects on the climate, environment and society at global and regional and global scales (Kasischke and Hoy, 2012; Carlson et al, 2012). Fire affects biogeochemical cycles through interacting with the biosphere, atmosphere and cryosphere when burning (Ward et al, 2012). Biomass burning emissions are a major source of air pollution impacting air quality, human health and climate on several space scales (Chen et al, 2017; Wu et al, 2018). Wildfires deteriorate air quality and adversely impact human health (Fann et al, 2018). Burning biomass material releases harmful diverse gases, including CO, CO_2, CH4, NOx, volatile organic compounds, and particulate matter (PM) (Sharratt and Auvermann, 2014). Greenhouse gases emission induced irreversible climate change trends, causing more frequent occurrence of wildfire which are unmanageable (Tavra, 2021).

Destructive wildfires with high fire frequency and high severity affect native fauna and flora that are less fire resilient (Lindenmayer, 2020). Plants and animal mortality from uncontrolled fire occurring in fire prone areas has affected endangered species from growing in numbers (Pausas

and Parr, 2018; Elliot et al, 2019; Kumari and Pandey, 2020). High fire frequency induces plant species richness but indirectly affect animals through changing their habitat and food availability (Heim et al, 2019; Pausus and Keeley, 2019). Ordinarily, controlled fires with low-intensity are used in ecosystem management to maintain habitat and wildfire management (Weiss and Brower, 2021). Uncontrolled fires with high fire intensity because of woody shrub encroachment induced extinction of small mammals in arid Australia grassland and savanna ecosystems (Gordon and Letnic, 2019). Increasing wildfire activities have driven extinction of amphibians due to canopy density thinning and higher temperatures that affects amphibian's thermoregulation and breeding sites (Spranger et al, 2020). Animals' physiological response from harsh wildfire events affects their phenotype and sexual ornament, hence females remain stressed and unlikely not to reproduce but maintain (Weiss and Brower, 2021).

Wildfire directly and indirectly affect physico-chemical property of soil including texture, pH, colour, bulk density, organic matter, nutrient and biota (Licas-Borja et al, 2020; Gomez-Sanchez et al, 2019; Isah et al, 2021). During burning, the fuel layers are consumed with heating soil minerals influencing change in soil texture, bulk density, colour, moisture content, and permeability (Isah et al, 2021). The degree of fire intensity, severity and frequency determines a variety of impacts on soil depending on weather, topography and fuel availability (Oyewole et al, 2019). Not all fires affect soil properties but fires that burn at high temperature (>300°C) affect surface and deep soils (Lambao et al, 2021). High temperature fires change soil colour resulting in decreasing organic matter and increasing bulk density, silt and clay content (Zhang et al, 2018)

2.6 Fire Regimes in South Africa

A fire regime is a general pattern in which fires vary in intensity, frequency, size, extent, type, seasonality and severity in an ecosystem over an extended period (Keeley et al, 2009; Weston, 2010; Rogers et al, 2020). Fire regimes are mainly determined by vegetation, weather and climate patterns (Pechony and Shindell, 2010). Climate change directly affects vegetation, fire severity and fire frequency due to prolonged dry days, abundant dead biomass and dry fuel load (Countryman, 1972). Fire regimes are also influenced by terrain features, slope exposure, fire management regimes and landscape patterns (Taylor and Skinner 2003). Topography, near surface winds and dead biomass available influences wildfire ignition, behaviour, the rate and direction of fire spread (Potter, 2012; Thurston et al, 2014;).

Changes in rainfall seasonality shows a decrease in the wet season duration and a prolonged the dry season over South African rainfall zones (Roffe et al, 2021). Rainfall zones distinguished are

summer rainfall zone (SRZ), winter rainfall zone (WRZ) and year-round rainfall zone (YRZ) play a significant role to South Africa ecosystem (Tyson and Preston-Whyte, 2000). The bulk of the country is a SRZ, the south-west region (Western Cape Province) is a WRZ, while the Cape south coast is classified as YRZ (Tyson and Preston-Whyte, 2000; Botai et al, 2018; Roffe et al, 2019). Distribution of rainfall throughout the year has established two fire seasons in South Africa (Strydom and Savage, 2016). The period December to April coincides with the dry season in the Western Cape which is also the fire season over the region whilst May to November is the fire season for the rest of the country (Santam, 2014). Rainfall absence during summer over the Western cape plays a significant role in the occurrence of wildfire during summer (Strydom and Savage, 2016). Wildfires occur in all months of the year but most wildfires frequently occur in July, August, September and October, as shown on Figure 2.4 (Strydom and Savage, 2016).

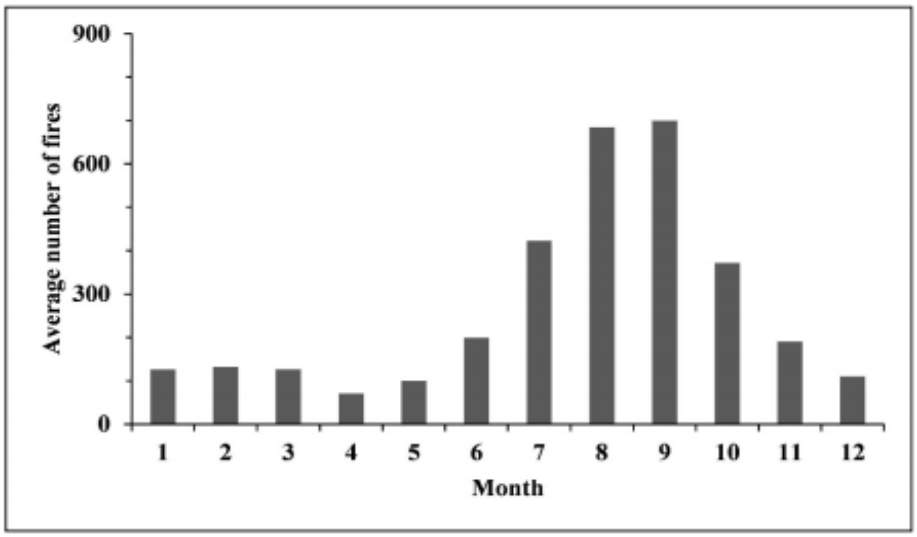

Figure 2.4 Mean annual number of fires per month from 2003 to 2013 in South Africa (Source: Strydom and Savage, 2016)

The frequency and intensity of wildfires peak during winter and spring seasons, because of windy and dry conditions that prevail over large parts of South Africa (Strydom and Savage, 2016). It is argued that the fire season over South Africa spans the period from May to November (Lui et al, 2010), May to October (Pricope and Binford, 2012), June to September (Scholes et al, 1996), or July to October (Archibald et al, 2010). These wildfires may be human induced or naturally occurring.

2.7 Influence of synoptic weather type on large fire activity

Synoptic weather types provide understanding of fire regimes and account for fire activities at different space and time scales (Duane and Brotons, 2018). Synoptic weather patterns and local weather conditions are critical to the development and rapid spread of wildfires (Schroeder et al, 1964; Duane and Brotons, 2018; Keely et al, 2021). Thus, weather conditions contribute significantly to the occurrence of large wildfires (Flannigan et al, 2000; Kraaj et al, 2018). Meteorological parameters including near surface temperature, precipitation, wind speed and direction, relative humidity, and atmospheric stability are anticipated when forecasting fire weather (Erickson et al, 2016; Dowdy and Pepler, 2018). The north-facing slopes are vulnerable to lightning-caused wildfire under low humidity conditions and prolonged drought period (Granger, 1984; Nampak et al, 2021).

The formation of a ridge and trough weather pattern has driven high to extreme fire spread rate (Tymstra et al, 2021). Ridge and trough weather types induce anomalous warm events with rapid fine fuel dryness and expected drought events, decreasing coarse fuels moisture (Rodrigues et al, 2020). Synoptic conditions responsible for wildfires in South Africa comprise of a ridging inland Kalahari high pressure cell which is associated with Berg winds near the coast during the austral winter (Chartan et al, 2018; Barnes et al, 2021). Berg winds also known as Foehn winds are strong drainage winds which are warm and dry, descending downslope the sharp escarpment from the plateau to the coast of South Africa influencing high fire danger rating (Sharples and Manzello, 2018; Adepoju and Adelabu, 2019; Barnes et al, 2021).

2.8 Fire danger Ratings System

Fire danger is defined as the resultant combination of both static and variable factors of the fire environment which affect the initiation, spread and difficulty of control of wildfires in an area and impact of fire (Deeming et al, 1972; Wotton, 2009). The constant factor is referred to as fuel and topography, whereas the variable factor is referred to as weather (Chandler et al, 1983). A fire danger rating system requires weather inputs from a specific weather station of interest to calculate an index under constant proposition of fuel, topography and ignition elements but weather forecasts will be used to predict the fire danger for the forthcoming period of time (Willis et al, 2001).

A Fire Danger Index (FDI) consists of fuel and meteorological information unified into several measures that are applied for issuing of warnings and estimating the suppression difficulty of a fire (Dowdy, 2009). An FDI is built to predict fire behaviour, declare fire bans, schedule prescribed

burns, and determine fire risk categories which are used by fire management authorities to identify danger and preparedness for unexpected wildfires outbreaks (Sharples et al, 2009, Khastagir et al, 2018). There are many fire danger indices used in different parts of the world, including "Grassland and Forest Fire Danger Index" (GFDI and FFDI) (McArthur, 1967) developed in Australia, "Canadian Forest Fire Weather Index" (FWI) System (Van Wagner, 1974), "Lowveld Fire Danger Index" (Meikle and Heine, 2010) developed in Zimbabwe and the "US National Fire Danger Ratings System" (NFDRS) (Deeming et al, 1977).

2.8.1 McArthur Grassland and Forest Fire Danger Index

"McArthur Grassland Fire Danger Index" (GFDI) (McArthur, 1966) and "Forest Fire Danger Index" (FFDI; (McArthur, 1967) are used by "Australian Bureau of Meteorology" to predict the role of weather variables on fire behavior and forecasts for use by fire authorities. Both GFDI and FFDI have similar basis but differentiated by fine fuel availability in the GFDI which is calculated using the degree of curing instead of Drought Index and Drought Factor components used in FFDI (Griffiths, 1999). The McArthur FFDI is broadly applied on all types of forests but fire behaviour differs with vegetation types and adaptation requires redefining the different fire danger classes. Nonetheless, the McArthur FFDI is based on an empirical model which requires several inputs including rainfall, air temperature, wind speed, and relative humidity time since last rainfall, and the "Keetch-Byram Drought Index" (KBDI) (Dowdy, 2009).

In order to calculate the FFDI, relevant information about the fuel moisture content, fuel load and terrain slope is also needed to define aspects of fire behaviour including the rate of forward spread of fire, heat output, fire line intensity, flame height, and spotting distance (Willis, et al, 2001, Noble et al, 1980). The formula to calculate FFDI is expressed by Willis et al, (2001).

$$FDI = 2e^{-0{\cdot}45 + 0.987ln(D) - 0.034RH + 0.0338T + 0.0234V}$$

Equation 2.1

Where, FDI is fire danger index (non-dimensional), D is drought factor (non-dimensional), RH is relative humidity (%), T is air temperature, particularly maximum temperature (°C), and V is 10 m wind speed (km h^{-1})

The drought factor (D) was introduced into the McArthur FFDI by Noble et al, (1980), then later improved by Griffiths (1999). Drought factor is defined as a variable representing the state of fuel and fine fuel availability derived from categories of the Keech-Byram drought index (Keech

& Byram, 1968). There drought factor is a non-dimensional parameter whose values range from 0 to 10 (Griffith, 1999). The formula to calculate D is expressed:

$$D = max\left[10 \cdot 5\left(1 - e^{-\frac{(I+30}{40}}\right)\frac{y + 42}{y^2 + 3y + 42}\right]$$

Equation 2.2

$$y = \max\begin{cases}\frac{(P-2}{N^{1.3}}, & N \geq 1 \; and \; P > 2 \\ \frac{(P-2)}{0.82^{1.3}}, & N = 0 \; and \; P > 2 \\ 0, & P \leq 2\end{cases}$$

Equation 2.3

Where, y is a past 20 day index variable, P is 24-hour accumulated rainfall (mm), N is period since the last rainy event (days), D is drought factor (Scale range between 0 and 10), and I is KBDI (mm).

Holgate et al, (2017) outlined the revised classification of FFDI and their assigned Fire Danger Rating (FDR) categories shown on Table 2.1. However, the revised threshold of FFDI presented in Table 2.1 differs from the original FFDI classification threshold shown on Table 2.2 (Dowdy et al, 2009).

Table 2.1 Revived classification of FFDI into Fire Danger Ratings (Source; Holgate et al, 2017)

"Fire Danger Rating"	**"FFDI Range"**
"Low–Moderate"	"0 –11"
"High"	"12 – 23 (12 – 31 in Western Australia)"
"Very High"	"24 – 49 (32 – 49 in Western Australia)"
"Severe"	"50 – 74 "
"Extreme"	"75 – 99"
"Catastrophic"	"≥ 100"

Table 2.2 Original FFDI classification into “Fire Danger Ratings” (source: Dowdy et al, 2009)

“Fire Danger Rating”	**“FFDI Range”**
“Low”	“0 – 5”
“Moderate”	“5 – 12”
“High”	“12 – 24”
“Very High”	“24 – 50”
“Extreme”	“50 +”

An equation to calculate the “McArthur Grassland Fire Danger Index” (GFDI) (McArthur, 1966) has evolved throughout time. The current GFDI Mark 5 equation (Noble et al 1980) is provided in terms of wind speed (km h $^{-1}$), relative humidity (%), dry-bulb temperature (°C), and grass curing (%) (Sharples et al, 2009). The GFDI Mark 5 equations are expressed as:

$$GFDI5 = \begin{cases} 3.35W^{(-0.0897m+0.0403U)}, & m < 18.8, \\ 0.299W^{(-1.686+0.0403U)}(30-m), & 18.8 \leq m < 30 \end{cases}$$

Equation 2.4

$$m = \frac{97.7 + 4.06H}{T+6} - 0.00854H + \frac{3000}{C} - 30$$

Equation 2.5

Where, m is fuel moisture content (%), H is relative humidity (%), T is air temperature (°C), C is degree of curing (%), $GFDI5$ is fire danger index, W is fuel load (kg/m^2). Including W in $GFDI5$ equation has affected its application over a regional scale unless they assume the fuel load to be constant (Sharples et al, 2009).

McArthur 1966 GFDI Mark V Fire Danger Rating Thresholds range: Low (0 – 2.5), Moderate (3 – 7.5), High (8 – 20), Very High (20.5 – 50), Extreme (>50 – 100/150) and Catastrophic/Code red (>150) (Cheney and Gould, 1995). “GFDI Mark IV Fire Danger Ratings GFDI thresholds Low (0 – 2.5), Moderate (>2.5 – 7.5), High (>7.5 – 20), Very High (>20 – 50) and Extreme (>50 – 200)” (Sharple et al, 2009).

2.8.2 Lowveld Fire Danger Index

The Lowveld Fire Danger Index (LFDI) was developed in Zimbabwe (Laing, 1978) and has been fully adopted as an official "South African National Fire Danger Rating System (Notice 1099 of 2013)". LFDI comprises burning index, rain correction factor and wind correction factor calculated together to simulate fire behaviour (Meikle and Heine, 1987). The formula to calculate the Burning index (BI) requires meteorological inputs from temperature and relative humidity (Notice 1099 of 2013).

$$BI = (T - 35) - \frac{(35-T)}{30} + 0.37(100 - RH) + 30 \qquad \text{Equation 2.5}$$

Where, T is Temperature and RH is Relative Humidity

The LFDI is calculated daily in the morning at 10h00 and afternoon at 14h00 Local Standard Time (LST) when maximum index values are expected.

Formula:

$$LFDI = (BI + WindFactor) \times RCF \qquad \text{Equation 2.6}$$

The wind factor is the additional FDI value that corresponds with the recorded wind speed (km/h). Rain correction factor (RCF) is determined by the accumulated rainfall over a single to many more days which have an assigned number value ranging from 0 to 1. The calculated LFDI is rated between 0 and 100 (Notice 1099 of 2013).

The "Fire Danger Rating System" used in South Africa has five fire colour codes categories which represent the fire behaviour, dangers, and severe damage associated with each colour code and FDI rating (Notice 1099 of 2013). The rating of FDI closer to zero, represents safer conditions, while rating score closer to 100 represents dangerous conditions. The colour codes are interpreted under a range of FDI rating: Blue (insignificance) 0 - 20, Green (low) 21 – 45, Yellow (moderate) 46 – 60, Orange (high) 61 - 75, and Red (extremely high) 76 – 100 (Notice 1099 of 2013).

The colour codes defined unique fire parameters calibrated in accordance to the FDI rating (Notice 1099 of 2013). Blue represents fire, with flame height less than 1m, with no spreading threat. Green colour code alert about fires with flame height between 1.0 and 1.2m and slight threat of spreading (Notice 1099 of 2013). Yellow colour code corresponds to extreme caution with 1.2-1.8m flame height driven by unfavourable weather and control burn being undertaken

within manageable conditions (Notice 1099 of 2013). Orange enforces maximum suppression effort to fires of any kind and estimated flame heights are 1.8-2.4m (Notice 1099 of 2013). Red colour code requires all firefighting teams on standby because of whirl-fire development, increase in wind speed, lots of spotting fires and flame heights above 2.4 meters (Notice 1099 of 2013).

2.9 Fire management in South Africa

Wildfires are very common in South Africa because of the vegetation types that are fire dependent and climate dependent to maintain their structure and composition (Kruger et al, 2006). South Africa has adopted the National Veld and Forest Fire Act, No. 101 of 1998 as a major tool and improved wildfires warning and management guide in South Africa (Kruger et al, 2006; Moyo et al, 2020). NVFFA is a tool to facilitate integration between owners (organ of state, private landowner, and communities on communal lands) in preventing and combating wildfire (Bridgett et al, 2003). Therefore, NVFFA requires owners to form and register a functional Fire Protection Association (FPA) to predict, prevent, manage and extinguish wildfires (Bridgett et al, 2003; Ballantyne, 2019).

“South African National Fire Danger Rating System” (NFDRS) has adopted the “Lowveld Fire Danger Rating System” by Meike and Heini (1987) developed in Zimbabwe (Lall and Mathibela, 2016). Lowveld Fire Danger Index (LFDI) alerts fire managers and foresters about the weather that may influence ease of ignition, harsh behaviour of fires and assess the risk of ordained burning activities, improving preparedness of real-time firefighting and allocating firefighting resources (Meikle and Heine 1987; de Groot et al, 2006). South African NFDRS considers the relevant features of every area including the vegetation type, topography, seasonal climatic cycle, recent, current and forecasted weather and also other relevant matter (Willis et al, 2001; Harrison, 2015).

South Africa’s 226 local municipalities are used as a division to represent wildfire risk assessment and the calculated LFDI which is used for fire danger rating (Kruger et al, 2006; Forsyth et al, 2010). Wildfire risk assessment has been adopted as a guide which classified fire-ecology types derived from South African biomes (Low and Rebelo, 1998; Dayaram et al, 2019). Fire-ecology types are classified as either fire dependent or climate dependent (Kruger et al, 2006). Fire-ecology types are composed of Forest, Thicket, Savanna (Sparse Arid, Arid, and Moist Woodland), Karoo (Succulent, Nama, and Grassy Nama Karoo), Grassland (Coastal, Sour and Sweet Grassland) and Fynbos (Renosterveld and Fynbos) (Low and Rebelo, 1998; Kruger et al, 2006; Harris et al, 2019; Dayaram et al, 2019).

2.10 Projected wildfire activities using GCMs

Climate change has manifested in long-term mean rainfall, temperature and circulation patterns, but also through a global increase in the frequency of extreme events (John et al, 2015). Extreme wildfire events estimated using multiple climate models based on KBDI, showed potential increase in intensity, duration and frequency (Brown et al, 2021). Modelling wildfire activities plays a significant role in understanding dynamics of fire regimes and their associated socio-economic, and ecological impacts under climate change (Dupuy et al, 2020). Improving climate models reduces biasedness hence increasing reliability in simulating the past and projected trends of regional climate variabilities and determining the magnitude and extent of climate signals (Irrgang et al, 2021; Watson-Parris, 2021).

GCMs have projected an increase in wildfire activities globally at the end of this century using the "Keetch-Byram Drought Index" (KBDI) (Lui et al, 2010; Brown et al, 2021). The KBDI is a tool used for estimating drought and forest fire potential risk by indicating the amount of moisture decreasing in the top soil layers (Srinivasan and Narasimhan, 1998; Johnson and Forthum, 2001; Xanthopoulos et al, 2006; Fujioka, 2019). Meteorological variables including wind speed, precipitation, and maximum temperature are used to measure the fire potential (Lui et al, 2010; Barbero et al, 2020; Keely et al, 2021).

Rising global average surface temperature reaching thresholds 3°C showed complex feedback between climate, fire, CO2, trees, and C4 grasses (Engelbrecht and Engelbrecht, 2016). Projections under "A2 scenario" of the "Special Report on Emission Scenarios" (SRES) showed expansion of hot steppe and hot desert zones, intrusion of savanna into grassland and more frequent fynbos fires in a drier and warmer climate (Engelbrecht and Engelbrecht, 2016). Fire and CO2 influences growth of trees in mesic savannas and grasslands (Bond et al, 2003; February et al, 2020). Rising levels of CO2 influence growth of trees which are more fire resistant to invade the savannas throughout the world (Bond and Midgely, 2012; Voelker et al, 2019).

Projections of vegetation change using a "dynamic-vegetation" model with exclusion of fire and results showed most of C4 grasslands and savannas were likely to become forest to a greater distinct (Bond et al, 2005; Quirk et al, 2019). The paleo-records showed forests existed in the ancient ecosystems over sites which are the current savannah biomes of South Africa but simulations from a dynamic vegetation model have shown a significant increase in tree numbers since the pre-industrial era (Bond et al, 2003). Catastrophic fires and low CO2 levels in the

atmosphere influenced the slow recovery of trees, which persuaded establishment of the current savannah and grassland ecosystem (Bond et al, 2003).

2.11 Summary

Climate observations are the crucial resource needed to understand and predict the climate and its influence on fire regimes. Projections of future wildfire regimes in a changing climate require consideration of current interactions between short-term climate variables and wildfire activity (Kennedy et al, 2021). However, incorporating “Fire danger Rating Systems” and biomass accumulation have played a significant role in predicting fire behaviour using meteorological observations (Anderson, 2009; Harris et al, 2012; Canadell et al, 2021). Since climate models can produce simulations of future climate on seasonal, annual, and longer time scales, fire danger and behaviour within the prescribed timeframes or forecasting scale (Littell, 2018). Climate models are the best tools to project the future climate considering different socio-economic pathways. This study employs climate models to project the risk of future fires over the Limpopo grasslands under a “business as usual” scenario.

Chapter 3: Research Methodology

3.1 Introduction

The change in climate variables and moisture content of live and dead vegetation influences wildfires (Halofsky, 2018). During the dry season, water stress is high and with less moisture in the fuel, fires ignite easily, and other driving forces, including wind, may cause rapid and intense fire to spread (Pierre-Louis and Schwartz, 2018). The data required for the present study was gathered and analysed using relevant methods to explain the relationship between climate change, wildfires, and fire regimes. Thus, this chapter describes the datasets and methods that were employed in the study. Climate observational data and climate models' simulations under the worst-case emission scenario RCP8.5 were used to simulate the present-day climate and project the future. Simulations from climate models need to be validated against historical observations using appropriate statistical parameters (Cannon et al, 2020).

3.2 Study area

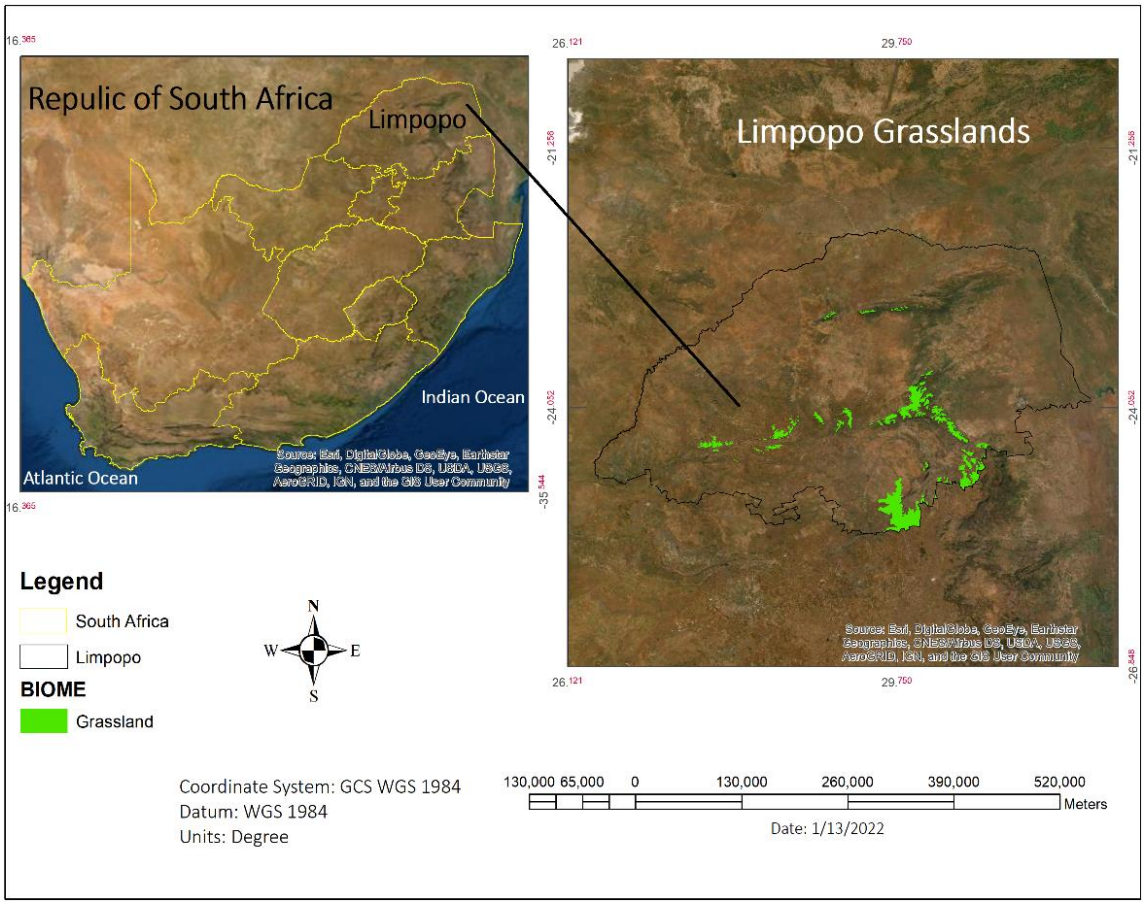

Figure 3.1 Map showing geographical location of the study area.

Limpopo is one of the nine provinces of South Africa, located on the north-eastern side of the country, as shown in Figure 3.1. The province is largely a semi-arid region that shares its boundaries with Zimbabwe (north), Botswana (west), and Mozambique in the east. The savanna and grassland biomes, but with patches of forest and alluvial, distinctively occupy the area (Val et al, 2021; Moshobane et al, 2021). The study area includes the Kruger National Park on the eastern boundary, one of South Africa's largest national parks (Mills et al, 2021).

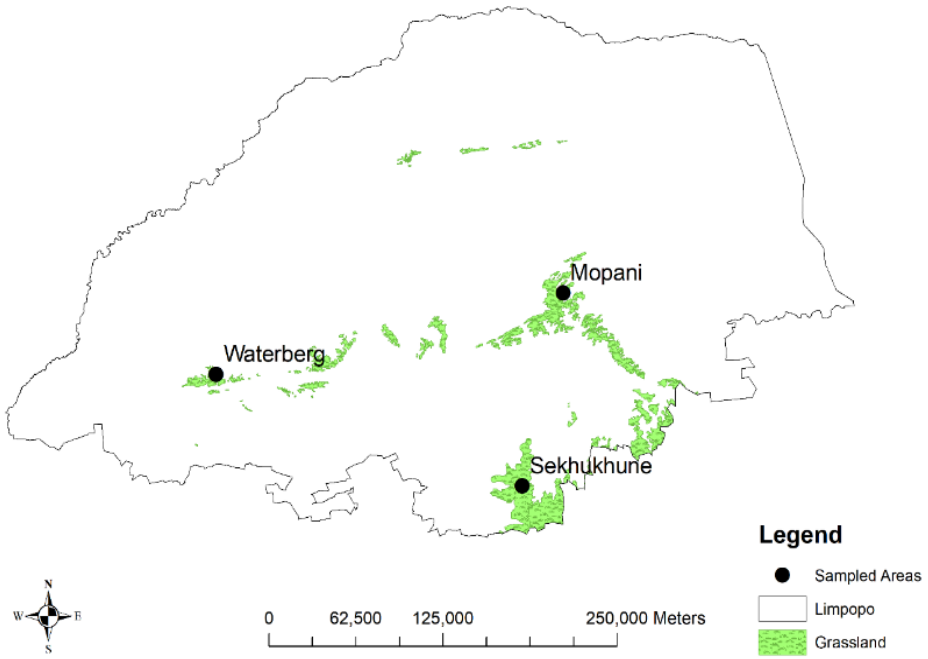

Figure 3.2 Point areas of interest within Limpopo grasslands

There are three geographical point areas of interest for the present study which include Waterberg (27.77 E; 24.45 S), Sekhukhune (29.73 E; 25.15 S), and Mopani (30.01 E; 23.91 S) as shown in Figure 3.2. These three locations derive their names from the district municipalities in which they are located, and were selected to investigate the impact of weather conditions on fire danger rating. Recent intense droughts in the past decade have triggered unprecedented large fires in Limpopo. The accumulated dead fuels during drought induced extreme fire events with high fire intensity and high spread rate.

3.3 Observational data

3.3.1 Key variables

3.3.1.1 Precipitation

Precipitation is any product of the condensation of the atmospheric water vapor that falls under gravity (Kumari et al, 2019). The amount, duration, and frequency of precipitation directly affect drought and fire activities (Chen et al, 2014). Declining summer rainfall and wetting rain days significantly drives an increase in fire activities (Holden et al, 2018). Fuel moisture is influenced by the amount and duration of the precipitation (Ruffault et al, 2018). Fine fuels rapidly react to change in precipitation by gaining or losing moisture, usually within one hour (Bilgili et al, 2019). It does not affect heavy fuels due to lengthy period they take to gain or lose moisture (Miller and Wilmore, 2020). Heavy rainfall over a short duration will not increase fuel moisture compared to light rainfall over a longer period where the fuels can absorb more moisture influenced by less run off (Ruffault et al, 2018).

3.3.1.2 Air Temperature

Air temperature is a measure of the degree to which air becomes cold or hot, in variation with time, location, and altitude. Changes in air temperature near earth's surface are influenced by dynamic activity, seasonality, diurnal cycles, and movement of weather systems (Ziter et al, 2019). Hot temperatures influence the ignition and behaviour of wildfires due to preheating fuels, whilst cooler temperatures have the opposite effect (Sun et al, 2021). Air temperature can be measured using thermometers and expressed in degrees Kelvin, Celsius or Fahrenheit (Wilson, 2021). If the reading of air temperature is in Kelvin, it can be converted to Celsius by subtracting 273.15 from the recorded value and conversely converted from Celsius to Kelvin by adding same value of 273.15 (Wilson, 2021).

3.3.1.3 Wind speed

Wind is the movement of air from an area of high pressure to an area of low pressure across earth surface comprises of zonal (U), meridional (V) and vertical (ω) components (Droste et al, 2018). The horizontal components of the wind vector are combined to give the speed and direction of the horizontal wind, measured in $m.s^{-1}$ (Chen et al, 2021). Wind determines advection of heat and moisture and therefore the weather conditions. It is the most significant weather element influencing behaviour of wild fires, the most unpredictable, and frequently changing over time and

space (Storey et al, 2020). The most significant role played by winds is driving the weather and climate at local and global scale (Holbrook et al, 2019).

3.3.1.4 Relative Humidity

Relative humidity, expressed as a percentage, is the ratio of the amount of moisture in the atmosphere at a given air temperature relative to the amount the air could hold when saturated at the same air temperature (Nui et al, 2020). Relative humidity ranges from 1% (very dry) to 100% (saturated), even though the atmosphere is never completely dry. It has an influence on wildfire behaviour making is a good indicator of high fire danger (Torres et al, 2018). In wild fire environment, relative humidity influences fuel moisture content depending on fuel types, hence varying over time and location (Torres et al, 2018). The relationship between temperature and relative humidity is inversed (Matsoukis et al, 2018). When temperature reaches its lowest point in the early morning, relative humidity reaches its highest point, and the temperature increases so does the water holding capacity, thus the relative humidity decreases (Jatta et al, 2018).

3.3.2 Weather Station Data

In the present study, daily weather station data comprises six key variables; rainfall (mm), minimum temperature (°C), maximum temperature (°C), minimum relative humidity (%), maximum relative humidity (%), and wind speed (m/s) was used as the present climate data spanning period from 1961 – 1980. Weather station data was obtained from the South African Agricultural Research Council (ARC-SA). The weather stations used are listed in Table 3.1 below:

Table 3.1 ARC weather station used in the present study

Station name	**Altitude**	**Latitude**	**Longitude**
Duiwelskloof: Westfalia Letaba	858 m	-23.96666718	30.18333244
Thabazimbi: Marakele Towers	2256 m	-24.45878	27.61334
Sekhukhune: Leeukraal	1446 m	-24.91583	29.83511

These weather stations are selected because they are located close to three geographical point areas of interest for the present study shown in Figure 3.2.

3.3.3 Climate Research Unit Observations

In addition to the weather station data, the gridded Climate Research Unit (CRU) Time-series (ts) data version 4.04 (Harris et al., 2020) was also used in this study. The CRU data comprises monthly averages of variable such as precipitation, daily minimum and maximum temperature.

Essentially, the CRU data are gridded weather station data with a spatial resolution of 0.5° x 0.5° (Harris et al., 2020). CRU datasets are reliable with long timeframe since 1901 to present (Jones and Harris, 2008; Harris et al., 2020). The designated period of study for this research is from 1961 to 1980 as the historical baseline. The variables used for the present study include; precipitation, minimum and maximum temperature.

3.4 Climate Models

3.4.1 Conformal Cubic Atmospheric Model (CCAM)

CCAM is a GCM developed at CSIRO (Australia), fully based on a variable-resolution conformal-cubic grid to “simulate regional scales” barring “lateral boundary conditions” (Thatcher et al, 2015; McGregor, 2005). It is among the first “cube-based three-dimensional” (3-D) atmospheric model which avoids lateral boundary stipulations and allowing coupling done together with the “global and regional spatial scales” on the equal grid (Figure 3.3; Thevakaran et al, 2015). The model uses a non-hydrostatic, semi-implicit, and semi-Lagrangian dynamical core that is cost-effective for regional climate modeling because of semi-Lagrangian methods that allow longevity of time-step (McGregor, 2005). It also has a sizable sequence of physical parameterizations to calibrate forces and energy transformation to describe the behavior of the radiation, convection, aerosols, cloud microphysics, boundary layer turbulence, gravity wave drag, and land surface (Thevakaran et al, 2015).

The CCAM spatial resolution ranges from the 200 km horizontal resolution provided using quasi-uniform C48 conformal-cubic grid (Schmidt factor 1) for global simulations to an ultra – high resolution of 1 km (Schmidt factor 200) over a specific area of study (Engelbrecht et al, 2011). In the present study, CCAM 8 km resolution simulations were obtained by nudging the output of 60 km resolution simulations shown by Figure 3.3 with Schmidt stretching factor 24.75 over South Africa for the period 1961 – 1980 (historical baseline), 2021 – 2040 (near future), 2041 – 2060 (mid future), and 2080 – 2099 (far future). McArthur high fire danger days', rainfall, maximum temperature, minimum relative humidity, and wind speed are the key variables projected using CCAM.

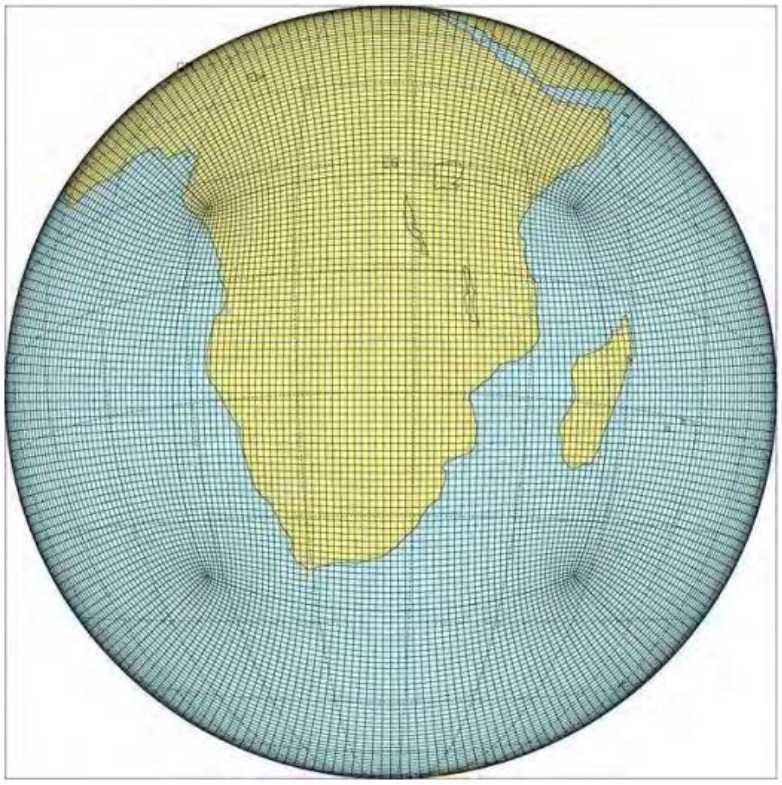

Figure 3.3 CCAM grid under Schmidt factor 3.3 used over Southern Africa and tropical Africa for downscale simulations at 60 km spatial resolutions (Engelbrecht et al, 2011).

3.4.2 Six Downscaled General Climate Models (GCM) from CIMP6

Simulations from six (6) downscaled GCMs were used in this study. The dynamical downscaling of six GCMs was performed through RCM CCAM to get a relatively high spatial resolution of 8 km over the study area.

3.4.2.1 Australian Community Climate and Earth System Simulator Coupled Model (ACCESS-CM)

ACCESS-CM is a climate model used for climate research (Bi et al, 2013) which contributed to Phase Five of the Coupled Model Inter-comparison Project (CMIP5). The model was developed in Australia through alliance between “Centre for Australian Weather and Climate Research (CAWCR), Bureau of Meteorology and CSIRO” (Bi et al, 2013). ACCESS-CM comprises two versions, including ACCESS1.0 and ACCESS1.3, both coupling the atmospheric Unified Model (UM), ocean model and sea-ice model from NOAA/GFDL and the UK Met Office, fully coupled using CERFACS4 OASIS3.2–5 framework (Bi et al, 2013).

Both ACCESS1.0 and ACCESS1.3 have unique land surface and atmospheric components. ACCESS1.0 is the basic version which runs through the Met Office's most considered HadGEM2 (r1.1) atmospheric physics and Surface Exchange Scheme version 2 (MOSES2) (Martin et al. 2011). ACCESS1.3 is considered as the experimental version to run projections of climate change at a century scale. Therefore, atmospheric physics of ACCESS1.3 is made up of prognostic cloud prognostic condensate (PC2) cloud scheme (Wilson et al. 2008; Hewitt et al, 2011) which assimilate the configuration of the "Met Office Global Atmosphere" (GA) version 1.0. The land components of ACCESS1.3 are assimilated from "Community Atmosphere Biosphere Land Exchange (CABLE) version 1.8" (Kowalczyk et al, 2006, 2013).

3.4.2.2 The Community Climate System Model (CCSM)

CCSM is a GCM comprising coupled components of atmosphere, land, ocean, and sea ice linked through interchanging of state information and fluxes (Gent et al, 2011). It was developed through collaboration between National Center for Atmospheric Research (NCAR) and various organisations including universities, national laboratories, and a community of scientists from different institutions (Gent, 2006). The most recent version CCSM is approved around the world to take part in the CMIP5 (Blackmon et al, 2001; Gent et al, 2011). Other previous versions CCSM were employed to study paleoclimate epochs, the most recent climate, and future climate change projections via coupled runs comprising 1° and 2° grid resolution of the atmosphere and land components (Gent et al, 2011).

3.4.2.3 CNRM-CM

CNRM-CM is a GCM developed to contribute to CMIP5 through collaboration between "Centre National de Recherches Meteorologiques-Groupe d'etudes de l'Atmosphere Meteorologique" (CNRM-GAME) and "Centre Europeen de Recherche et de Formation Avancee" (Cerfacs) (Voldoire et al, 2013). CNRM-CM version 5.1 comprises components of atmosphere, land, ocean and sea ice models coupled through the OASIS system with reoccurring frequency of 6 hours (Voldoire et al, 2013). The model contributed to the long term control experiment in both CMIP5 and CMIP6 (Séférian et al, 2016). The 6th version of CNRM-CM can represent heat source and moisture sink properties integrated in a single-column approach (Abdel-Lathif et al, 2018).

3.4.2.4 Geophysical Fluid Dynamics Laboratory Earth System Models (GFDL-ESM)

GFDL-ESM is a model that merges advanced component in atmospheric chemistry, carbon, and ecosystem all-inclusive within a single coupled climate framework (Dunne et al, 2020). The most recent version, GFDL-ESM Version 4.1 (ESM4.1) is contributing to the CMIP6 (Dunne et al,

2020). GFDL-ESM v4.1 features double horizontal resolution of both atmosphere 2° to 1° and ocean 1° to 0.5° which significantly helps to represent the climate mean patterns and variability (Horowitz et al, 2020). The model comprehensively focuses on earth system interactions through improved couplings for chemistry, carbon, and dust in contrast to previous version (Horowitz et al, 2020).

3.4.2.5 Max Planck Institute Earth System Model (MPI-ESM)

The latest version MPI-ESM1.2 is the CMIP6 baseline and mainly used to study current seasonal and decadal climate predictions (Müller et al, 2018). The MPI-ESM1.2 consists of coupled higher-resolution version (MPI-ESM1.2-HR) and lower resolution version (MPI-ESM1.2-LR) (Gutjahr et al, 2019). The MPI-ESM1.2-RH has an equilibrium radiation budget and stable ocean circulation (Müller et al, 2018). Both versions consist of a coupled atmospheric model and ocean model (Mauristen et al, 2019).

The coupling of oceanic and atmospheric components is performed using the 4th version of "Ocean- Atmosphere-Sea-Ice" coupler without flux adjustment (Müller et al, 2018; Mauristen et al, 2019). The CMIP5 version have coupling frequency of one day, hence CMIP6 coupling frequency has been improved to one hour (Müller et al, 2018). Due to the improved coupling frequency, projection tropical Pacific diurnal cycle of convection improved and Niño events has been enhanced and improved (Müller et al, 2018). The computing resources to run MPI-ESM-HR are not cost-efficient compared to MPI-ESM LR (Müller et al, 2018). Components of MPI-ESM1.2HR and MPI-ESM1.2-LR are shown in Table 3.2 below.

Table 3.2 Component of MPI-ESM

Components		**MPI-ESM1.2-HR**	**MPI-ESM1.2-LR**
Atmospheric	Model	"ECHAM6.3"	"ECHAM6.3"
	Horizontal resolution	"T127 (~100 km)"	"T63 (~200 km)"
	Vertical resolution	"L95"	"L47"
Oceanic	Model	"MPIOM 1.6.3"	"MPIOM 1.6.3"
	Horizontal resolution	"0.4°"	"Nominal 1.5°"
	Vertical resolution	L40	L40

3.4.2.6 Norwegian Earth System Model (NorESM)

NorESM is a model that assimilated CCSM4 (Gent et al, 2011) framework, developed by "University Corporation for Atmospheric Research" (Iversen et al, 2013). The difference between NorESM and CCSM4 is an isopycnic coordinate which was adopted from ocean model and atmospheric component that has adopted advanced interaction system between chemistry, aerosol, cloud and radiation (Seland et al, 2020). NorESM1-M is core version comprising atmosphere and land components at the horizontal resolution of 2°. Lower resolution version (NorESM1-L) and a version that includes prediction of biogeochemical cycling is also available (NorESM1-ME) (Iversen et al, 2013). The ocean and ice components have horizontal resolution of 1° (Iversen et al, 2013; Guo et al, 2019). The main goal behind developing and improving NorESM is to verify climate processes at northern high latitude around the north pole (Bentsen et al, 2012).

3.5 Representative Concentration Pathways (RCPs)

RCPs are scenarios that describe trajectories and time series of emissions and concentrations GHGs, aerosols and other active gases, along with land use/land cover (Moss et al, 2010; Su et al, 2021). The RCPs are innovation among incorporated assessment modelers, climate modelers, terrestrial ecosystem modelers and emission inventory experts (Gütschow et al, 2021). Integration between modellers induced comprehensive high-resolution datasets that project future climate conditions from the current climate and radioactive forcing values between 2.6 to 8.5 W/m^2 (van Vuuren et al, 2011). Integrated Assessment Models produced four RCPs corresponding emission scenarios (RCP2.6, RCP4.5, RCP6.0 and RCP8.5) to draw trajectories of emission and concentration of atmospheric pollutants influencing gradual rise of temperature before 2100 and projected further to 2300 (Yuan and Kopp, 2021; Reddy et al, 2021).

In this present study, the high emission 'RCP8.5' global warming scenario was used. The RCP8.5 is usually referred as worst-case or "business as usual" scenario, with the notion of society not taking initiatives and any effort to limit greenhouse gas emissions (Nordgren, 2021; Nguyen et al, 2021). The RCP8.5 scenario assumes rapid population growth, slow economic growth, increased poverty, low technology development and high emissions from energy use (Mendelsohn, 2021).

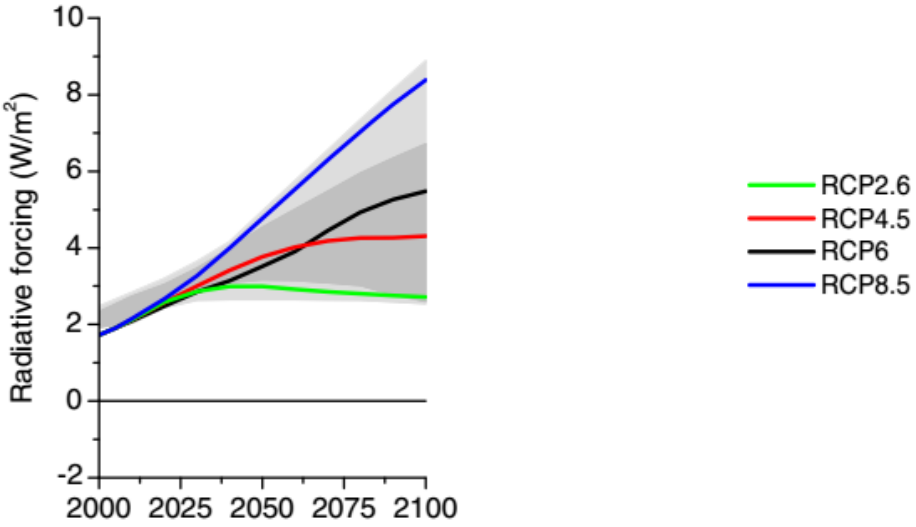

Figure 3.4 Four RCPs trends from 2000 to 2100 (Source: Maule et al, 2017)

3.6 McArthur Forest Fire Danger Index

The McArthur Forest Fire Danger Index (FFDI) is the most reliable and consistent fire danger predicting model that takes into consideration all significant drivers of fire behaviour (Willis et al, 2001). The Mark 5 Forest Fire Danger Meter is the currently used version of FFDI with thresholds range from a value 0 to 100 and divided into five fire danger categories namely; low, medium, high, very high and extreme (Sharples et al., 2009). The FFDI is calculated using meteorological variables, such as “wind speed, temperature, relative humidity, and rainfall” (Stephenson, 2015). The equation to calculate the FFDI is expressed in Equation 3.1 below (Hadisuwito and Hassan, 2021). The daily FFDI data used for the study was calculated using the CCAM future projections.

$$\mathrm{FDI} = 2\mathrm{e}^{-0{\cdot}45 + 0.987\ln(\mathrm{D}) - 0.034\mathrm{RH} + 0.0338\mathrm{T} + 0.0234\mathrm{U}} \qquad \text{Equation 3.1}$$

where, FDI is fire danger index (unitless), D is drought factor (unitless), RH is relative humidity (%), T is air temperature, either maximum or measured at noon (°C), and U is average wind speed (km/h) at a height of 10 m.

The drought factor in FFDI was calculated using Equation 3.2, with recorded daily precipitation and time parameters since the last rain (Khastagir, 2018).

$$DF = \frac{0.191(i + 104)(N + 1)1.5}{3.52(N + 1)1.5 + P - 1} \; if\; DF > 10, D = 10$$

Equation 3.2

where i is the Keetch–Byram Drought Index (KBDI) in millimetre (mm), N is the time since the last rain in days and P is the last recorded daily precipitation in mm.

KBDI is a drought index that has been widely used for forewarning the danger of wildfires (Jain, 2020). The drought index increases with the potential risk of ignition of wildfires. Crane (1982) reformulated the drought factor (DQ) on the International System unit scale written in equation 3.3 (Keetch and Byram, 1968; Alexander, 1990; Abrha and Adhana, 2019).

$$DQ = \frac{[203.2 - Q]\left[0.968e^{(0.0875T\ +\ 1.5552)} - 8.30\right]d\tau}{1 + 10.88e^{(-0.001736R)}}10^{-3}$$

Equation 3.3

Where Q is moisture deficiency (mm), T is daily maximum temperature (°C), R is mean annual precipitation (mm), and $d\tau$ is time increment (1 day).

The high fire danger rating was used in the present study by counting total number of days which the FFDI rank between 7.5 and 20 thresholds.

3.7 Model Validation

3.7.1 Taylor diagram

A Taylor diagram is a two-dimensional (2-D) graph that summarizes the strength of the relationship between a set of models and observations (Taylor, 2001; Montgomery, 2019). It is employed to evaluate how close models match observations. It comprises the centered Root Mean Square Error (RMSE), correlation coefficient (r), and standard deviation plotted simultaneously on a single quadrant (Taylor, 2005). The values of different variables used in the present study, including rainfall, maximum temperature, minimum relative humidity, and wind speed, are plotted with normalized variance to show the relative amplitude of the model and observed variations (Hu et al, 2019). Taylor diagrams were used to evaluate models' performance (Montgomery, 2019) for the historical baseline (1961 – 1980) in the present study.

3.7.2 Root Mean Square Error (RMSE)

The RMSE is the standard deviation of the residuals (prediction errors) (Muthyalappa and Sreedhar, 2021). Residuals measures how far are data points are from the regression line, hence RMSE measures how spread out are these residuals (Mawlood et al, 2021; Yan et al, 2021). It shows how concentrated the data are near the line of best fit. RMSE is commonly used in climatology, forecasting, and regression analysis to validate experimental results (Lou et al,

2021). The equation 3.4 below, O_i is the ith observed value and M_i the ith modelled value for a total of n observations.

$$RMSE = \left(\frac{\sum_{i=1}^{n}(M_i - O_i)}{n}\right)^{\frac{1}{2}} \qquad \text{Equation 3.4}$$

3.7.3 Standard deviation

The standard deviation is a statistic that measures the dispersion of a dataset relative to its mean and is calculated as the square root of the variance (El Omada and Sergent, 2021). It is calculated as the square root of variance by determining the variation between each data point relative to the mean (Baker et al, 2021). The distance between point data and the mean, indicates deviation or variability within the data set; thus, the more outspread the data, the higher the standard deviation (El Omada and Sergent, 2021). The formula is expressed in Equation 3.5.

$$\sigma = \sqrt{\frac{\Sigma(O_i - \bar{O})^2}{n-1}} \qquad \text{Equation 3.5}$$

Where, O_i is the value of observed data, $\bar{O}$ is the mean value of the data set n is the number of data points in the data set.

3.7.4 Correlation coefficient (r)

Correlation coefficient (r) is a statistical measure that calculates the strength of the relationship between the linear association of two variables (Ali and Medhat, 2021). The values of correlation coefficient range between -1.0 and 1.0 (Fu et al, 2020). However, if a calculated value exceeds the thresholds of 1.0 and -1.0, it means that there was an error in the correlation measurement (Li et al, 2022). A positive correlation implies that as one variable increases, so does the other, whilst the converse is true for a negative correlation. A correlation of 0.0 suggests that no relationship exists between two variables. The equation 3.6 below, O_i represents the ith observed value and M_i represents the ith modelled value for a total of n observations. Furthermore σ_M is the standard deviation for modelled value, σ_O represent the standard deviation for observed value, $\bar{M}$ is the mean of the Modelled value and $\bar{O}$ is the mean of the observed values.

$$r = \frac{1}{(n-1)}\sum_{i=1}^{n}\left(\frac{M_i - \bar{M}}{\sigma_M}\right)\left(\frac{O_i - \bar{O}}{\sigma_O}\right) \qquad \text{Equation 3.6}$$

3.8 Climate change projections

Climate change projections in this study are presented as percentiles. Percentiles are used in statistics to translate and interpret data in which the Nth percentile of a set of data is the value below the Nth percent of the data (Taylor, 2020). Percentiles arrange a dataset into divisions of 100 equivalent segments, deciles of ten equivalent parts, and quartiles four equal parts (Kaur et al, 2018). Differences between percentiles and quartiles are minor and often disappear with many values in a dataset. The lower quartile (25th percentile) is the point at which 25% of values in a dataset lies below and 75% of values lie above. The second quartile (50th percentile) is the median (midpoint of the dataset). The upper quartile (75th percentile) is the point at which 75% of values in a dataset lies below and 25% of values lie above (Kaur et al, 2018). The 10th, 50th and 90th percentiles were used to analyse a number of high fire danger days in the future. However, the discussion in Chapter 5 focuses on the 50th percentile. Percentile formula is expressed in equation 3.7.

$$n = \left(\frac{P}{100}\right) \times N \qquad \text{Equation 3.7}$$

Where, n is ordinal rank of given value P is Percentile N is Number of values in a dataset.

This study considered three future periods i.e., 2021 – 2040 (near future), 2041 – 2060 (mid future), and 2080 – 2099 (far future). The projections are made against historical baseline period from 1961 to 1980 using the RCP8.5 “business as usual” emission scenario.

3.9 Data Display

3.9.1 R

R is an open-source software and programming language developed as an environment for statistical computing and graphics (Winter, 2019; Ihaka and Gentleman, 1996). It provides facilities for data manipulation, calculation and graphical displays which have effective data handling and storage facility from a large collection of packages (Venable and Smith, 2021). Calculations are processed on arrays and matrices in particular matrices to manipulate datasets of different dimensions (Gandrud, 2018). R uses a simple and effective programming language called ‘S’ which includes conditionals, loops, user defined recursive functions and input and output facilities as platform for interactive data analysis (Venable and Smith 2021).

3.8.2 Grid Analysis and Display System (GrADS)

GrADS is an interdependent computer software used to retrieve, manipulate, and visualize spatial data of different dimensions (Wang, 2019). It processes the data in 5-Dimensions (5-D) comprising the four conventional dimensions such as longitude, latitude, vertical level, and time whilst an optional 5th dimension for grids is implemented but designed to be used for ensembles (Wang, 2019). The data descriptor file is used to integrate datasets within the 5-D through the entering command line in FORTRAN expression (Kumar, 2020). GrADS supports various file formats, including binary, GRIB, NetCDF, HDF, and BUFR (Dmitruk, 2020; Wang, 2019). Graphics used to display data in GrADS include line and bar graphs, scatter plots, smoothed contours, shaded contours, streamlines, wind vectors, grid boxes, shaded grid boxes, and station model plots, which are saved as PostScript or image formats (Sato et al, 2018).

3.8.3 Climate Data Operator (CDO)

CDO software is an integration of numerous operators for processing and manipulating climate datasets in a user-friendly format (Schulzweida, 2019). The operators encompassing simple statistical and arithmetic functions, data selection and sub-sampling tools, and spatial interpolation (Koffe et al, 2019). It was developed with a mandate to have similar set of processing functions for GRIB and NetCDF datasets in one package (Schulzweida, 2019). Features that are crucial to CDO include available operators above 700, modular design and assimilated open source for extendable new operators (Koffe et al, 2019). It uses an uncomplicated UNIX “command-line interface” which processes dataset using a number of operators, saving output on designated pathways and fast processing of missing values within large datasets (Wachsmann, 2020; Schulzweida, 2019).

3.8.4 ArcGIS

ArcGIS is a complete software suite for desktop and cloud-based Geographic Information System (GIS) (Kholoshyn et al, 2019). Both desktop and cloud-based ArcGIS softwares provide powerful applications that are used to create maps, perform spatial analysis, manage geographical data and imagery (Price, 2019). It comprises optional extensions that feature tools in areas of 3D modelling and analysis, network analysis, spatial analysis, image analysis, geostatistical, workflow management, data quality control, comprehensive data interoperability, and industry-focused workflows (Law and Collins, 2019)

3.9 Summary

This chapter has detailed the datasets and data analysis techniques applied to obtain the results based on the objectives of this study. Meteorological observations from 1961 – 1980 were used as the baseline and six downscaled GCMs through RCM CCAM provided climate simulations for the near future (2021 – 2040), mid future (2041 – 2060) and far future (2070 – 2099). Precipitation, maximum and minimum temperature, wind speed, relative humidity and FFDI are used as key variables to investigate influence of climate change on fire regimes. Correlation co-efficiency, standard deviation and root mean square error are used for model validation. Several data display tool was used in the present study including the Grid Analysis Display System (GrADS), ArcGIS and R were used to visualize and interpretation the results using spatial maps and graphs.

Chapter 4: Historical baseline

4.1 Introduction

Climate models have become significant tools to simulate the past and future climate systems at different spatial and temporal resolutions (Beaumont et al, 2008; Hausfather et al, 2018). However, it is crucial to begin with model verification against observation to determine the skill/bias of the models before using them to project the future. Thus, the aim of this chapter is to perform model verification to evaluate models' performance in reflecting the present-day observed climate, hence gaining confidence in using the model to simulate the future climate. In the present study, six GCMs were downscaled with RCM CCAM to attain a high resolution of 8 km under the RCP8.5 emission scenario. The CRU data and ARC weather station data were used as the observation for model validation. The validation process focuses on models' capabilities to reproduce the spatial and temporal variation of climate variables such as rainfall, maximum temperature, minimum relative humidity, wind speed and McArthur high fire danger days. A Taylor diagram (Taylor, 2001) was used to investigate models' reliability in producing results that are consistent with observational data in the Limpopo grasslands.

4.2 Spatial verification of the models

4.2.1 Annual means over Limpopo

4.2.1.1 Rainfall

Mean annual rainfall over the Limpopo province varies significantly, with lower rainfall in the north (~22-23°S) near the boundary between with Botswana and Zimbabwe and Mozambique, whilst more rainfall is observed over interior and south region where the Limpopo grasslands are located (Mosase and Ahiablame, 2018). The panel plots of observation (CRU ts4.04) and six downscaled GCMs show similar spatial variations in mean rainfall distribution over the study area as shown in Figure 4.1. The observed CRU rainfall varies from less than 30 mm/month to well above 75 mm/month in some locations (Figure 4.1a). The region north-south along ~30°E experiences high rainfall (>90 mm/month), consistent with the presence of the northeastern escarpment which enhances rainfall through orographic lifting. Similarly, high rainfall along ~23°S is associated with the influence of the Soutpansberg mountain range. In fact, some of the highest rainfalls in South Africa occur along this range with some stations recording ~1800 mm/year. The general pattern is for lower rainfall (<45 mm/month) in the border areas with Botswana, Zimbabwe and Mozambique which is the lowveld.

Rainfall simulations of the historical baseline for six downscaled GCMs are shown in Figure 4.1 (b – g) in relation to the CRU observation. All models simulated significant high rainfall along the great escarpment over the study area. Similar patterns of mean annual rainfall over the study area was presented by Mpandeli et al, (2015). Lower mean annual rainfall variabilities (30 mm/month) were simulated widely extending in the north region of the study towards Botswana and Zimbabwe by CCAM_CCS85, CCAM_ACC85 and CCAM_CNR85 models. Historical simulations from models CCAM_GFD85 and CCAM_MPI85 showed close spatial variabilities with observation around the transboundary between Limpopo, Botswana and Zimbabwe. CCAM_NOR85 simulations generally overestimated mean annual rainfall over the study area than other models and the CRU observation during the period 1961 - 1980.

Model verification was employed to evaluate the performance of six downscaled GCMs against observations. A Taylor diagram shown in Figure 4.3 was used for model validation, hence standard deviation, correlation coefficient, and RMSE are integrated to rank the performance of the GCMs. Results from Taylor diagram have shown high performance by all models in terms of correlation with positive values above 0.9 calculated. The highest correlation of 0.99 relative to the observation was achieved by CCAM_ACC85, CCAM_CNR85 and CCAM_MPI85.

Standard deviations showed close variability to the observation from CCAM_GFD85 and CCAM_CCS85. Model CCAM_ACC85 have less variability than observation, while models CCAM_CNR85, CCAM_MPI85 and CCAM_NOR85 have more variabilities than observation. RMSE between observation and models' simulations were low. The overall performance of all models showed model CCAM_NOR85 to be the worst performing model because of high RMSE, whereas the CCAM_ACC85 and CCAM_CCS85 have shown the best performance in simulating rainfall over the Limpopo grasslands.

4.2.1.2 Maximum temperature

Observed and projected annual mean maximum temperatures during the period 1961 - 1980 are shown in Figure 4.2. The mean observed pattern (Figure 4.2a) shows generally high temperatures (>28°C) in the lowveld areas, corresponding to the low rainfall areas shown in Figure 4.1. The interior region of the study area showed mean maximum temperatures between 23°C and 27°C. Lower annual mean maximum temperatures in the interior region are influenced by high altitude on the African plateau, while high observed annual mean maximum temperatures along the north and east regions were influenced by low altitude. All six GCMs simulated mean annual maximum temperature of about 30°C in the Limpopo River valley between Limpopo province and Zimbabwe,

and in the east region towards Mozambique. The CCAM_NOR85 model (Figure 4.2e) projected lower maximum temperatures than all models over the study area.

Model validation has shown high performance from all models with regard to maximum temperatures (Figure 4.4). The CCAM_NOR85 showed high variability while CCAM_CCS85, CCAM_CNR85, CCAM_ACC85, CCAM_MPI85 and CCAM_GFD85 showed less variability from observation. Meanwhile, CCAM_NOR85 and CCAM_GFD85 simulated temperature variability close to observation. The models performed very well in terms of high correlation coefficient above 0.95, as shown in Figure 4.4. CCAM_MPI85 had the highest RMSE, resulting in it being the worst performing model because it was the furthest from the 'observed' value of mean annual maximum temperature.

4.2.1.3 Minimum relative humidity

Annual mean minimum relative humidity was calculated from three weather stations that are located in the Limpopo grasslands. The weather stations are located between 23.9°S – 25°S latitude and 27.5°E – 30.5°E Longitude. Models' annual means were calculated using Limpopo Province domain ranging from 22°S – 25.5°S and 26°E – 32°E. In terms of standard deviation, all six models overestimated variabilities from observation, as shown in Figure 4.5. Meanwhile, CCAM_ACC85 and CCAM_GFD85 exhibited a closer variability from the observation. Models CCAM_ACC85 and CCAM_GFD85 showed least RMSE while CCAM_CCS85, CCAM_MPI85, CCAM_CNR and CCAM_NOR85 showed high RMSE. High correlation coefficients around 0.8 were calculated with model CCAM_ACC85, CCAM_GFD85 and CCAM_MPI85. The least performing model in terms of correlation was CCAM_NOR85, which was measured below 0.7. Therefore, model CCAM_NOR85 was the least performing model because of high RMSE, lower correlation and high standard deviation variability compared with observed values.

4.2.1.4 Wind speed at 10m

Annual mean wind speeds on the Limpopo grasslands were calculated from the same three weather stations used for minimum relative humidity above. The models' annual means were calculated using the domain ranging from 22°S – 25.5°S and 26°E – 32°E, which is the geographical area of Limpopo. In terms of standard deviation, an ensemble of six models overestimated variabilities when compared with the observed wind speed shown in Figure 4.6. All models have shown poor performance in terms of standard deviation due to more variabilities than observation in simulating wind speed over the study area, which was also determined by the highest RMSE. Perhaps, the models failed to perform better due to low observed wind speeds

influenced by the location/siting of weather stations. The wind field itself is one of the most variable meteorological parameters in time and space. Positive correlations calculated between observed values and model simulations were around 0.7.

4.2.2 Seasonal means over Limpopo

4.2.2.1 Rainfall seasonal means

Limpopo province is largely a semi – arid region which forms part of Limpopo River Basin which is one of the largest river systems in southern Africa. It is prone to frequent drought events mostly associated with the El Niño Southern Oscillation (Landman et al, 2020; Jimoh et al, 2021; Nembilwi et al, 2021) and destructive flood events frequently due to tropical storms from the southwest Indian Ocean (Rapolaki et al, 2019). Synoptic scale weather systems that drive the occurrence of rainfall include Temperature Tropical Troughs (TTTs), tropical low-pressure systems, mesoscale convective systems and cut-off lows (Rapolaki et al, 2019). On occasion, tropical storms which are remnants of landfalling tropical cyclones from the southwest Indian Ocean bring floods to the study region. High rainfall regions over the study area are largely influenced by high altitude (mountains and the northeastern escarpment) due to orographic effects (Hart et al, 2013).

December-January-February (DJF) seasonal mean rainfall over Limpopo province is shown in Figure 4.7. DJF rainfall seasonal observation from CRU ts4 (Figure 4.7a) have shown a minimum of ~60 mm to a maximum of ~160 mm. All six models' simulations recorded maximum rainfall of about 160 mm/month in some regions along the great escarpment and grasslands in the study area, as shown in Figure 4.7 (b – g). Models CCAM_CCS85, CCAM_ GFD85, CCAM_ACC85 and CCAM_CNR85 simulated lowest summer rainfall (60 mm) in the north and north-western region extending towards Zimbabwe and Botswana. CCAM_NOR85 and CCAM_MPI85 overestimated summer rainfall over the study area. Summer rainfall in the Limpopo exhibits a very high coefficient of variability largely due to the influence of the El Nino Southern Oscillation phenomenon (Chikoore, 2016). El Nino events are mostly linked to drought and high temperatures over the Limpopo whilst La Nina phases bring higher rainfall to the region and more likelihood for landfalls of tropical cyclones from the Mozambique Channel.

March – April – May (MAM) rainfall is distinguished by decreasing rainfall as the tropical rain belts shift equator ward as shown in Figure 4.8. The CRU ts4 observation shows MAM rainfall variabilities of about 40 mm/month throughout the study area, except the interior region with 60 mm/month observed rainfall. Rainfall below 20 mm/month in the north region has been simulated

by models CCAM_CCS85, CCAM_GFD85, CCAM_ACC85, CCAM_CNR85 and CCAM_MPI85, as shown in Figure 4.8. High MAM rainfall variabilities during 1961 – 1980 were simulated with model CCAM_NOR85.

During the austral winter months from June – July – August (JJA), both observations and models showed rainfall variabilities of about 20 mm/month over the study area, as shown in Figure 4.9. The spring season from September – October – November (SON) rainfall variabilities showed an increase in the interior region of the study area shown in Figure 4.10. The mean rainfall for SON ranges between 80 mm/month and 100 mm/month in the interior region with low variabilities of 40 mm/month in the west and 60 mm/month in the east region. It must be stated that the austral spring marks the beginning/onset of the rainfall season which can be October or November in this region. This season also corresponds to the peak of the fire season on the Limpopo grasslands such that any changes to the climate in this season may affect fire regimes significantly in future.

4.2.2.2 Maximum temperature seasonal means

The Limpopo province is located in the subtropics of the Southern Hemisphere under the subsiding limb of the Hadley Cell such that high temperatures prevail and the region is highly vulnerable to heatwaves. As shown in the rainfall analyses, the northern part of Limpopo is rather dry and particularly vulnerable to hot temperatures and heat waves. DJF is the hottest, with an average maximum temperature ranging above 22°C and below 34°C recorded by CRU ts4 and all six downscaled GCMs in the north region towards Zimbabwe and east region towards Mozambique, as shown in Figure 4.11(a – g). Model CCAM_ACC85 projected DJF maximum temperature (>34°C) expanding along the northern boundary between Zimbabwe and Limpopo Province. Spatial distribution of DJF means maximum temperature from CCAM_ACC85, CCAM_CCSS85 and CCAM_CNR85 showed variabilities of 30°C – 32°C expanding over the west region of study area along the boundary between Botswana and Limpopo in relation to CRU ts4 observation. Simulation from CCAM_NOR85 underestimated DJF mean maximum temperatures during period 1961 – 1980.

MAM mean maximum temperatures cooled down to a peak mean maximum temperature below 30°C, as shown by CRU ts4 observation in Figure 4.12a. Spatial distribution of MAM maximum temperature showed the north and east region remained hot while the south and interior regions where grasslands are located were becoming cooler. Models CCAM_CCS85, CCAM_GFG85, CCAM_ACC85, CCAM_CNR85 and CCAM_MPI85 showed gradient spatial variabilities below 32°C mean maximum temperature in the north and east regions of the study area. CCAM_NOR85

underestimated MAM maximum temperature over the west region of Limpopo province in relation to observation and other models' simulation.

During JJA, the observed mean maximum temperatures across grasslands were simulated below 26°C in the north region, 24°C in the interior and 22°C over the southern region, as shown in Figure 4.13. Observation showed significant spatial distribution of 26°C – 28°C JJA mean maximum temperature over the north (~23°S), and east region (~31°E) of Limpopo province. Model CCAM_NOR85 simulated JJA mean maximum temperature below 22° across grasslands in the study area, resulting in overestimated cooling of maximum temperature. JJA mean maximum temperatures 28°C – 30°C were overestimated by CCAM_CCS85, CCAM_ACC85, and CCAM_CNR85 in the north and east region of the study area. Spatial distribution of JJA mean maximum temperature with close variabilities to observation were projected by models CCAM_GFD85 and CCAM_MPI85, as shown Figure 4.13.

Observed SON mean maximum temperature (Figure 4.14a) showed a gradient from 24°C in the interior to 30°C – 32°C in the west, north and east regions of the study area. Limpopo grasslands are well established in area which maximum temperature is relatively low. SON spatial distribution of mean maximum temperature in the northern region was projected to reach a maximum of 32°C – 34°C along the boundary with Zimbabwe by model CCAM_CNR85. In the meantime, model CCAM_NOR85 projected underestimated SON mean maximum temperatures with spatial variabilities of 28°C in the west region of study area towards Botswana. Thus, CCAM_CCS85, CCAM_GFD85, CCAM_ACC85 and CCAM_MPI85 projection showed close variability with observation, as shown in Figure 4.14.

4.3 Mean annual cycle

4.3.1 Rainfall

Limpopo province is a summer rainfall region with most rainfall accumulated the during austral summer from October to March (Rapolaki et al, 2020). High rainfall accumulated during the summer is largely influenced by synoptic scale cloud bands, also known as TTTs (Harrison 1984; Reason et al, 2006; Rapolaki et al, 2020). Low accumulated rainfall thresholds in the study area are influenced by prevailed semi-arid climate associated with El Niño phenomenon, causing frequent drought events over the region (Reason et al, 2006). Annual mean rainfall of CRU ts4 observation and ensemble of six downscaled GCMs from CMIP6 is shown in Figure 4.15 with a threshold range of 0 to 120 mm/month.

Observations and model simulations showed closed variability in mean annual rainfall during period 1961 – 1980. Model CCAM_NOR85 showed high variability from the January to June when related to CRU ts4 rainfall observations. High rainfall activities with 90 mm/month were recorded during austral summer, including November, December, January and February. Mean annual rainfall rapidly declines from March to the lowest mean annual threshold in June, July and August (winter). Both observation and models showed a gradual increase in rainfall from September to December, as shown in Figure 4.15.

4.3.2 Maximum Temperature

The models simulated significantly close variabilities to the observed mean annual maximum temperature (Figure 4.16). Warmer conditions prevailed during austral summer were recorded from both CRU ts4 and six downscaled GCMs from CMIP6. Mean maximum temperature of above 30°C was recorded in January from both CRU ts4 and models. CCAM_NOR85 underestimated mean annual maximum temperature from January to September. Model CCAM_MPI85 showed an increase in maximum temperature from January to March.

Mean annual cycle showed a decline in maximum temperature from the mid-summer to the low mean maximum temperature of 22.5°C recorded in June and July, followed by a gradual increase from July to December. High temperatures are significantly influenced by the Tropic of Capricorn at 23.5° south latitude, which the sun is directly overhead at noon during summer. It can be can be concluded that extreme maximum temperatures associated with heatwaves over the Limpopo province are influenced by climate change (Maposa et al, 2021).

4.3.3 Minimum relative humidity

Minimum relative humidity observations used in the present study were obtained from three local weather stations located between 23.9°S – 25°S latitude and 27.5°E – 30.5°E Longitude in Limpopo grasslands. Mean annual minimum relative humidity was calculated using three weather stations to represent the study area. Models' annual means were calculated using Limpopo province domain ranging from 22°S – 25.5°S and 26°E – 32°E. Due to the small domain of the study area represented by three used weather stations, the models projected high variability of minimum relative humidity against weather station observation. Models such as CCAM_ACC85, CCAM_GFD85 and CCAM_MPI85 were found with a strong correlation coefficient (r) of 0.8.

Mean annual minimum relative humidity cycle is shown in Figure 4.17. Both observation and models' projection showed a high percentage of minimum RH during austral summer (November, December, January, February and March). Observed minimum relative humidity declined until

July, where it remained constant until September, then increases towards early austral summer. Models' simulation showed similar declining pattern until reaching minimum limits in September succeeded by a rapid rise October towards December.

4.3.4 Windspeed at 10m

The observed annual mean windspeed was calculated from three weather stations located between 23.9°S – 25°S latitude and 27.5°E – 30.5°E longitude in Limpopo grasslands. The models' annual means were calculated using the domain encompassing 22°S – 25.5°S and 26°E – 32°E. Therefore, weather stations only covered southern region of Limpopo province, resulting in high variability between observed and models projected mean annual values. At the same time, the wind itself is highly variable in space and time. A correlation coefficient of 0.7 was measured during model verification in Figure 4.6. Annual mean wind speed cycles of both observations and model projections are plotted in Figure 4.18.

Models varied closely from January to December, hence showing similar trends and patterns with weather stations observations. Meanwhile, weather station observations showed a slight decrease in wind speed (<1 m/s) from January to March but remained consistently low until gradual increase from June to October. The models projected mean annual wind speed of 3 m/s and 4 m/s during summer and spring, while autumn and winter varied relatively between 3 m/s and 2 m/s. In Figure 4.18, models showed mean annual wind speed varied below 3 m/s from March to the lowest values of 2 m/s in June followed by a gradual rise until October then declined during period 1961 – 1980.

4.4 Summary

In this chapter, spatial verification of models, seasonal means, and mean annual cycles were employed to analyse variations during the historical baseline from (1961–1980) in relation to observation and six downscaled GCMs from CMIP6. Taylor diagram comprising standard deviation, correlation coefficient and RMSE was used to validate models projection over the study area. Observation dataset were obtained from CRU ts4 gridded weather station data with spatial resolution of 0.5°× 0.5° and ARC-SA three weather stations within grassland over the study area. Models simulation was derived from six GCMs from CMIP6 dynamically downsacled with RCM CCAM comprising high resolution of 8 km. Spatial verification of models using CRU ts4 showed best performance from all models, but CCAM_NOR85 was the least performing model.

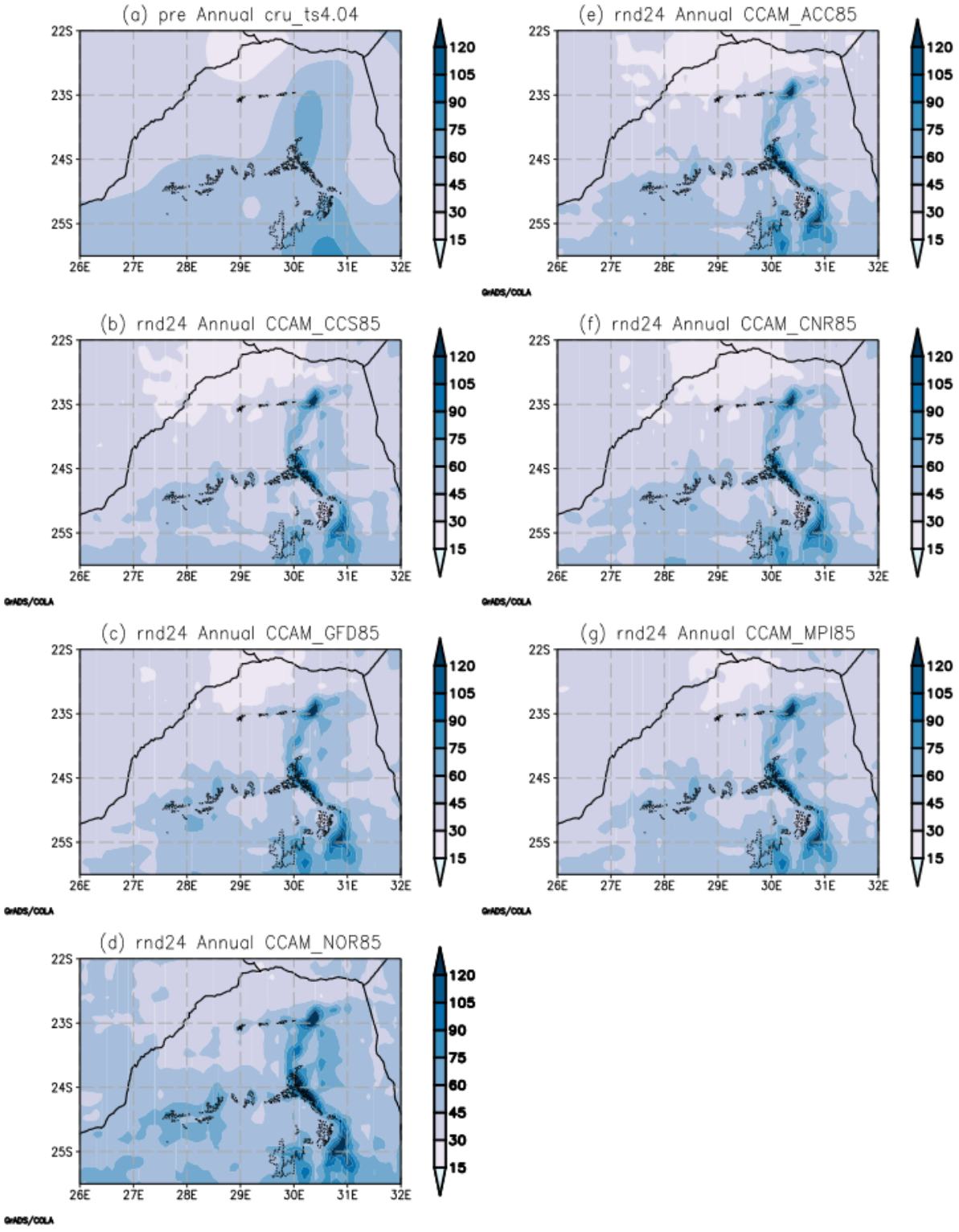

Figure 4.1 Limpopo annual mean rainfall (mm/month) from observation (a) and models (b – g) for the historical baseline 1961 – 1980.

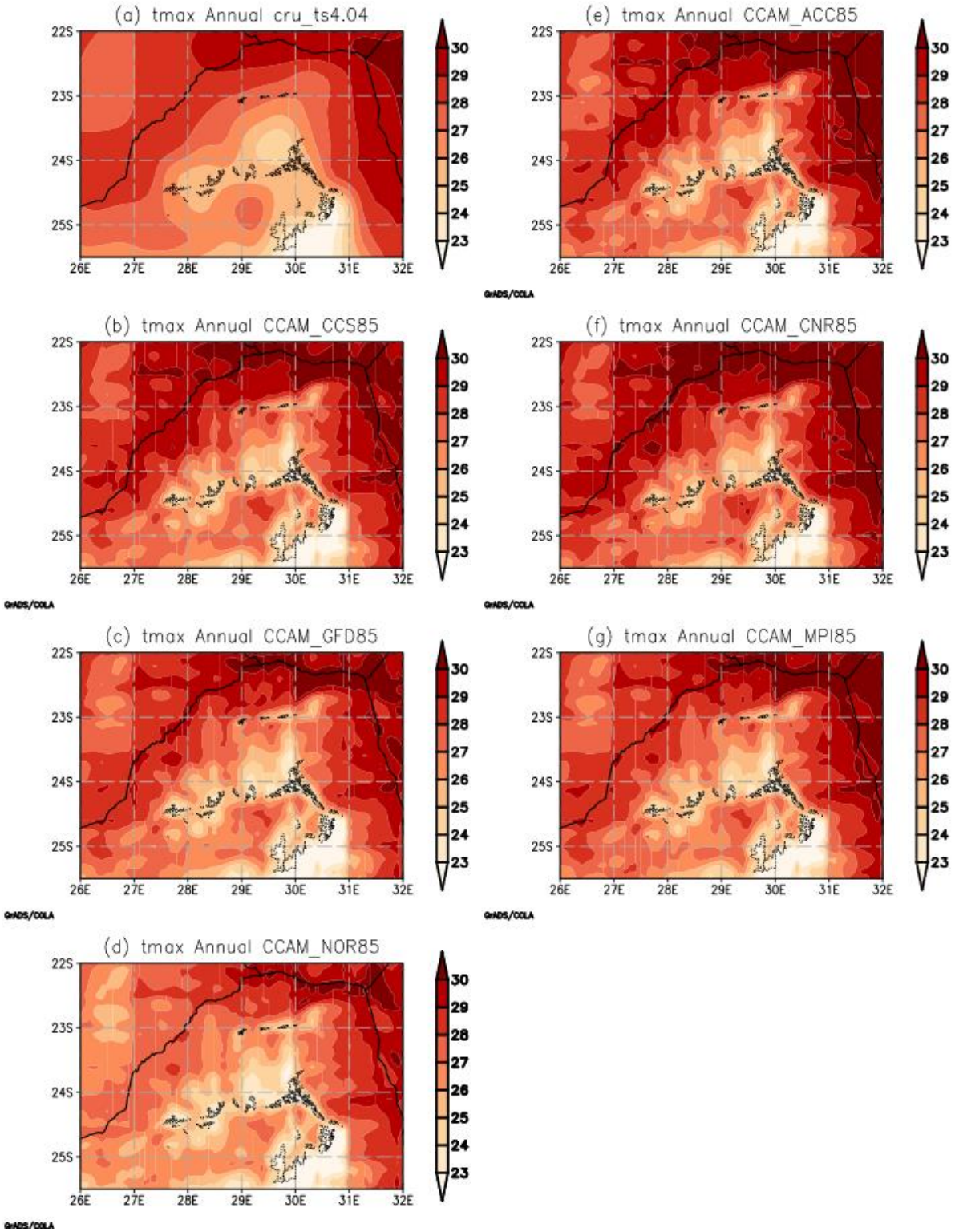

Figure 4.2 Limpopo annual mean maximum temperature from observation (a) and models (b – g) for the historical baseline 1961 – 1980.

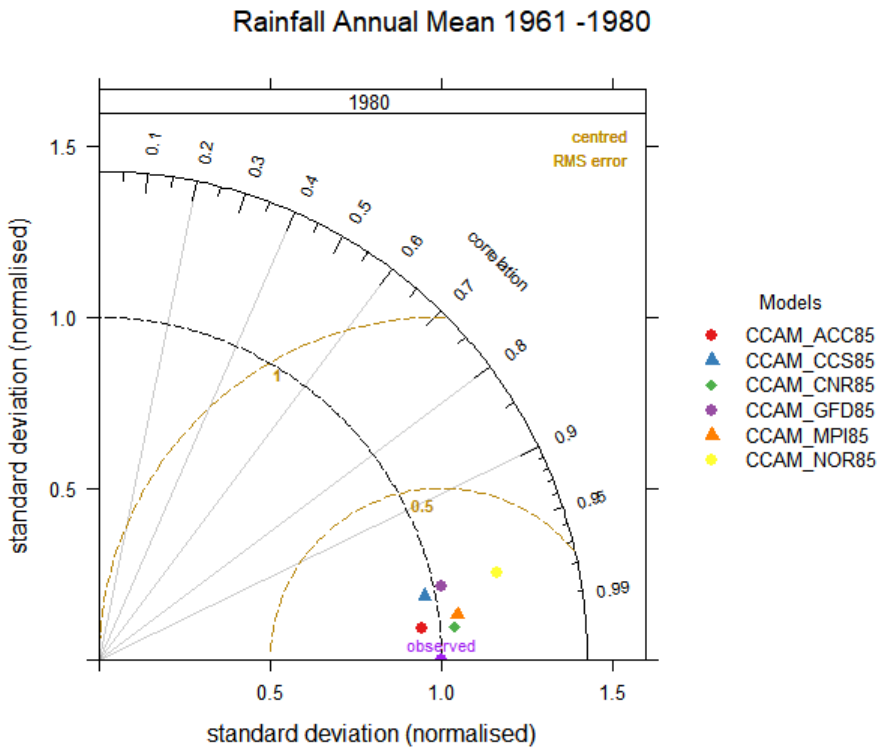

Figure 4.3 Taylor diagram showing rainfall model validation.

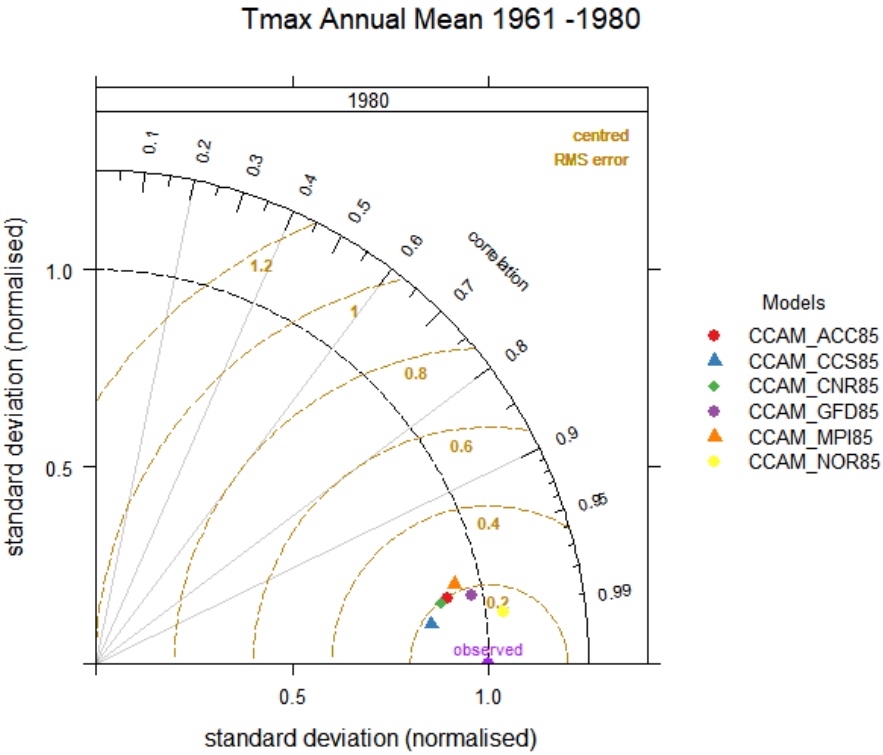

Figure 4.4 Taylor diagram showing maximum temperature model validation.

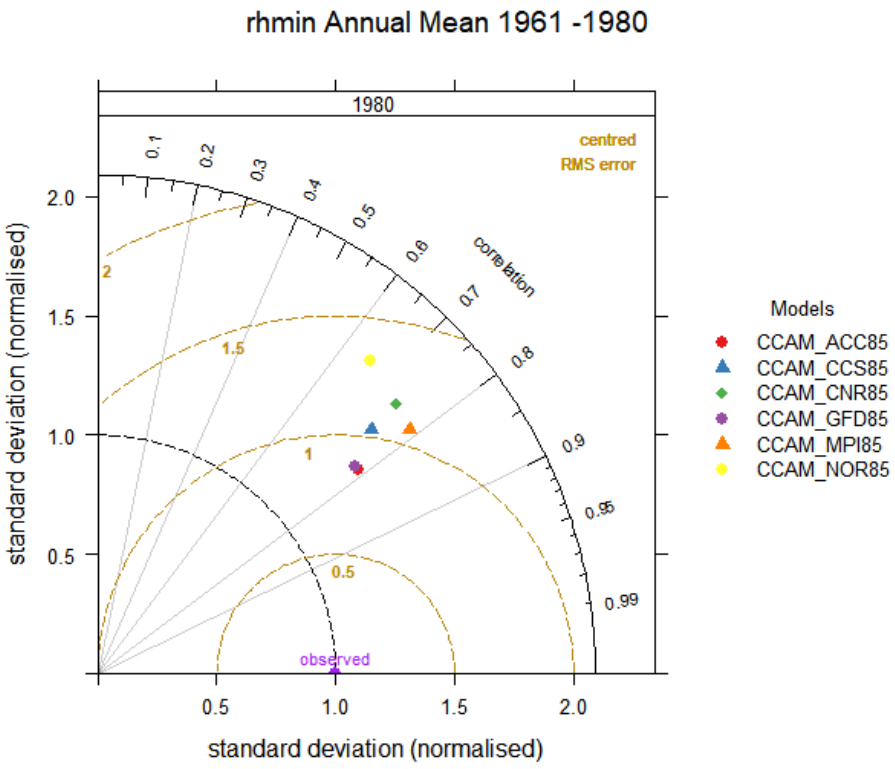

Figure 4.5 Taylor diagram showing minimum relative humidity model validation

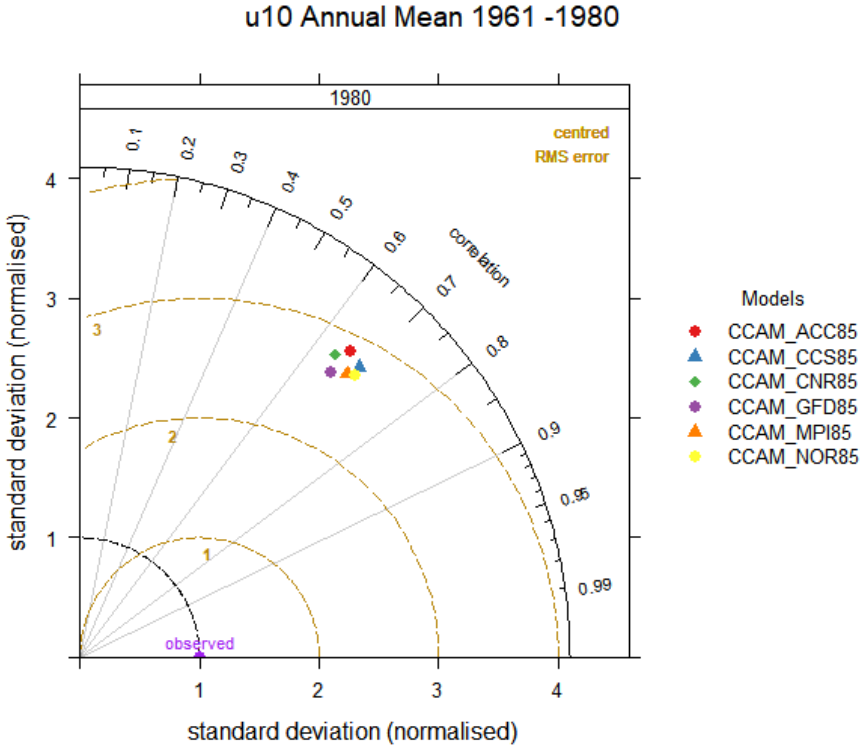

Figure 4.6 Taylor diagram showing windspeed model validation

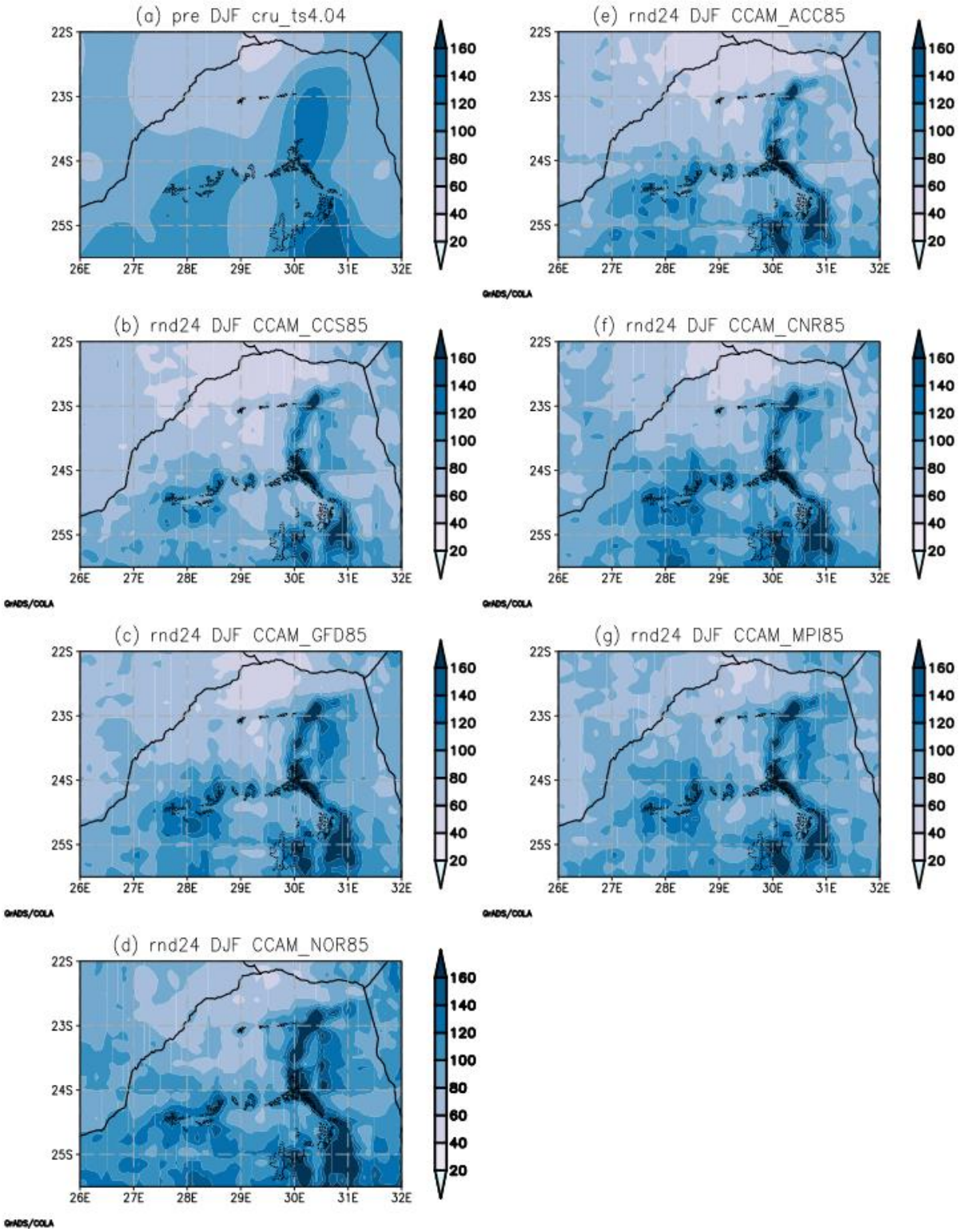

Figure 4.7 DJF seasonal mean rainfall for the period 1961 – 1980.

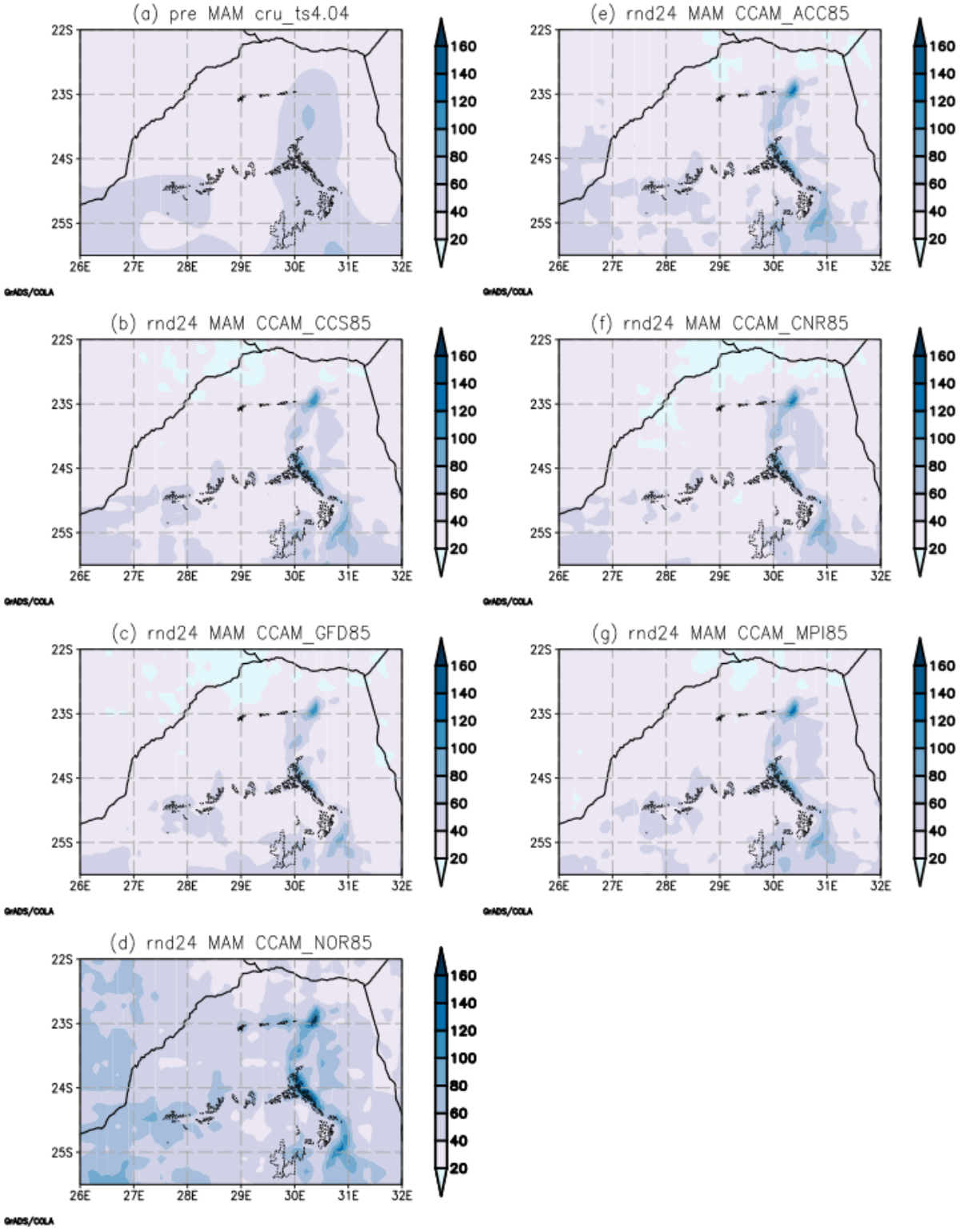

Figure 4.8 MAM seasonal mean rainfall for the period 1961 – 1980.

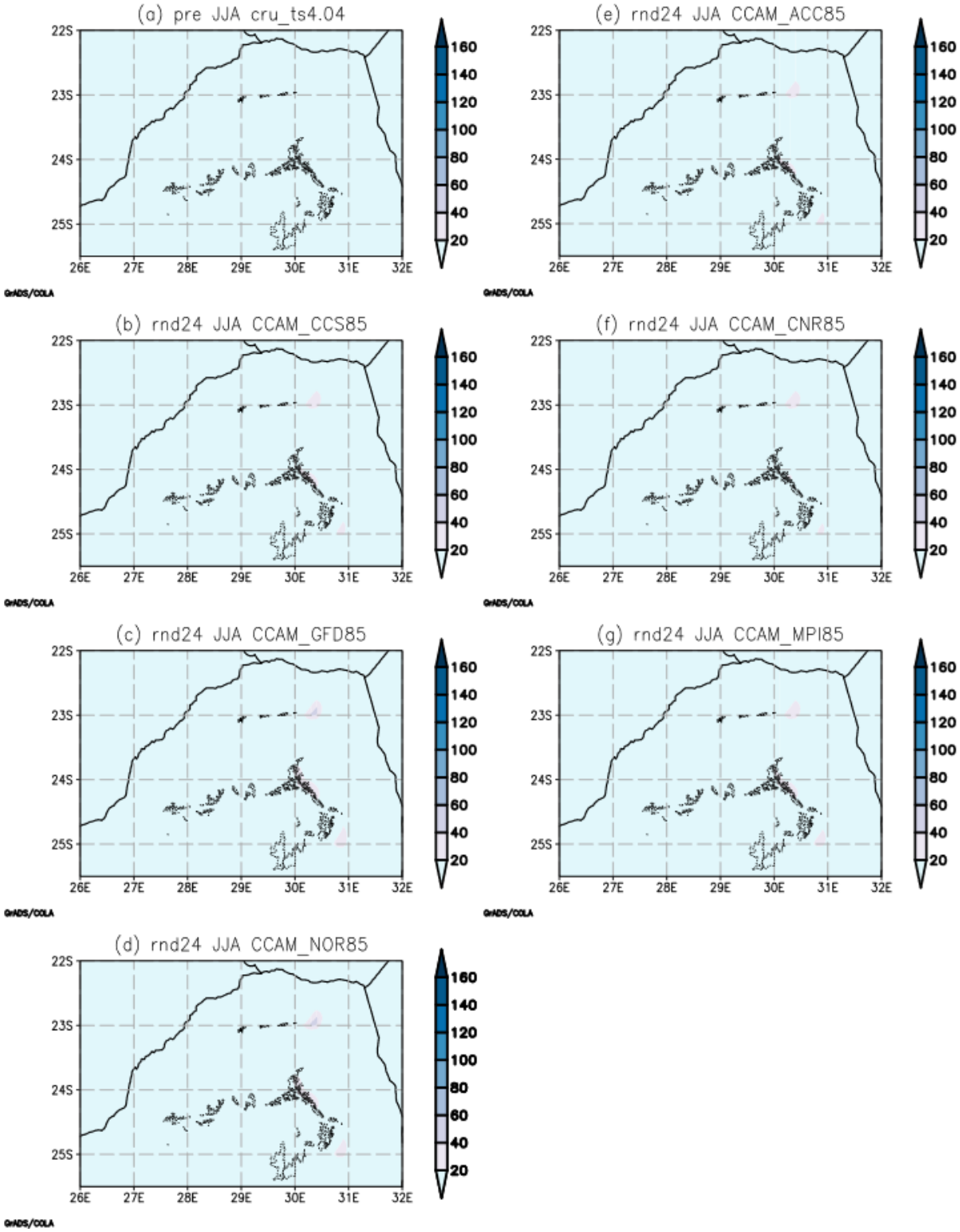

Figure 4.9 JJA seasonal mean rainfall for the period 1961 – 1980.

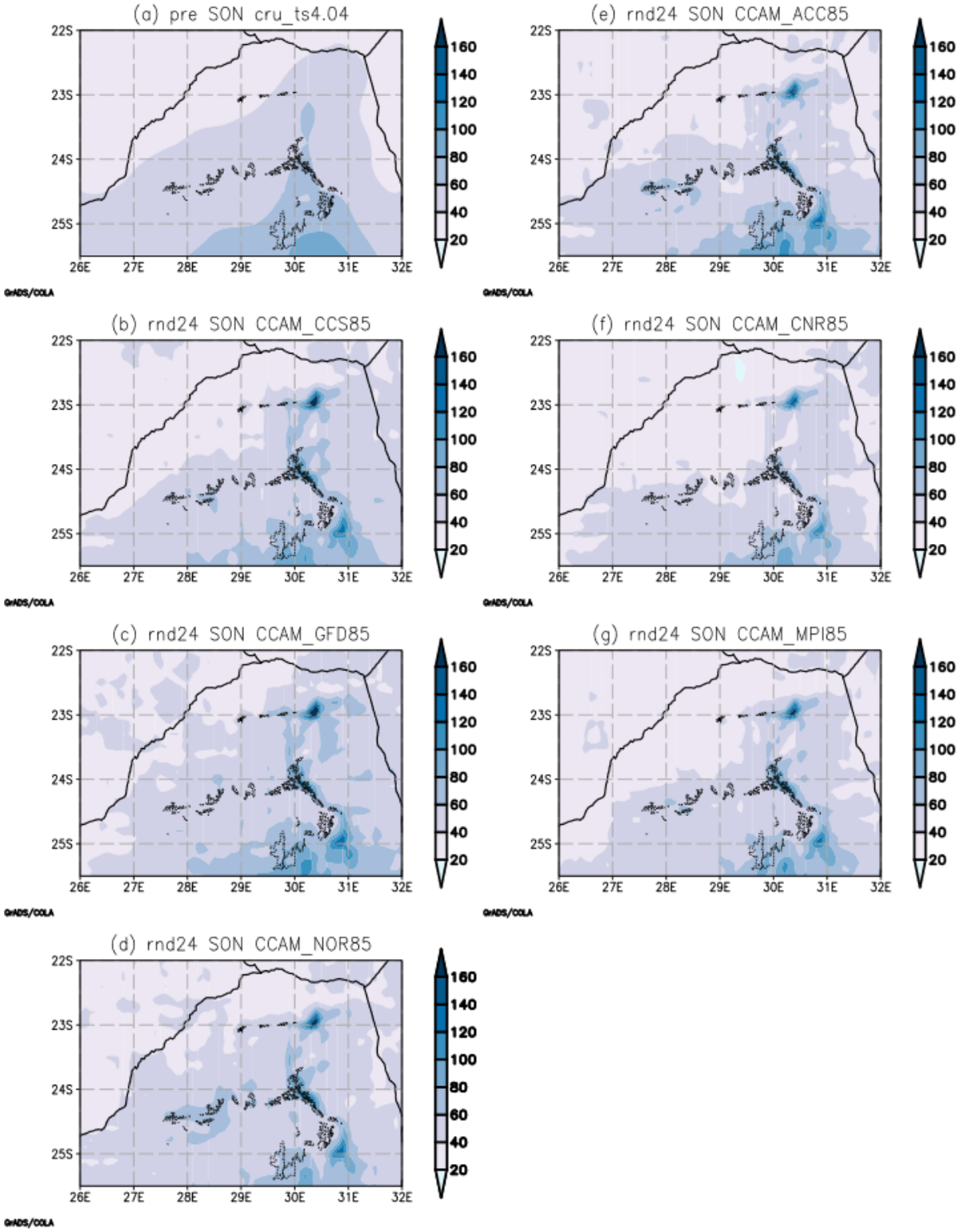

Figure 4.10 SON seasonal mean rainfall for the period 1961 – 1980.

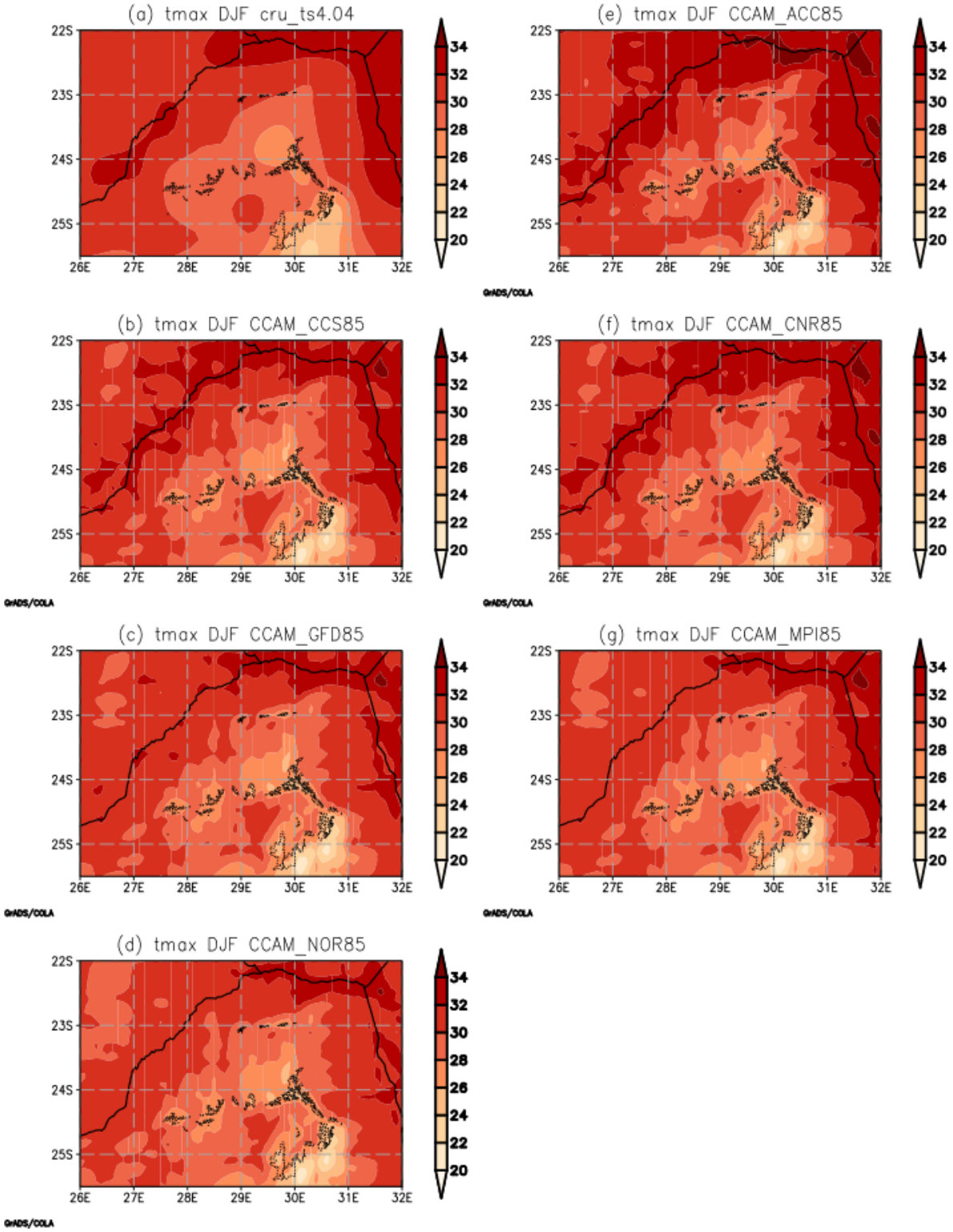

Figure 4.11 DJF seasonal mean maximum temperature for the period 1961 – 1980.

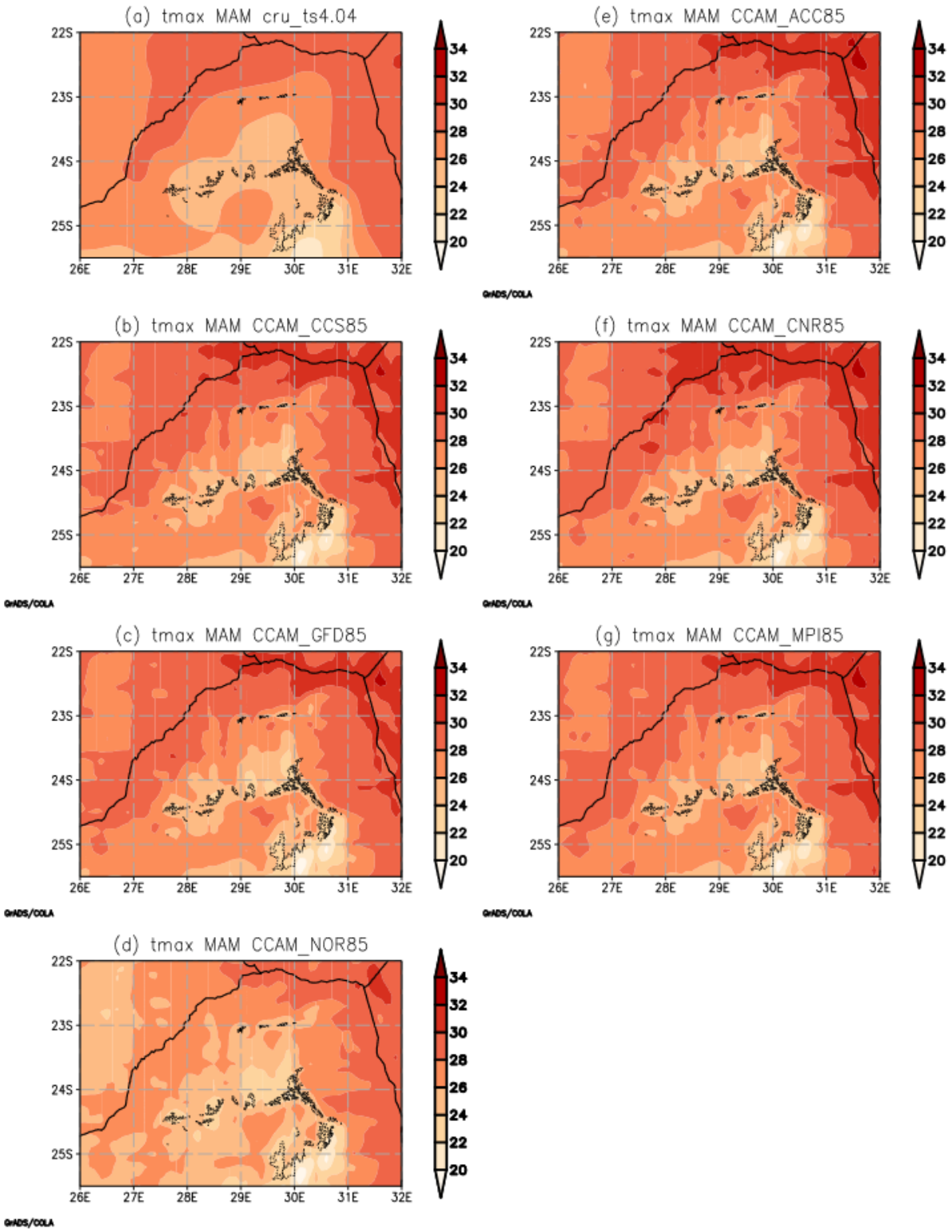

Figure 4.12 MAM seasonal mean maximum temperature for the period 1961 – 1980.

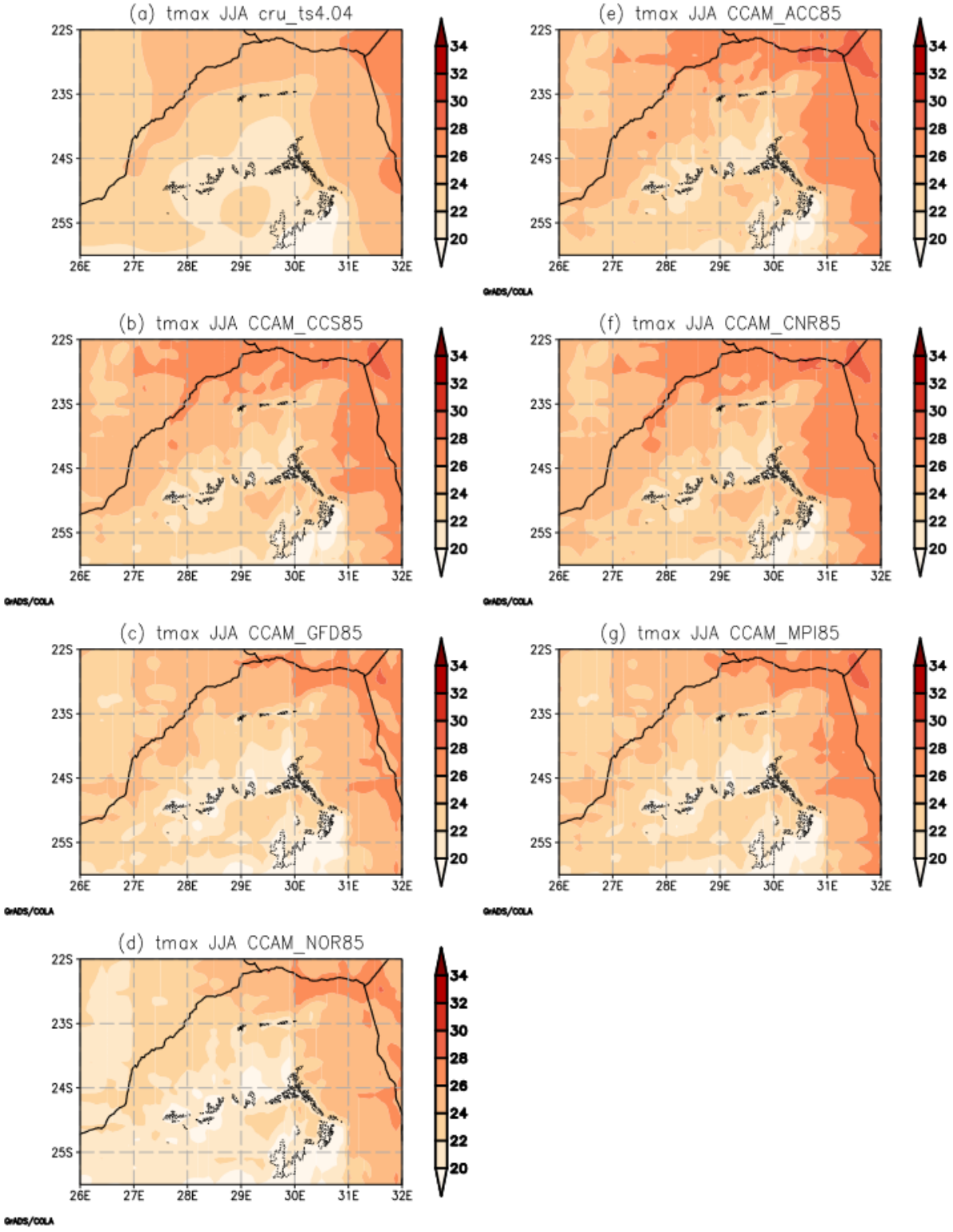

Figure 4.13 JJA seasonal mean maximum temperature for the period 1961 – 1980.

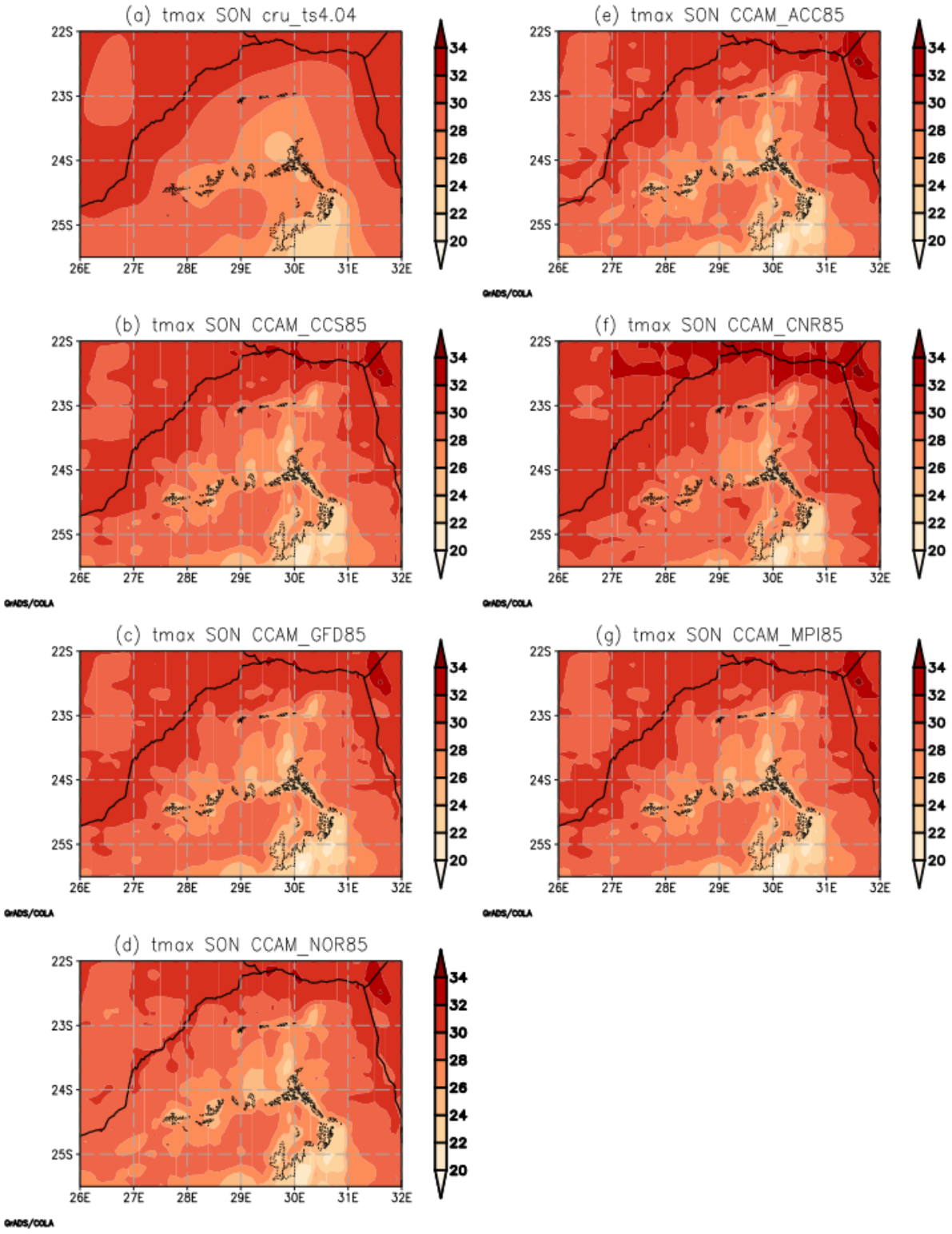

Figure 4.14 SON seasonal mean maximum temperature for the period 1961 – 1980.

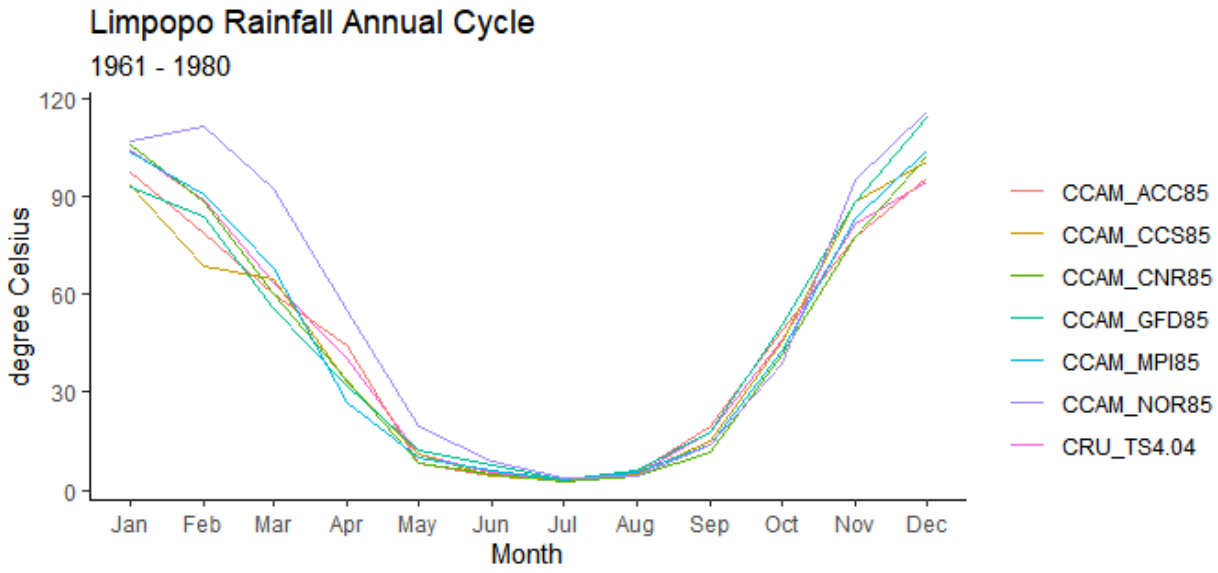

Figure 4.15 Limpopo rainfall mean annual cycle (mm/month).

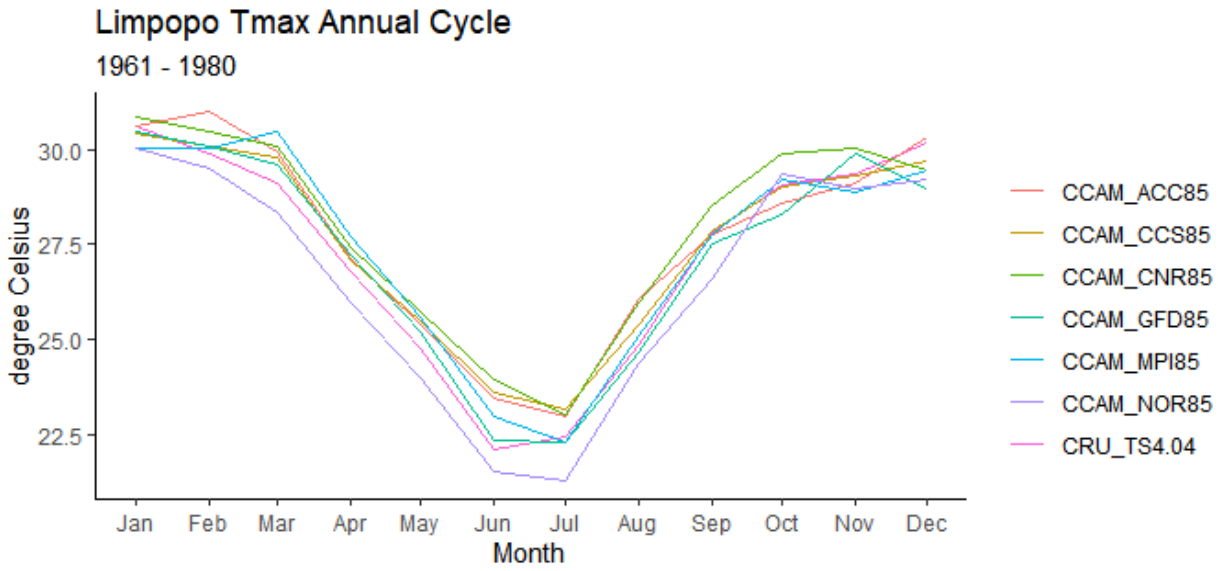

Figure 4.16 Limpopo maximum temperture mean annual cycle.

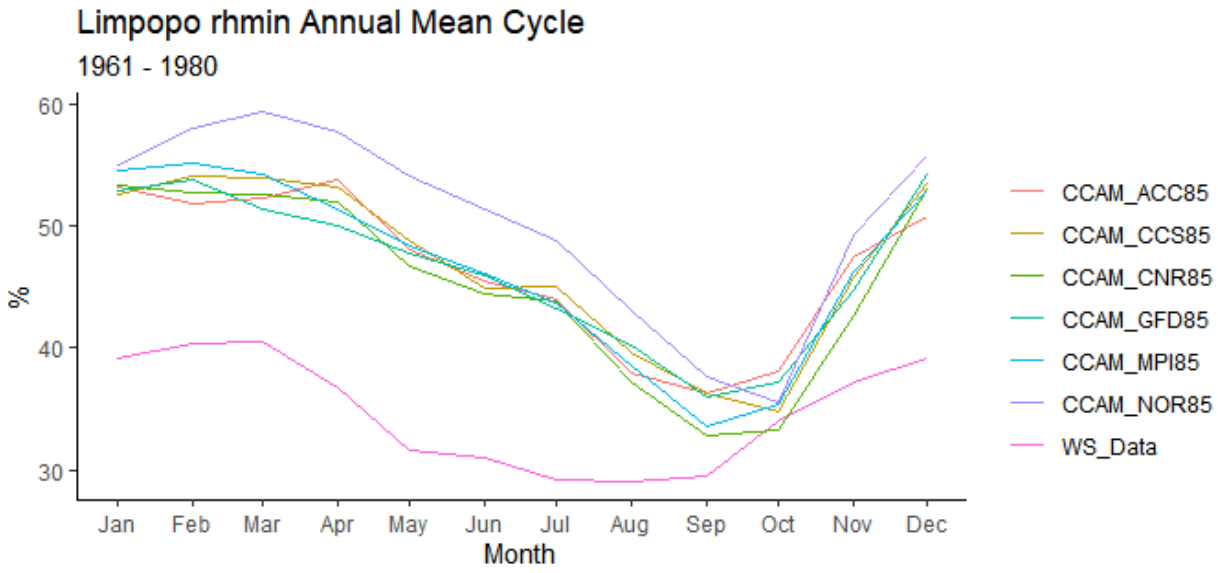

Figure 4.17 Limpopo minimum relative humidity mean annual cycle.

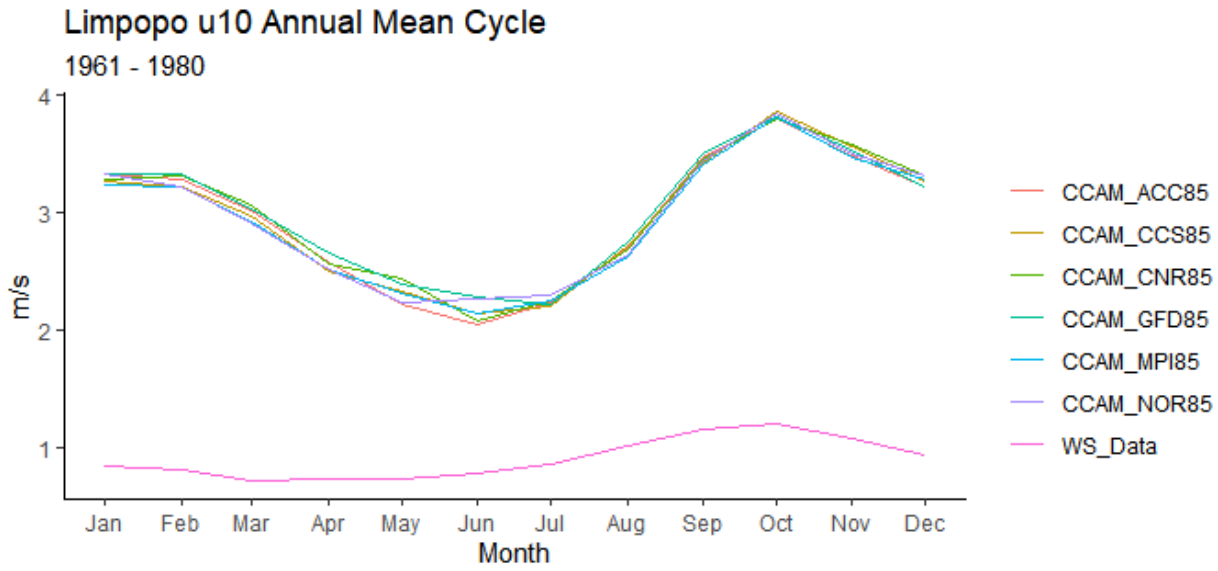

Figure 4.18 Limpopo windspeed at 10 m mean annual cycle.

Chapter 5: Future projections of climate change and fire risk over the Limpopo grasslands

5.1 Introduction

This chapter aims to detail future projections of climate change and fire risk over the Limpopo grasslands for three future periods including the near future (2021 – 2040), mid future (2041 – 2060) and far future (2080 – 2099). The projections are derived from an ensemble of six GCMs from the CMIP6, which were dynamically downscaled through RCM CCAM (McGregor 2005) to get relatively high spatial resolution of 8 km. The study focused on the RCP8.5 emission scenario, also known as low mitigation or "business as usual" scenario. Whilst several percentiles were calculated, only the median quartile (50th percentile) was selected for presentation in this chapter. Spatial analysis was applied to investigate the future of five key variables including rainfall, maximum temperature, minimum relative humidity and wind speed at 10 m. Changes in the mean annual cycle were used to investigate fire risk over the study area using McArthur FFDI high fire danger days comparing changes between three future periods.

5.2 Future climate projections

5.2.1 Rainfall

Future rainfall projections for three periods, i.e., 2021 – 2040, 2041 – 2060 and 2080 – 2099, were analysed using the 50th percentile to distinguish spatial variabilities of future rainfall in the study area. The key message is that rainfall is projected decreasing over most of the study area. During period 2021 – 2040, all models projected more rainfall variabilities varying along the Great Escarpment and grasslands in the interior regions between longitudinal line 30°E and 31°E as shown in Figure 5.1. The influence of orographic lifting on rainfall will remain despite changes induced by global warming and climate change.

The ensemble of six downscaled GCMs showed a mean annual rainfall below 30 mm/month spatially distributed over much of the study region apart from the escarpment and the mountain ranges as shown in Figure 5.1(a – f). Models CCAM_CNR (Figure 5.1b) and CCAM_GFD (Figure 5.1e) projected mean annual rainfall of 35 mm/month rainfall over the grasslands in the west region of study area extending to the south-western region with increasing rainfall to 40 mm/month. Mean annual rainfall of less than 30 mm/month is projected in the west region, expanding to Botswana by models CCAM_ACC and CCAM_MPI as shown in Figure 5.1a and Figure 5.1b. The east region toward Mozambique showed fewer variabilities with rainfall below

30 mm/month from an ensemble of six downscale GCMs, as shown in Figure 5.1. The CCAM_GFD model projected slightly more rainfall in the southeast than the other 5 models (Figure 5.1e).

In the mid future (2041 – 2060), the models projected high rainfall of above 55 mm/month along the Great Escarpment in the interior and south region of the study area as shown in Figure 5.2. Model CCAM_CCS (Figure 5.2d) projected extremely low mean annual rainfall of less than 15 mm/month over the north and north-western regions of Limpopo province. CCAM_GFD (Figure 5.2e) projected more rainfall variabilities over the east region into Mozambique. CCAM_NOR projected more rainfall variabilities in the study, with 40 mm/month expanding from south-west region into grassland as shown in Figure 5.2f.

The far future projections (2080 – 2099) showed extreme low rainfall of 10 mm/month over north and west region from Botswana and Zimbabwe as shown in Figure 5.3. More rainfall variabilities were projected along Great Escarpment and increase spatial extent over the south region. Model CCAM_MPI (Figure 5.3c) showed small spatial extent of projected rainfall in the south region of the study area. CCAM_CNR and CCAM_NOR projected rainfall varying below 30 mm/month over the west region. Overall, all models project significant drying over the Limpopo grasslands into all three futures under investigation.

5.2.2 Maximum Temperature

Maximum temperature projections for the near future, mid future and far future have shown a gradual increase in the study area, consistent with the global warming trend. Near future projections showed maximum temperature ranging between 25°C and 29°C varying in the interior region and grasslands over the study area. Models projected fewer variabilities of highest maximum temperature (34°C) expanding from north-east region of study area as shown in Figure 5.4. CCAM_ACC projected spatial extent of 33°C along the boundary between Limpopo and Zimbabwe. CCAM_NOR (Figure 5.4f) underestimated maximum temperature, resulting in projections of low maximum temperature (28°E – 31°E and 23°S – 25.5°S) in the study area during 2021 – 2040.

In the mid future (2041 – 2060), CCAM_CCS projected increasing spatial extent of maximum temperature (34°C) along the boundary line between Limpopo and neighbouring countries (Figure 5.5). The models projected increasing maximum temperatures throughout the domain of study area. Patches of grasslands in the west region are projected under significant vulnerabilities due to increasing maximum temperatures. During the 2080 – 2099 (far future) period, models

projected extreme hot climate over the study area. Maximum temperatures ranging between 25°C and 31°C are projected expanding in the interior region and grassland along the Great Escarpment. Models CCAM_ACC, CCAM_MPI and CCAM GFD projected extreme hot climate increasing in the interior region of the study area, as shown in Figure 5.6(a, c, d).

5.2.3 Minimum relative humidity

The models' projections of minimum RH into the future showed more spatial variability from west to east region of the study area, similar to the rainfall variabilities. In the near future (2021 – 2040), all models showed spatial gradients in minimum relative humidity gradually increasing from west (Botswana) to the east region (Mozambique) as shown in Figure 5.7. It is also important to highlight that the dominant moisture source region for the province is the southwest Indian Ocean in the east. The models projected minimum RH of 45% - 60% varying from west to east in the southern regions (~25°S – 25.5°S) of the study area. More spatial variabilities were projected in the interior with a high minimum RH (65%) along the Great Escarpment and decreasing in the west region. The east region of grasslands showed less variation, but high minimum RH ranging from 45% to 55% as shown in Figure 5.7.

During the mid-future period from 2041 – 2060, model CCAM_CCS (Figure 5.8d) projected more variabilities of low minimum RH from west into the interior of study area. CCAM_ACC, CCAM_CNR and CCAM_MPI have shown a less change in comparison with near future projections. Model CCAM_GFD (Figure 5.8d) have shown decreasing minimum RH over grasslands expanding from the interior to west of study area compared to near future variabilities. The east region remained ranging between 45% and 55% minimum RH as shown in Figure 5.8. In the far future (Figure 5.9), all models projected more variabilities of low minimum RH (35% and below) expanding from west region to the interior. The east region (~31°E) was projected consistently ranging from 45% to 60% minimum RH in the near and mid future. The far future is projected decreasing to minimum RH range between 40% and 55% as shown in Figure 5.9.

5.2.4 Windspeed at 10 m

Spatial variabilities of projected wind speed at 10 m showed no significant change from all three future periods, as shown in Figure 5.10, Figure 5.11 and Figure 5.12. All models projected wind speeds of between 3 m/s and 5.5 m/s from the interior to the north and west region of the study area. The high wind speed may be related to the nocturnal low-level jet stream, locally known as Limpopo Jet, responsible for transporting water vapour over Limpopo River valley (Riffe et al, 2010; Munday et al, 2021). South region of the study area extending from 24°S latitude poleward was projected with uniform windspeed variabilities by all models through all three future periods.

The wind field itself is one of the most complex variables, considering wind gusts and local winds due to topography or thermally induced circulations.

5.3 High fire danger days in the future climate

5.3.1 McArthur high fire danger days

Projections of the McArthur FFDI high fire danger days were used to investigate fire behaviour in the near future, mid future and far future. Ten days were used as a scale to distinguish high fire days' spatial variabilities from an ensemble of six downscaled CMIP6 GCMs. High fire danger days spatial variabilities would vary under highs and lows projected by rainfall, maximum temperature, minimum RH, and wind speed through each model and period.

Projected high fire danger days for the near future are shown in Figure 5.13(a – f). All model projected high fire danger days above 10 days over the north and west region. The east region projected with 7 to 8 days of high fire danger hence, the interior and south region were entirely ranging between 1 – 4 days, as shown in Figure 5.13. Meanwhile, model CCAM_CCS (Figure 5.13 d) projected low vulnerabilities over the east region towards Mozambique. The models also projected 5 – 9 days expanding south-westerly from 24°S – 25°S and 29°E – 30°E during the near future period.

In the mid future, model CCAM_GFD (Figure 5.14e) projected least vulnerability than others model in the east region whilst, CCAM_CCS (Figure 5.14d) projected high variabilities ranging from 7 to 10 high fire danger days. The number of days expanding south-westerly from 24°S – 25°S and 29°E – 30°E increased in all models. Far future projections (Figure 5.15) have shown a further increase in high fire danger days in the study area. All models showed 10 days of high danger days throughout the study except along the Great Escarpment, where the number of days remained uniform.

5.3.2 Projected future mean annual cycles

In the present study, three locations including Mopani (30.01 E; 23.91 S), Sekhukhune (29.73 E; 25.15 S), and Waterberg (27.77 E; 24.45 S) were selected for analysis. Mopani was excluded in this section because of outcomes with minimum threshold that were uninterpretable.

5.3.2.1 Sekhukhune

Mean annual high fire danger days in Sekhukhune for three future periods were analysed using an ensemble of six downscaled CMIP6 GCMs. Projected near future mean annual high fire danger days showed no variation in the number of high fire danger days from January to June,

as shown in Figure 5.16. However, the models showed variations in high fire danger days from July increasing to a close range between 10 – 15 days from September and October, then descends through November back to zero in December. CCAM_ACC85 and CCAM_CCS85 projected 15 days and above in September, while CCAM_CNR85 projected over 15 days of high fire danger in October. The lowest high fire danger days were projected by model CCAM_GFD85 (Figure 5.16).

During the 2041 – 2060 period (Figure 5.17), the model projected an increase in the number of high fire danger days to maximum high between 15 and 20 days. Other models showed fewer variabilities from January to June, with an early increase in number of high fire danger days from May. CCAM_CCS85 projected highest number (>20 days) in September, hence in October, CCAM_MPI85 projected highest number (>20 days). CCAM_GFD85 constantly projected lowest days (15 days) during period 2021 – 2040 as shown in Figure 5.17.

In the far future (Figure 5.18), the models projected high fire danger days above 20 per annum. Mean annual high fire danger days varied from between 0 – 10 days until July, followed by a rapid rise to above 20 days in September and October. High fire danger days are projected increasing in Sekhukhune from near to far future.

5.3.2.2 Waterberg

Waterberg is in the west region of study area, where future projection from models showed extreme arid climate conditions. In the near future, high fire danger days projected varied below 5 days from January to July, as shown in Figure 5.19. CCAM_ACC85 and CCAM_CCS85 projected 20 days in September, hence CCAM_CCS85 and CCAM_MPI85 projected more than 20 days of high fire danger in October. CCAM_GFD85 projected lower high fire danger days in September and October.

During period 2041 – 2060, model projections showed an increasing high fire danger day in Waterberg. All models projected over 20 days in September and October. CCAM_CCS85 projected highest number of high fire danger days, as shown in Figure 5.20. In the far future, the models projected increasing number of days from January to June. CCAM_GFD85 projected more days of high fire danger days than all models. Increasing high fire danger days early from March showed extremely hot climate expected from Waterberg. Models projected mean annual high fire danger of 30 days in September and October, as shown in Figure 5.21.

5.4 Discussion

In the present study, the 50th percentile climate variabilities were projected and analysed to distinguish changes between the near future, mid future and far future. Projected variables which are most relevant to wild fires include rainfall, maximum temperature, minimum relative humidity, wind speed at 10 m and McArthur FFDI high fire danger days. Projections under low mitigation showed extreme dry and hot conditions over the study area from an ensemble of six CMIP6 GCMs forced with high resolution (8 km) regional climate model CCAM. Several studies have projected hot and dry condition over the study area under 1.5°C, 2°C, 3°C, and 4°C global warming levels into the future (i.e., Engelbrecht et al, 2015; Mbokodo et al, 2020; Engelbrecht and Monteiro, 2021).

Several other studies have projected the Limpopo province to become drier under the low mitigation emission scenario (e.g., Engelbrecht et al, 2011; Archer et al, 2018; Engelbrecht and Monteiro, 2021). Tropical cyclone tracks are also projected continuously varying northwards to northern Mozambique, hence becoming fewer over Limpopo province (Malherbe et al., 2013). CORDEX regional climate models projected decrease in rainfall by 0.2 and 0.3 mm /day under 1.5° and 2° global warming levels (Maure et al, 2018). Some studies have projected decreasing rainfall spatial extent varies with increasing intensity of drought under increasing global warming levels over southern Africa (James and Washington 2013; Maúre et al, 2018). Meteorological drought is projected increasing consistently in southern Africa under both 1.5°C and 2°C global warming levels (Hoegh-Guldberg et al, 2018). Besides projected decreasing rainfall variabilities, daily rainfall intensities are expected in some regions (Hoegh-Guldberg et al, 2018).

Projected increasing maximum temperatures are associated with occurrence of heatwaves over the study area (Engelbrecht et al, 2015; Mbokodo et al, 2020) and expansion of arid climate zone (Engelbrecht and Engelbrecht, 2016). Projected maximum temperature will increase frequency of heatwaves over the study area due to mid-level high pressure systems that prevail over this region, influenced by expansion of the Hadley cell over southern Africa (Engelbrecht et al, 2011). Rising temperature may support growth of tress and expansion of Limpopo savanna into patches grasslands (Engelbrecht and Engelbrecht, 2016).

The study projected decreasing rainfall and rising temperatures inducing drastic high fire danger days over the study area in the future. A key finding of this study is the projected increase in fire risk over the Limpopo grasslands via a steady rise in future high fire danger days. The study by Engelbrecht et al, (2015) also made a similar projection, suggesting that high fire danger days

may lead to occurrence of catastrophic wildfire events. Since rising temperature favour growth of woody vegetation, frequent occurrence of wildfire may reserve grassland from spatial expansion of savanna over the study area. Mean annual cycles of high fire danger days in the future showed a peak in September, which is similar to peaks in the number of fires observed during fire season in Limpopo by Strydom and Savage (2016). The assumed strong relationship between fire and climate requires climate models to assess human impacts in the system (Archibald et al, 2010).

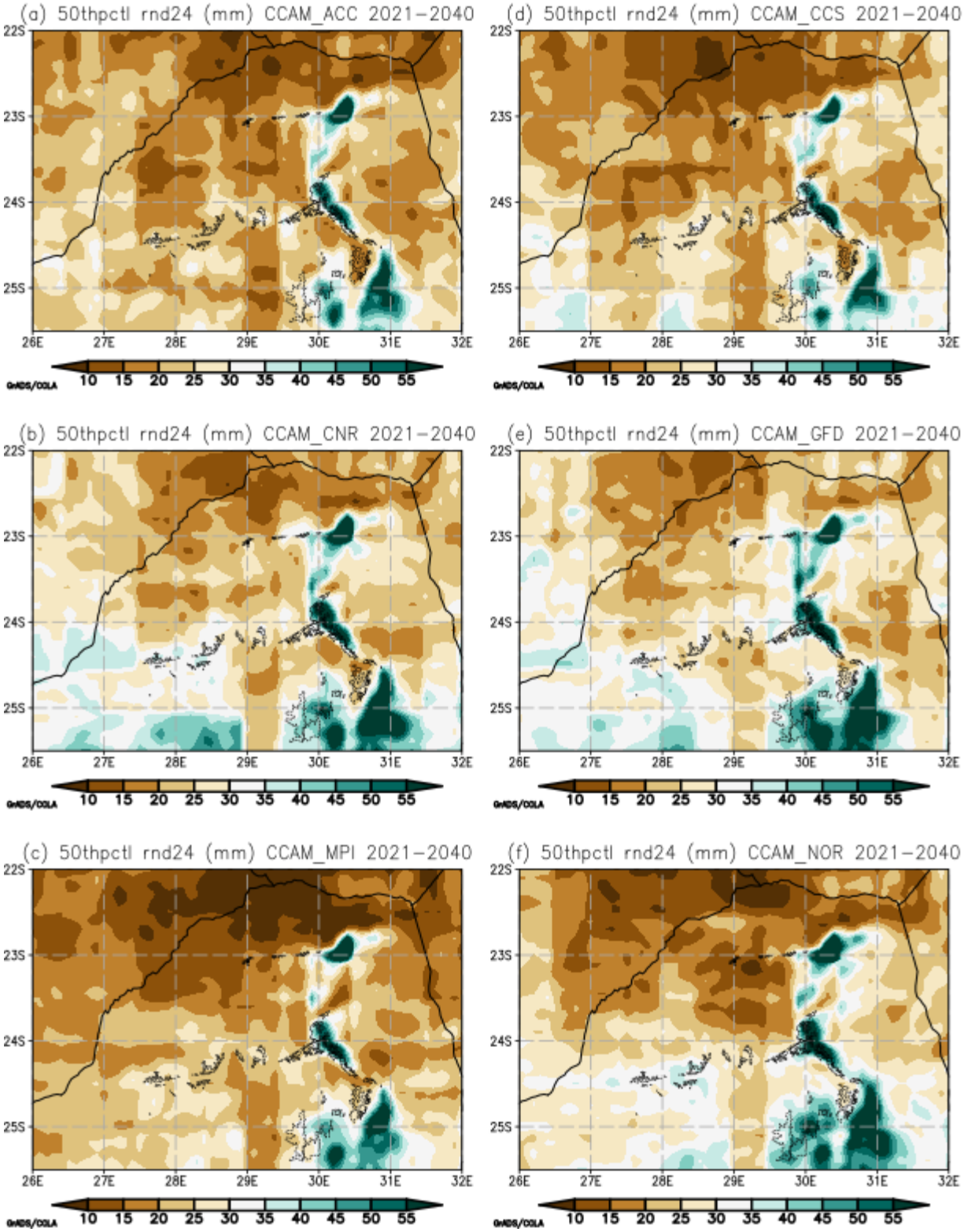

Figure 5.1 Near future rainfall projection from an ensemble of six downscaled CMIP6 GCMs

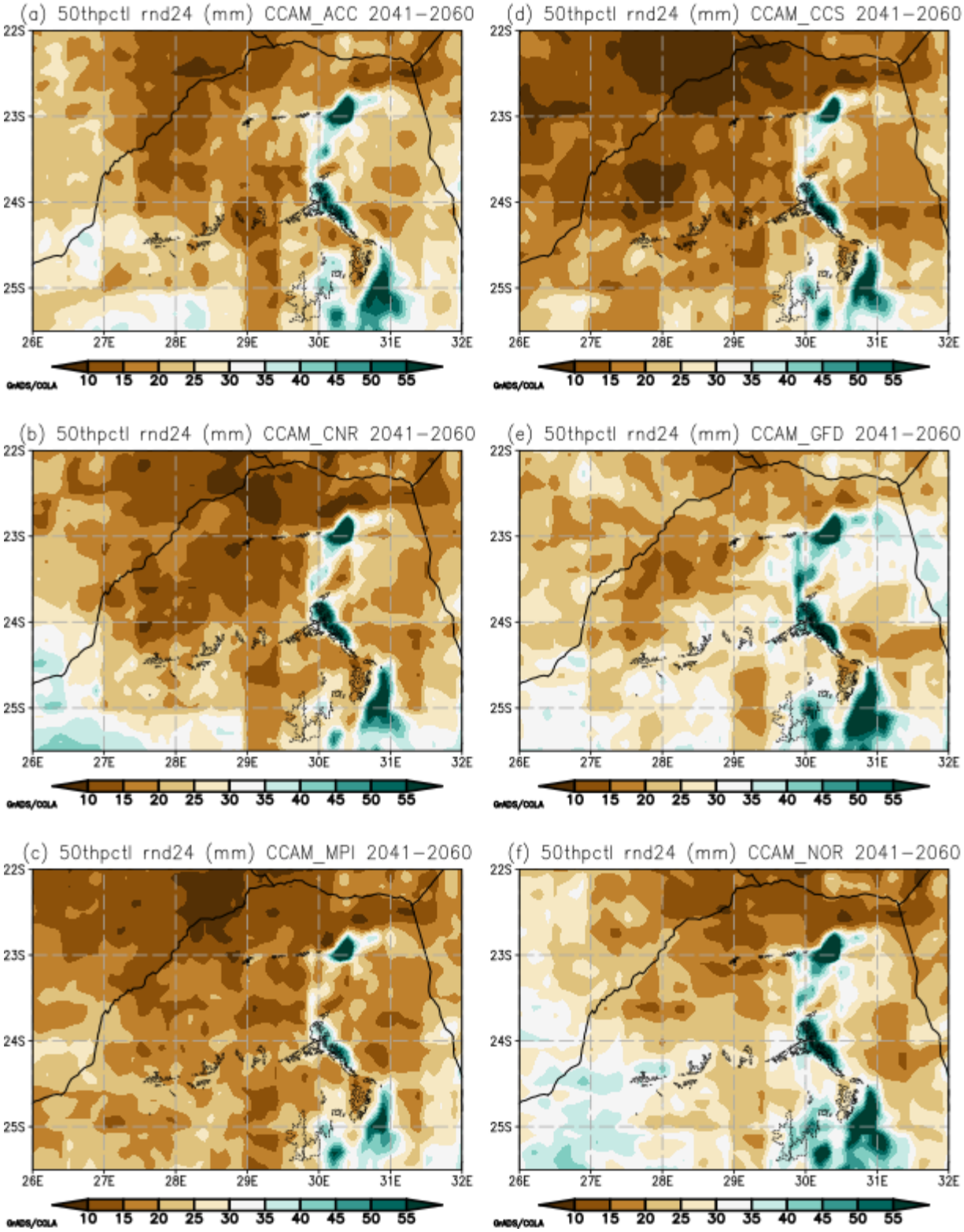

Figure 5.2 Mid future rainfall projection from an ensemble of six downscaled CMIP6 GCMs

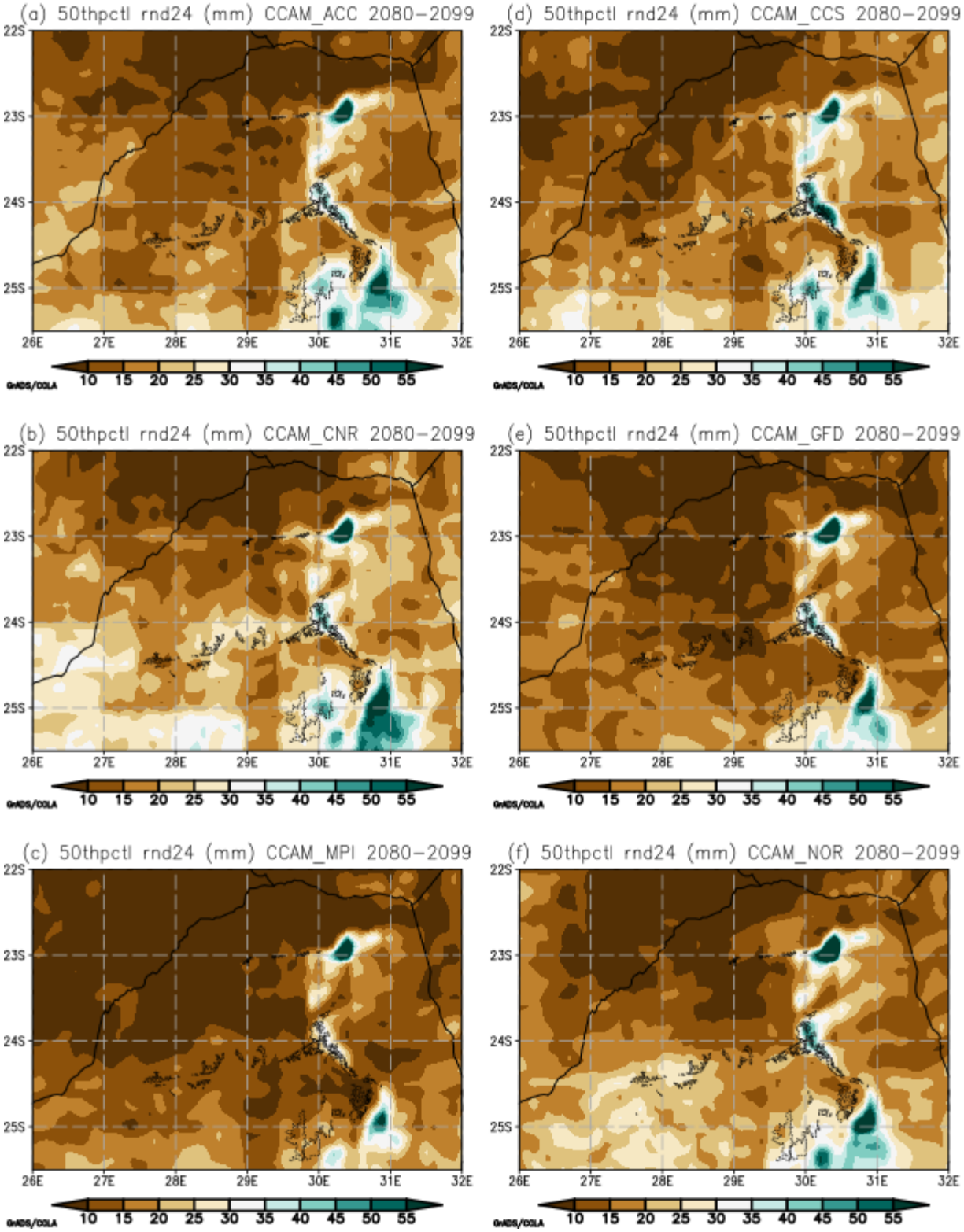

Figure 5.3 Far – future rainfall projection from an ensemble of six downscaled CMIP6 GCMs

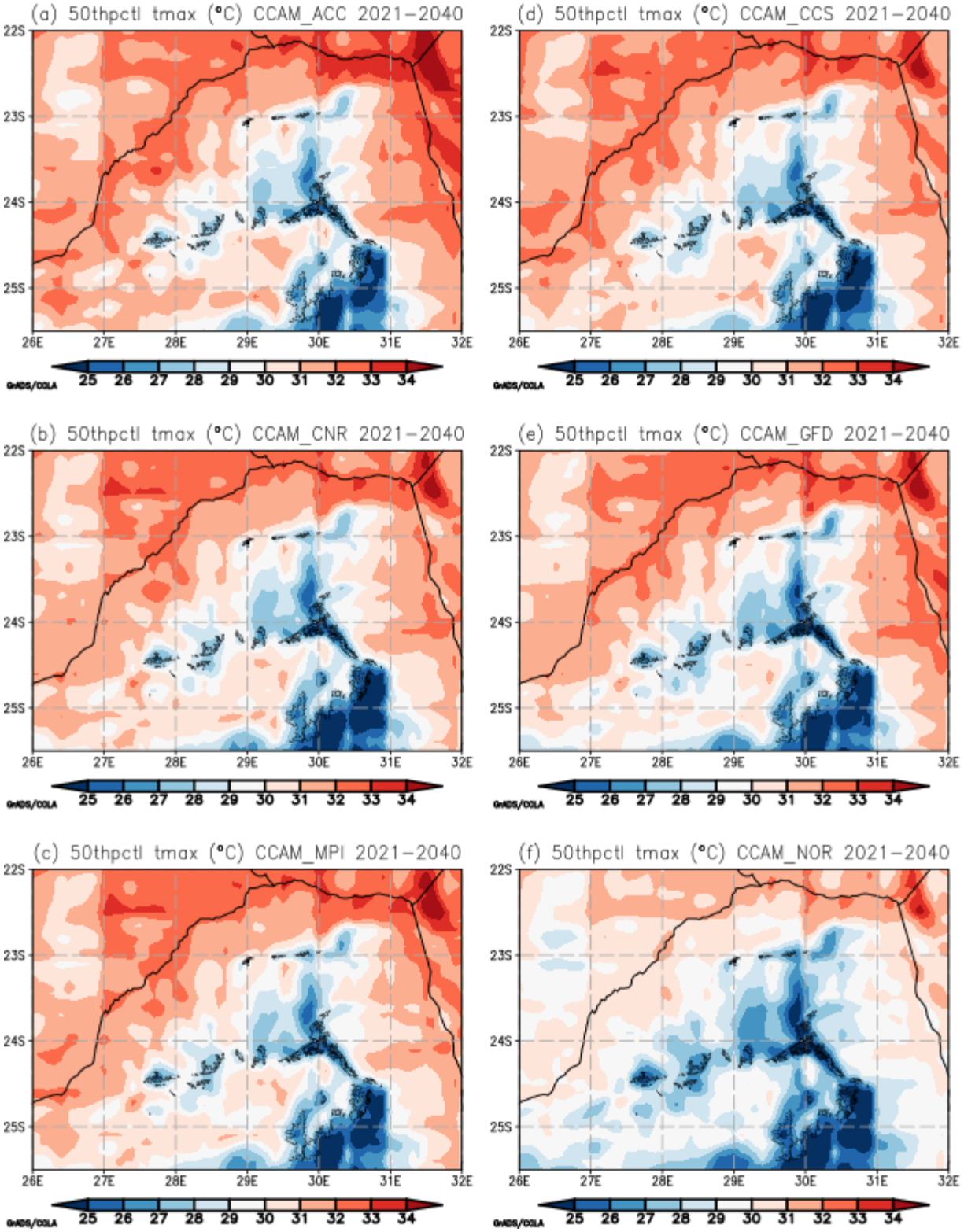

Figure 5.4 Near – future maximum temperature projection from an ensemble of six downscaled CMIP6 GCMs

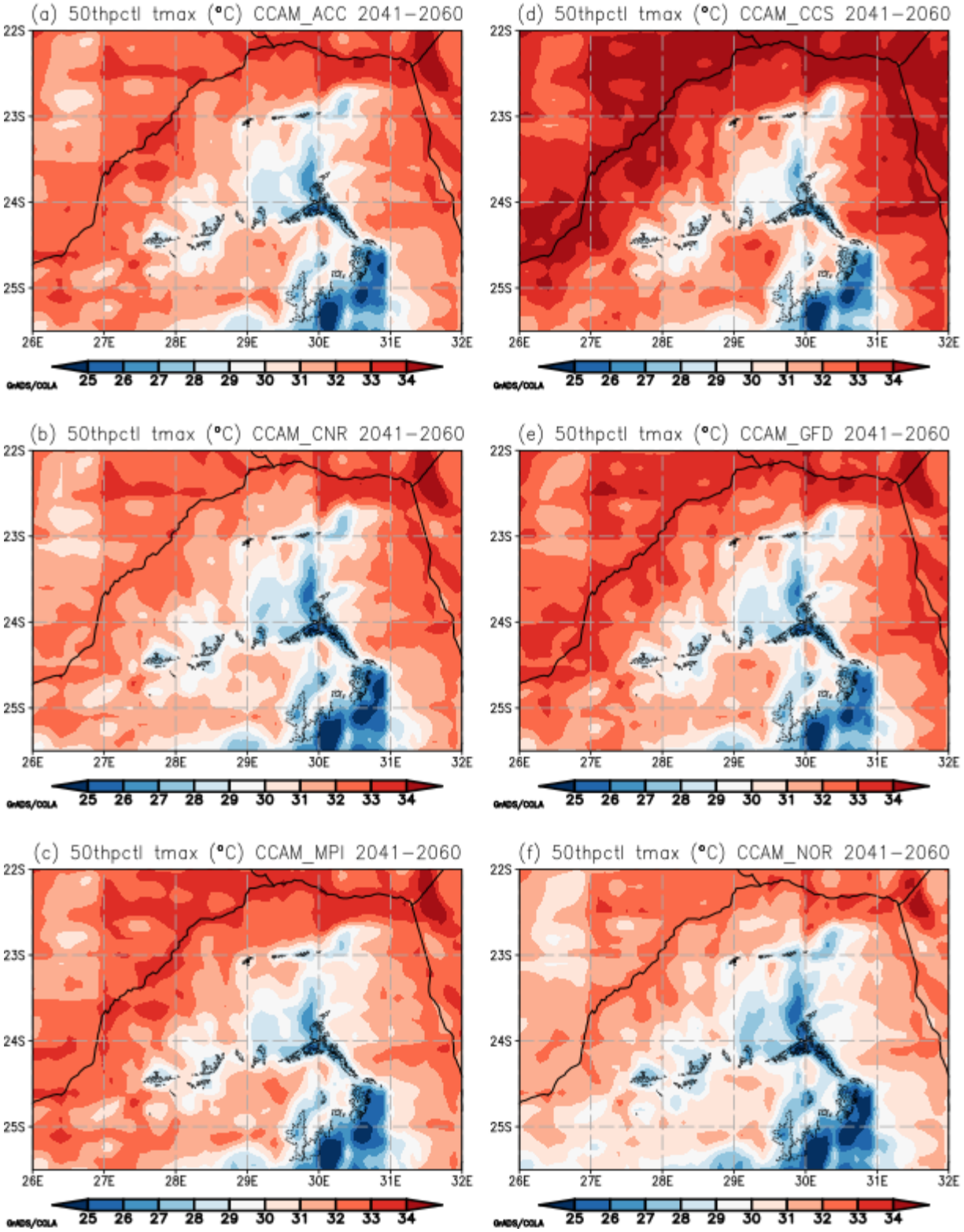

Figure 5.5 Mid – future maximum temperature projection from an ensemble of six downscaled CMIP6 GCMs

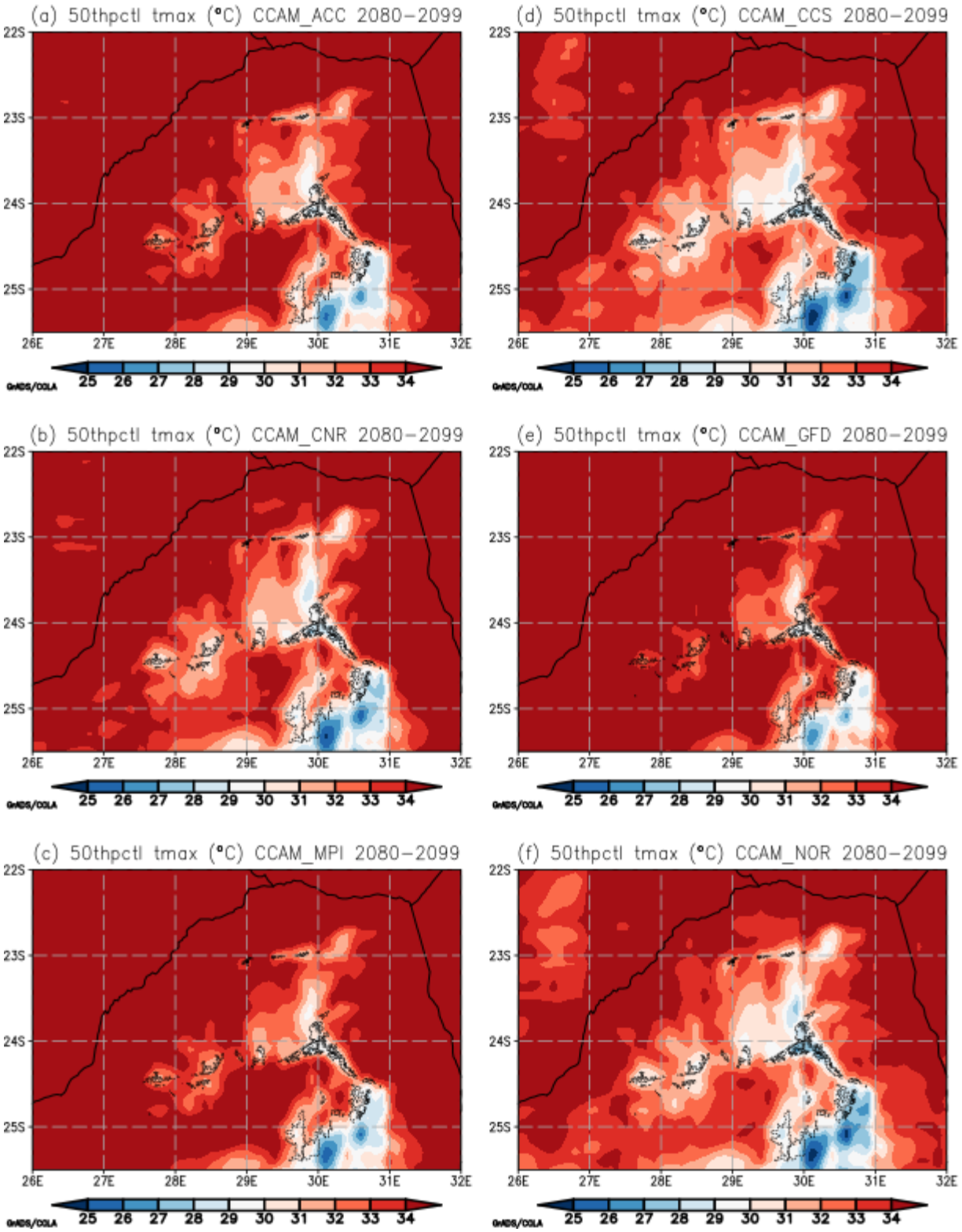

Figure 5.6 Far – future maximum temperature projection from an ensemble of six downscaled CMIP6 GCMs

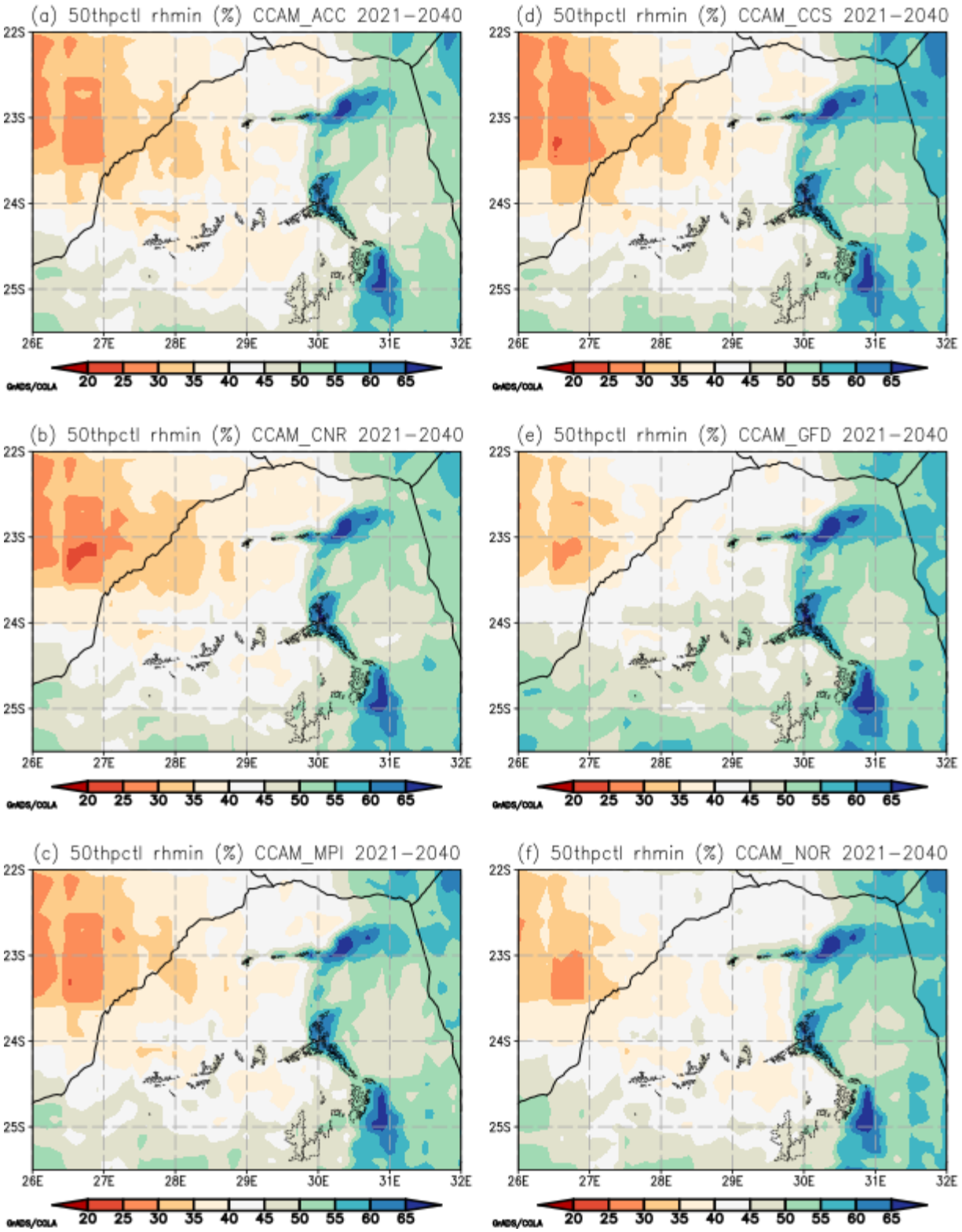

Figure 5.7 Near – future minimum relative humidity projection from an ensemble of six downscaled CMIP6 GCMs

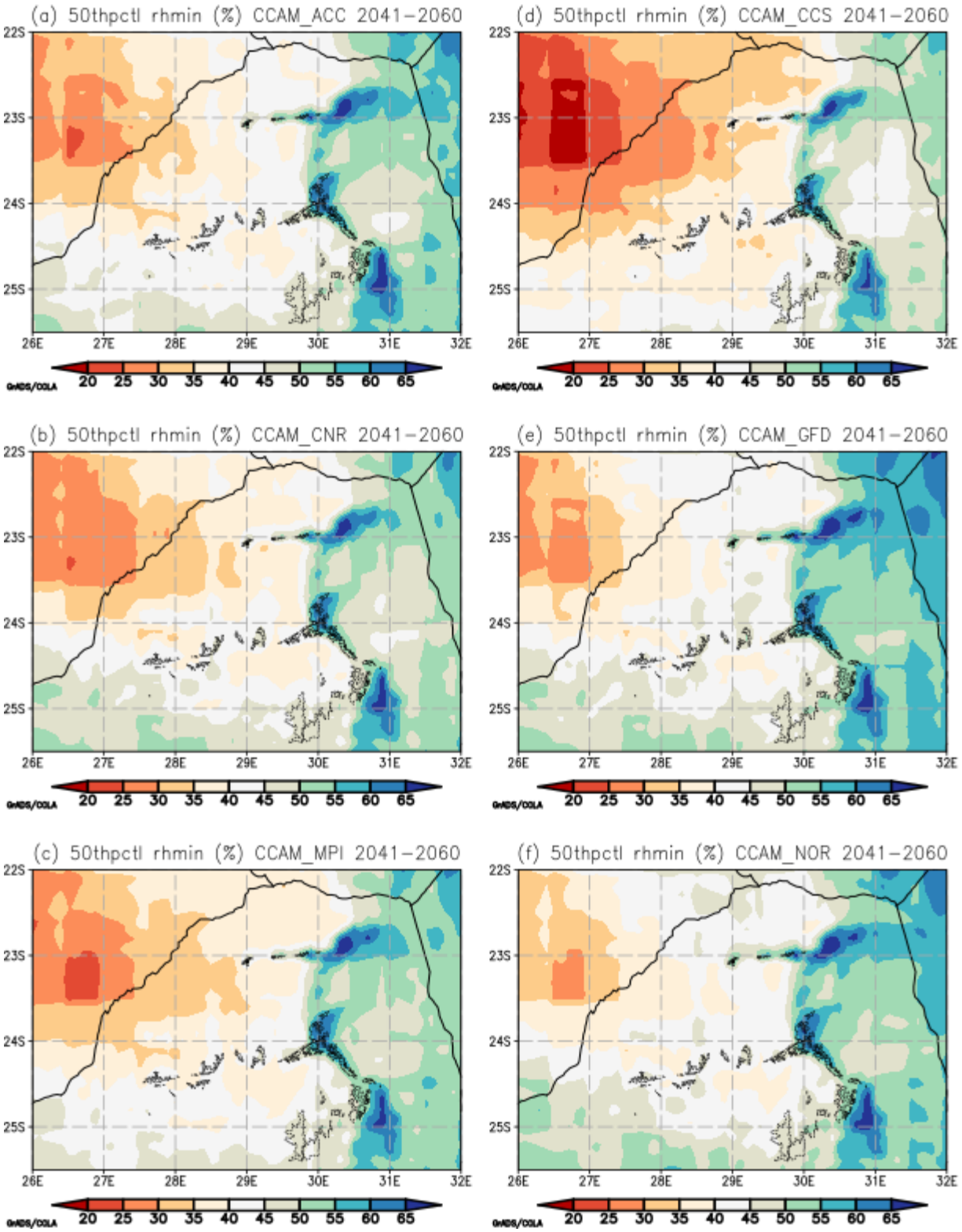

Figure 5.8 Mid – future minimum relative humidity projection from an ensemble of six downscaled CMIP6 GCMs

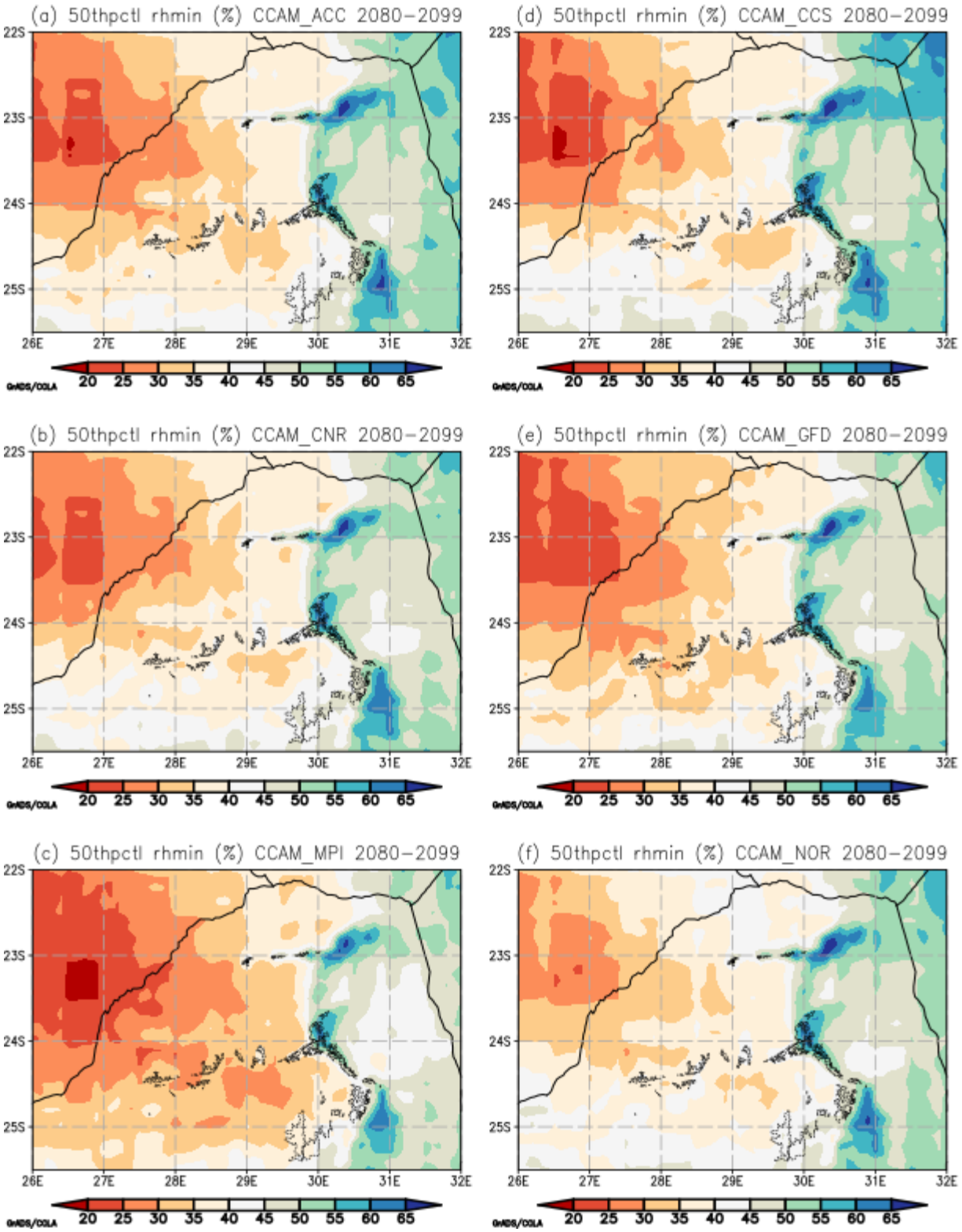

Figure 5.9 Far – future minimum relative humidity projection from an ensemble of six downscaled CMIP6 GCMs

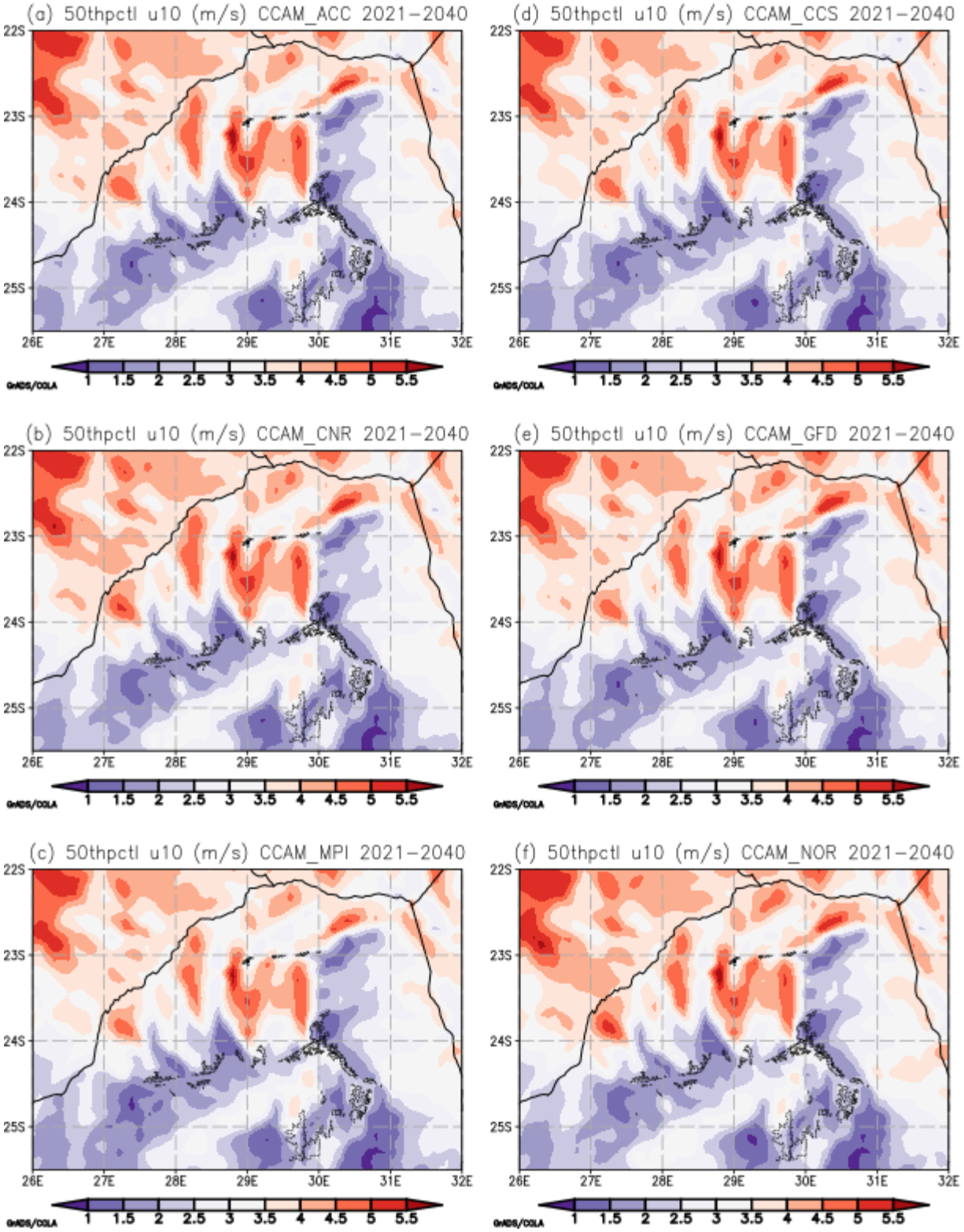

Figure 5.10 Near – future wind speed at 10 m projection from an ensemble of six downscaled CMIP6 GCMs

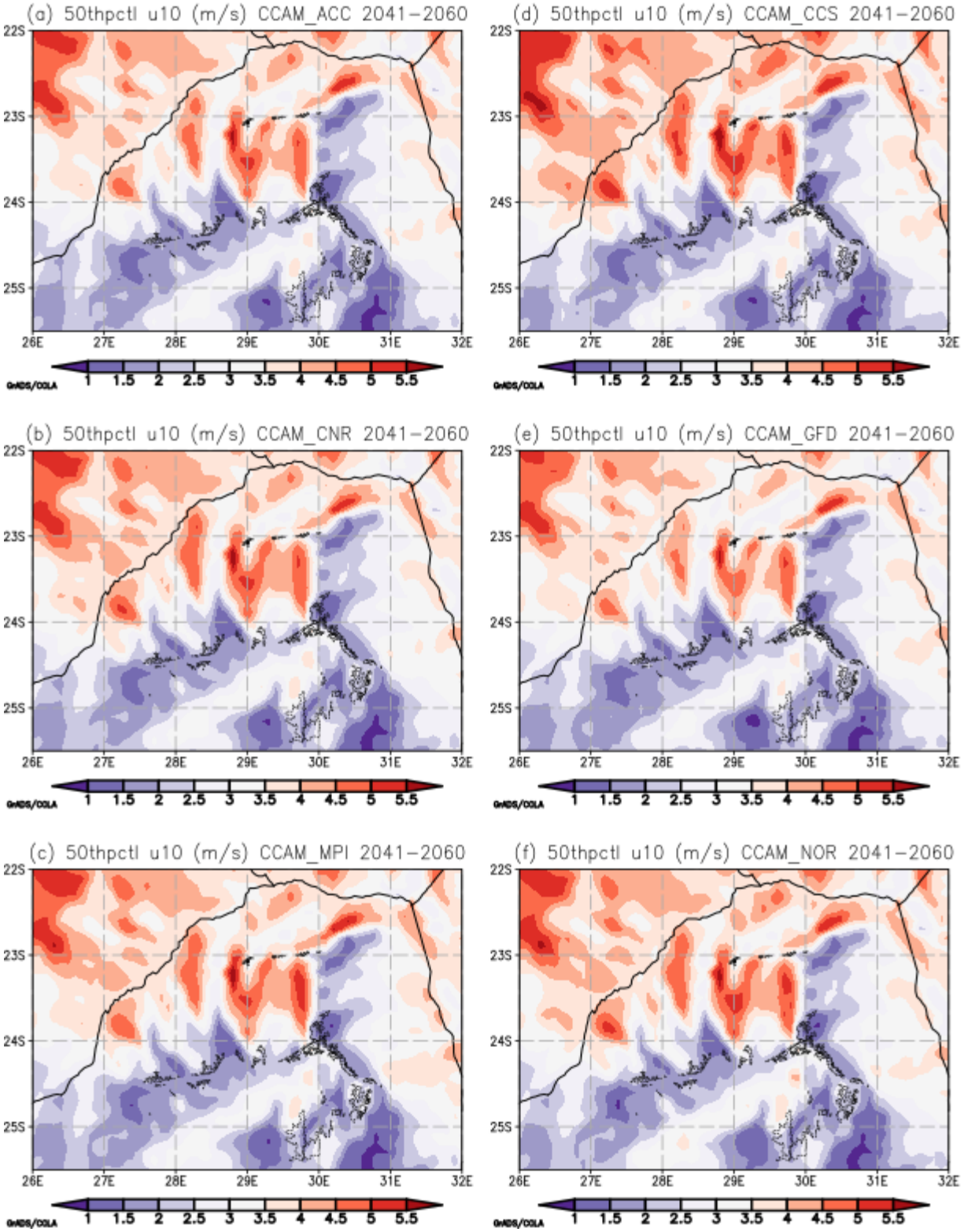

Figure 5.11 Mid – future wind speed at 10 m projection from an ensemble of six downscaled CMIP6 GCMs

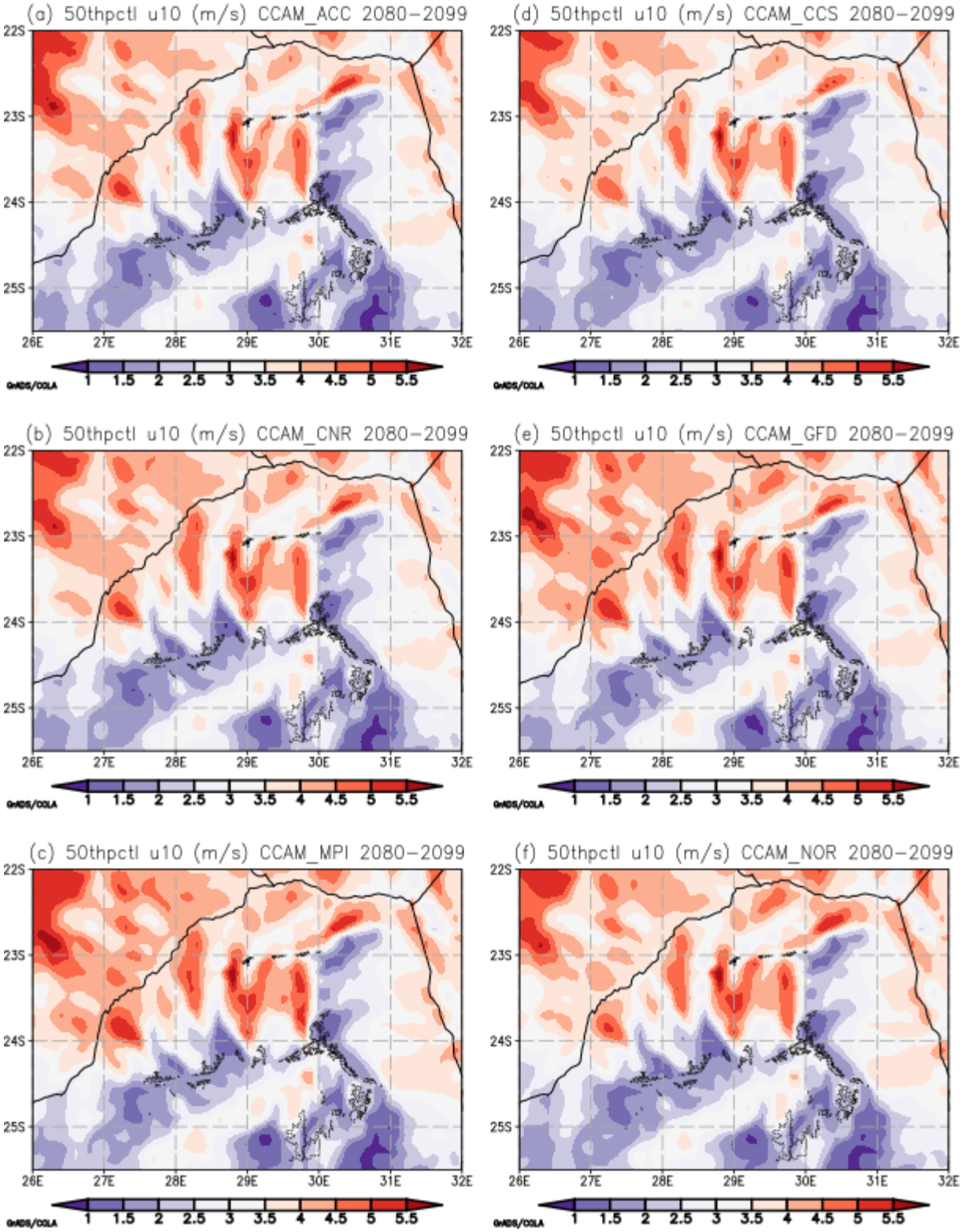

Figure 5.12 Far – future wind speed at 10 m projection from an ensemble of six downscaled CMIP6 GCMs

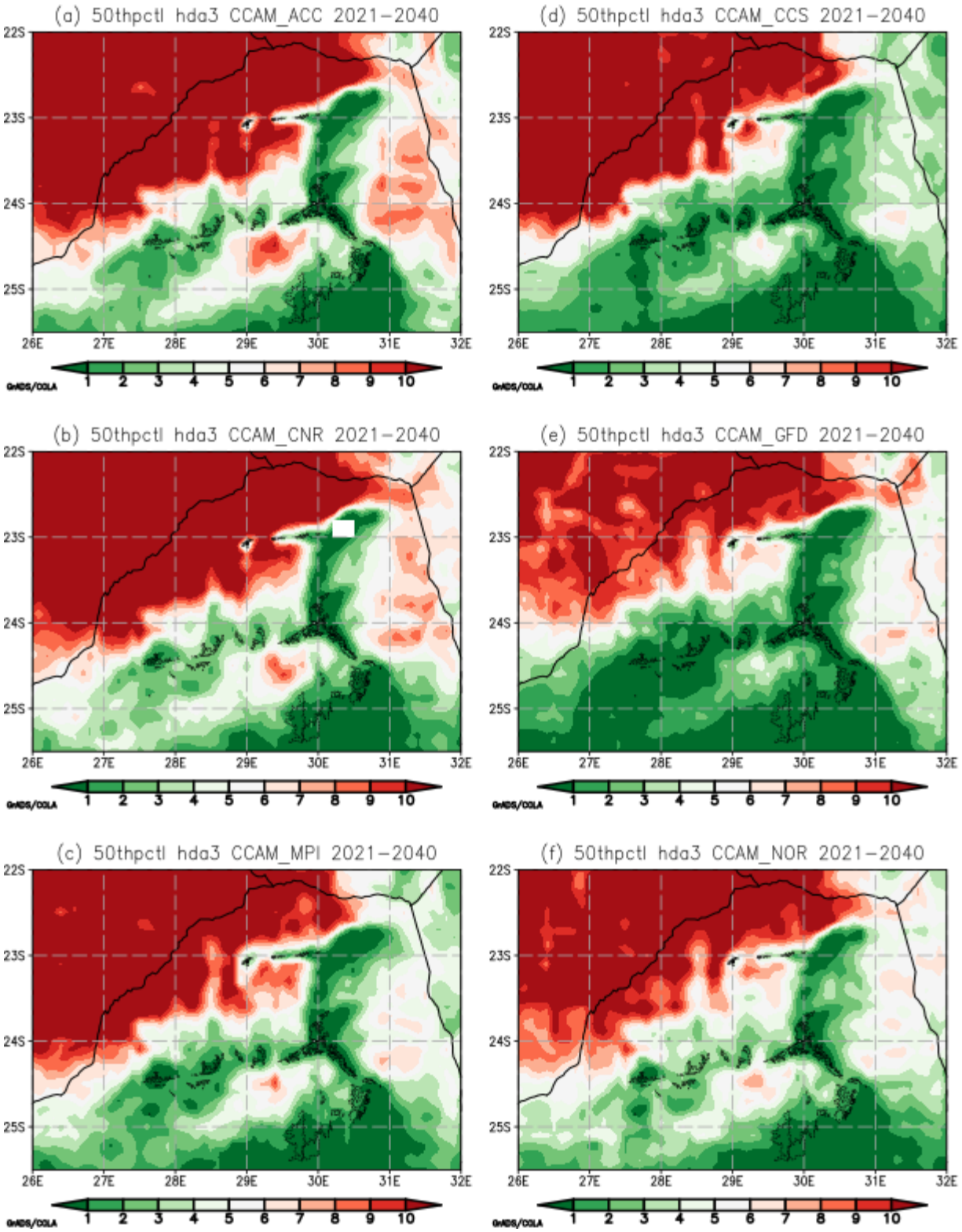

Figure 5.13 Near – future McArthur FFDI high danger days projection from an ensemble of six downscaled CMIP6 GCMs

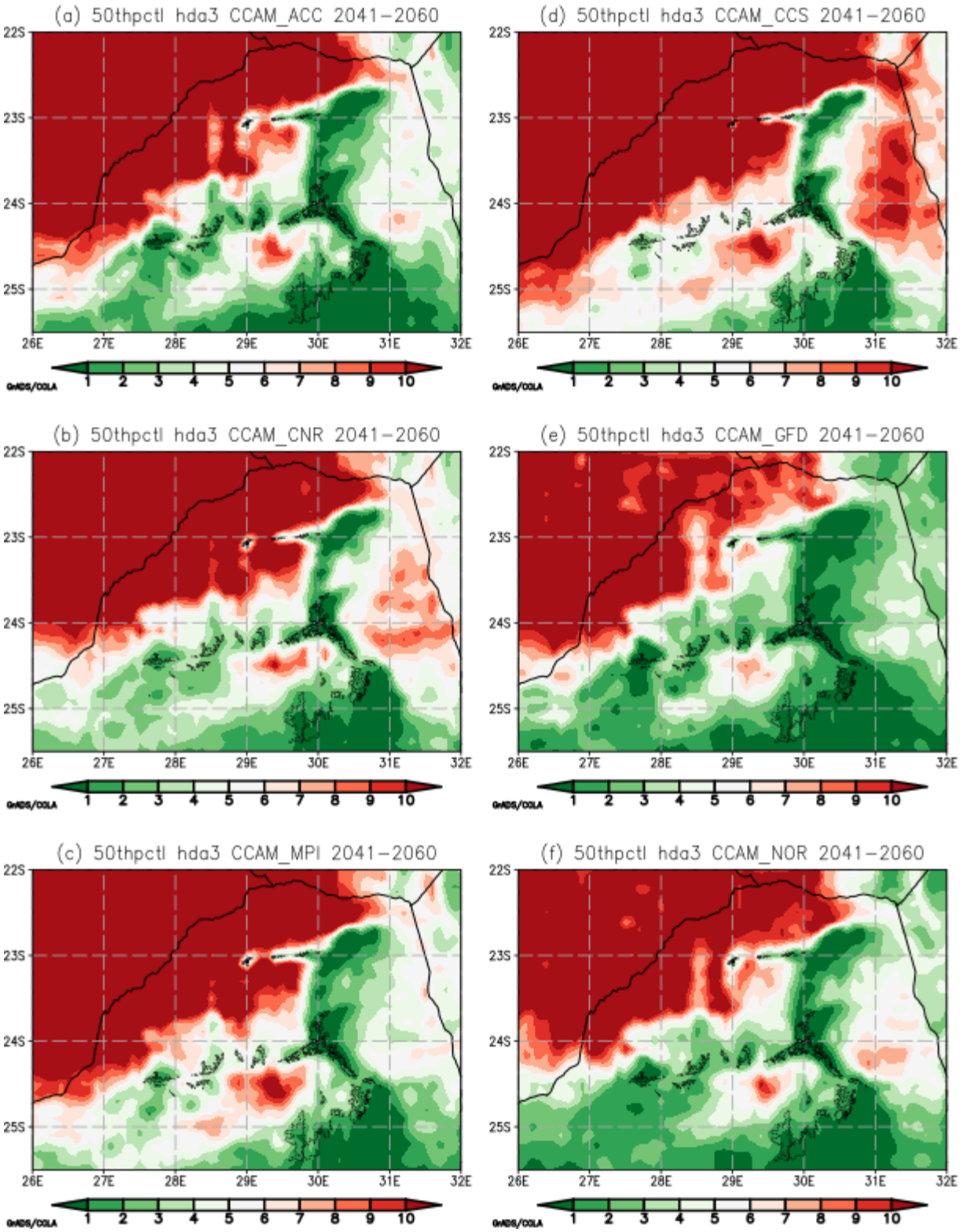

Figure 5.14 Mid – future McArthur FFDI high danger days projection from an ensemble of six downscaled CMIP6 GCMs

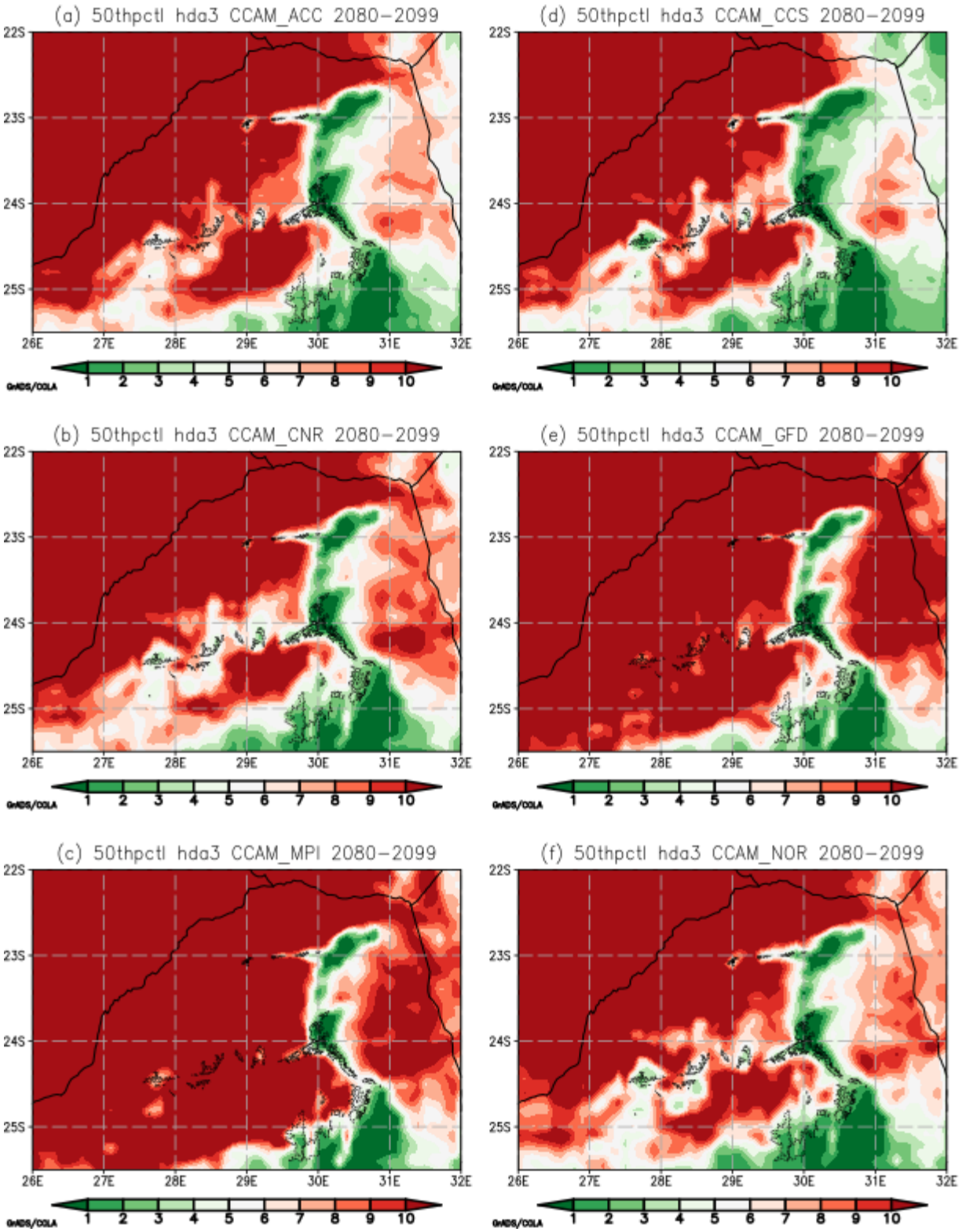

Figure 5.15 Far – future McArthur FFDI high danger days projection from an ensemble of six downscaled CMIP6 GCMs

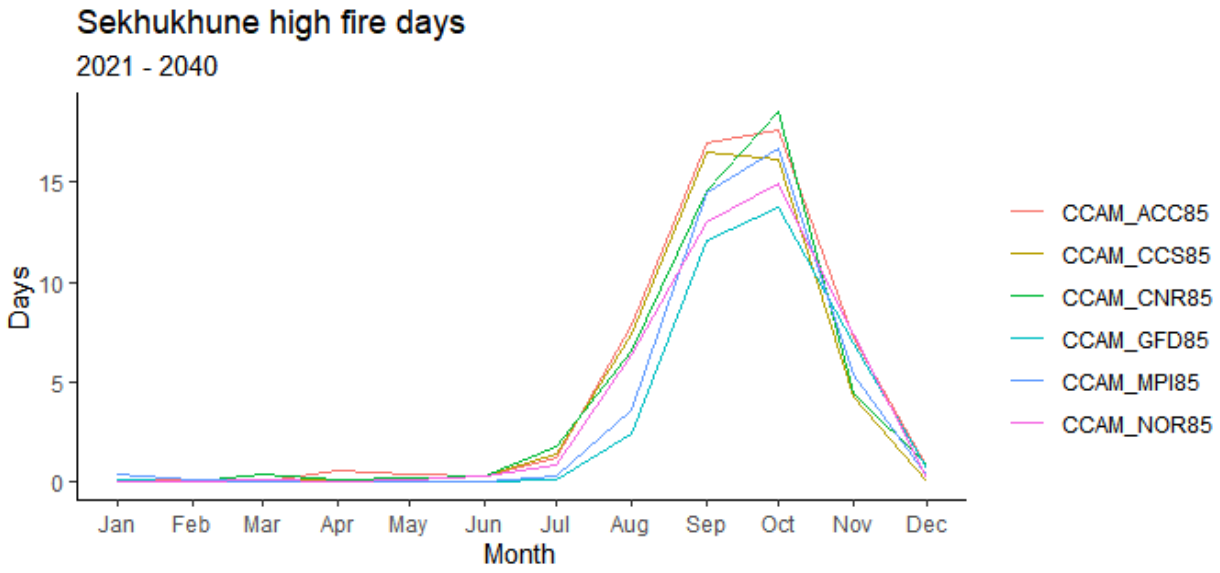

Figure 5.16 Sekhukhune mean annual McArthur FFDI high danger days from an ensemble of six downscaled CMIP6 GCMs (near – future).

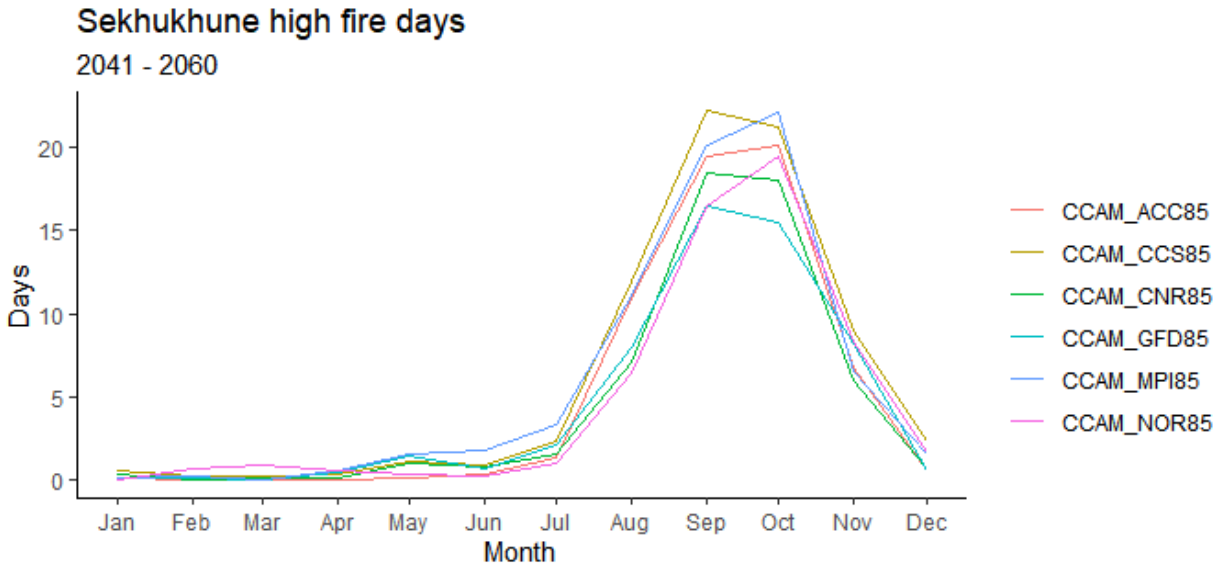

Figure 5.17 Sekhukhune mean annual McArthur FFDI high danger days from an ensemble of six downscaled CMIP6 GCMs (mid – future).

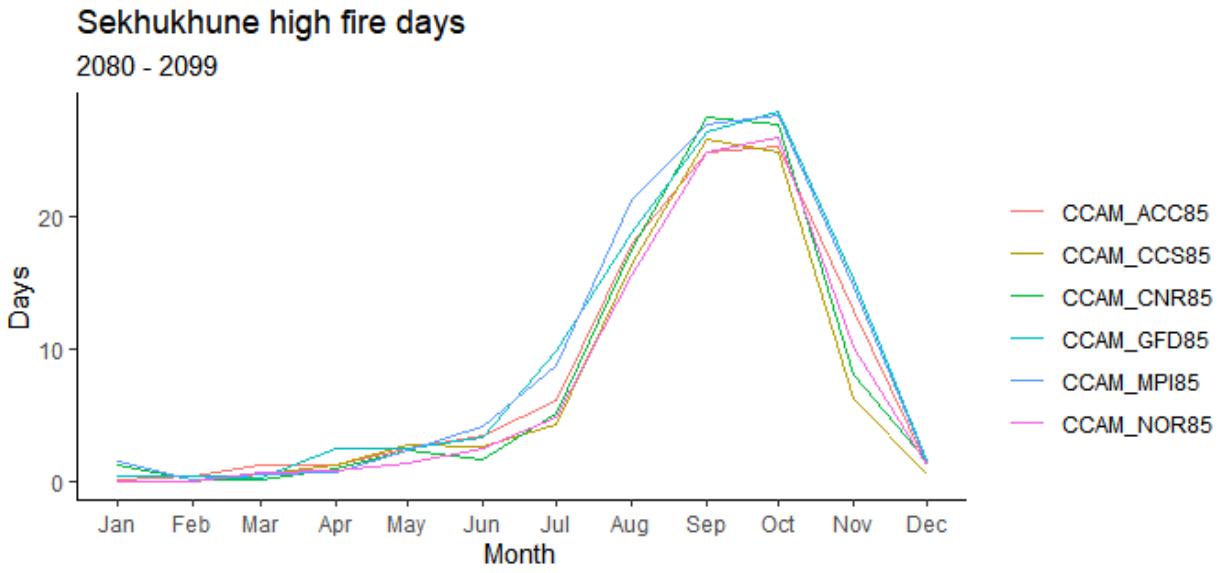

Figure 5.18 Sekhukhune mean annual McArthur FFDI high danger days from an ensemble of six downscaled CMIP6 GCMs (far – future).

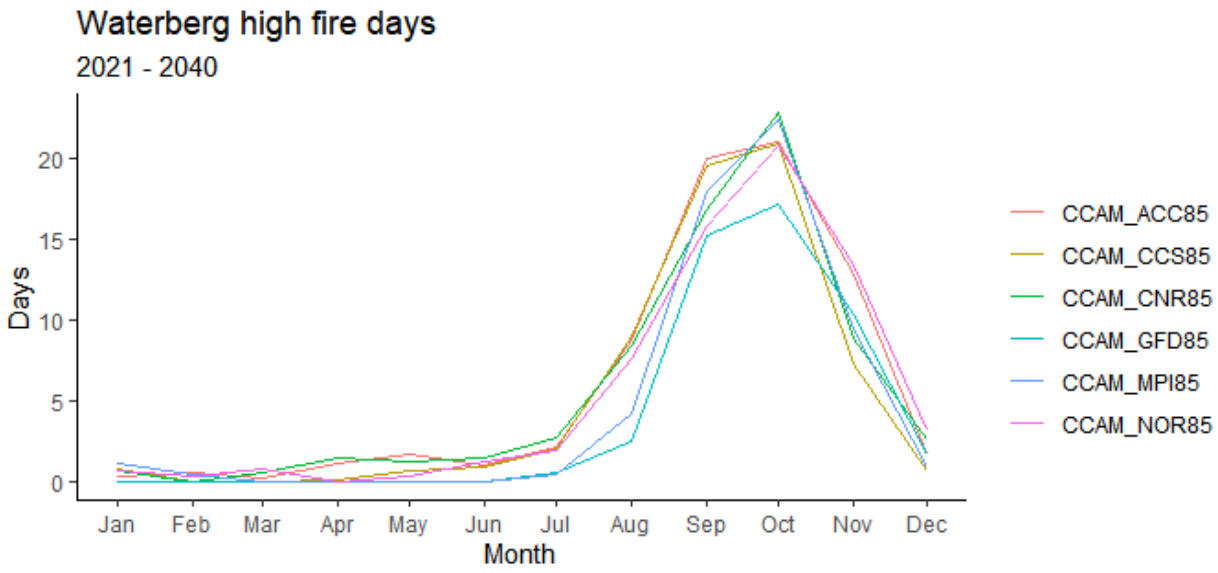

Figure 5.19 Waterberg mean annual McArthur FFDI high danger days from an ensemble of six downscaled CMIP6 GCMs (near – future).

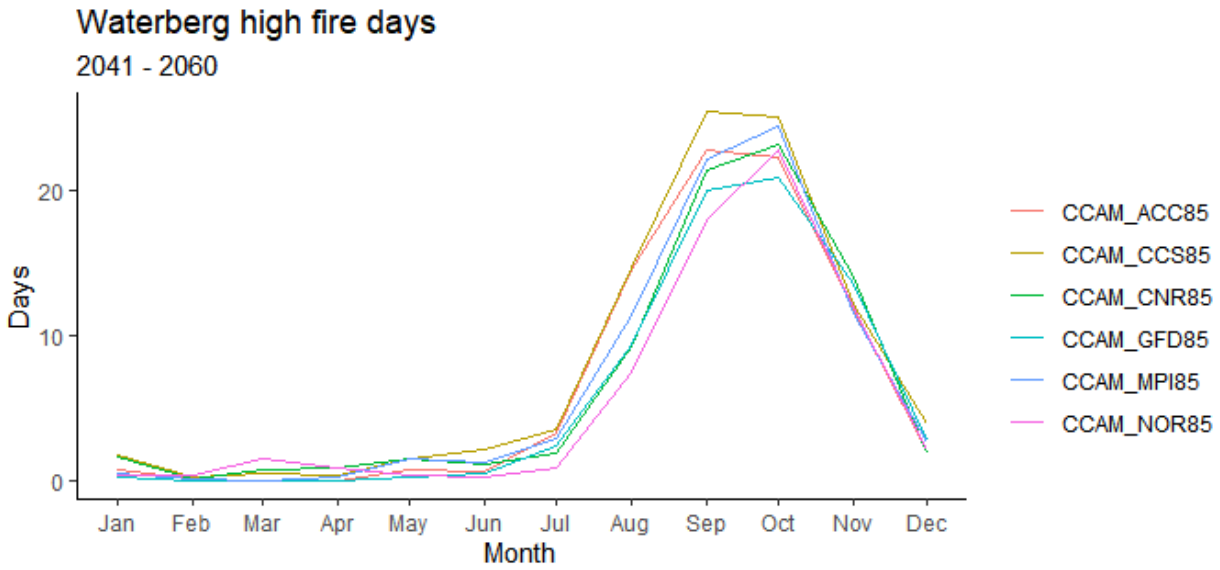

Figure 5.20 Sekhukhune mean annual McArthur FFDI high danger days from an ensemble of six downscaled CMIP6 GCMs (near – future).

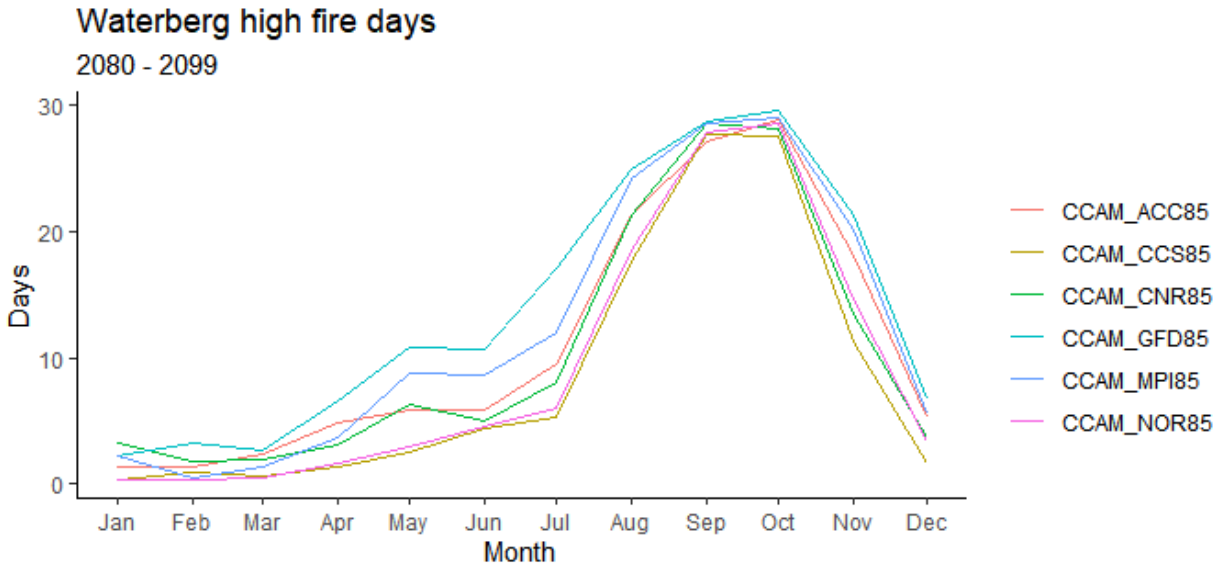

Figure 5.21 Sekhukhune mean annual McArthur FFDI high danger days from an ensemble of six downscaled CMIP6 GCMs (near – future).

Chapter 6: Conclusions and Future work

6.1 Introduction

Fire is a common and essential process in the ecology of the savanna grasslands of Limpopo, located northeast of South Africa. However, increasingly, the burned area is growing due to a prolonged fire season as the climate warms and changes. Recurrent drought on the grasslands coupled with high temperatures and heat wave conditions (Lyon, 2009; Chikoore and Jury 2021) create conditions conducive for frequent and intense wildfires. This study aimed to investigate changes in fire risk on the Limpopo grasslands due to climate change. It is well established in the literature that weather and climate variables such as temperature, precipitation, humidity and wind play an important role in the occurrence and spread of wildfires. Precipitation promotes fuel accumulation, temperature influences dryness of fuels, relative humidity regulates fuel moisture content, whilst wind speed affects fire spread rate.

This concluding chapter provides a synthesis of the key findings of this work, while providing recommendations for future research and fire management practices.

6.2 Discussion of Key Findings

6.2.1 Model verification

This study employed an ensemble of six models from the CMIP6 models forced with the high resolution CCAM model. The period 1961-1980 was employed as the historical baseline, whilst CRU TS4.04 data and ARC-SA weather station observations were used to verify the models. The Taylor diagram was employed to investigate models' performance against observations. Statistical tools featured in a Taylor diagram include standard deviation, correlation coefficient and RMSE. For this study of fire regimes, key variables used for model verification include rainfall, maximum temperature, minimum relative humidity, and wind speed.

Rainfall model verification showed CCAM_ACC85, CCAM_CCS85, CCAM_CNR85, CCAM_GFD85, and CCAM_MPI85 exhibited the closest variability, highest correlation and least RMSE compared with observation, whilst CCAM_NOR85 had the least skill. As expected, maximum temperature showed highest correlation and least RMSE from all models compared with observation, with CCAM_GFD85 and CCAM_NOR85 having high skill. In terms of minimum relative humidity, CCAM_ACC85, CCAM_GFD85 and CCAM exhibited high correlation (r=0.8), whilst the same models had least RMSE and close variability compared with the CRU ts4 observation. Under wind speed, the models showed worst performance in terms of standard

deviation and RMSE, hence having correlation (r=0.65) compared with observation. Therefore, the black dashed line in the Taylor diagram measures magnitude of variability compared with observations. All models that lie below the black dashed line are underestimating variability of observation and ones that lie above the dashed black line are overestimating observations.

6.2.2 Climate change projections

Future projections showed an increasing magnitude and spreading of aridity over the study area, consistent with Jury (2021). Rainfall is projected decreasing, suggesting increasing the intensity and frequency of drought on the grasslands. Spatial distribution of rainfall showed more activities occurring in the interior of study area. Maximum temperature is projected increasing to thresholds that will influence frequent occurrence of heatwaves. It has been found that drought is often accompanied by very high temperatures and heat waves (Lyon 2009). The models projected decreasing minimum relative humidity suggesting increased risk for vegetation and the agricultural sector. Reduced rainfall and high surface temperatures imply increasing evapotranspiration and reduced soil moisture. Manifestation of climate change through increased drought and heatwaves can be associated with food insecurity, water scarcity, decimation of livestock. Several studies have shown the Limpopo province is prone to heatwaves, which pose significant threats to agricultural sector, human lives and livelihoods (Mbokodo et al, 2020; Maposa et al, 2021; Nyoni et al, 2021).

6.2.3 Future changes in fire risk on the Limpopo grasslands

Limpopo grasslands are projected to become more vulnerable to increasing high fire danger days in the future. The projected increasing high fire danger days may influence frequent occurrence of wildfires that are destructive. In the near future (2021 – 2040), high fire danger days are projected ranging from 0 to the peak of 15 days over the grasslands in the south of the study region. In the west region, high fire danger days projected over the grasslands were varying from 0 to 20 days. The peak high fire danger days are projected to occur in September and October.

In the mid future (2041 – 2060), high fire danger days are projected increasing throughout the grasslands. Mean annual cycles analysed in chapter 5 showed relatively low fire risk from January to July across Limpopo grasslands. The peak high fire danger days have increased by 5 days from September to October, hence increasing fire risk in the grasslands. In the far future (2080-2099), the grasslands are vulnerable to high fire risk due to an increasing mean annual high fire danger days. The mean annual cycles projected drastic increases of high fire danger days from early autumn (March) until reaching the peak of 30 days high fire danger in spring.

6.3 Future work

Whilst this study has employed the McArthur FFDI, a comparison of the simulations of future fire risk based on different fire danger indices might be more revealing. Fire danger indexes, including fire weather index (FWI) and Lowveld Fire Danger Index (LFDI) are also employed in different part of the world. A comparison between fire danger indexes would provide different input and arguments to support the results because index values vary assessing impact of fire danger between different regions (Dowdy et al, 2010). Such a comparison of the performance of the different indices is therefore necessary.

Climate change projections of the present study were based on low mitigation effort (RCP8.5) and did not consider other RCPs. Future projections of fire risk using illustrative greenhouse emission scenarios referred to as Shared Socio-economic Pathways (Popp et al, 2017) showing climate variability from best effort mitigation to low mitigation (IPCC, 2021) would construct a firm fire risk assessment under current climate change uncertainty. Based on the projections of increasing fire risk under climate change in the future, fire managers and disaster risk reduction authorities need to take proactive prevention measures to reduce the impacts of future fires. The recent fires in the Western Cape of South Africa, in Knysna and on the Table Mountain have increased awareness of the potential harm due to runaway fires.

High resolution climate models, such as CCAM, would be useful in projections of future fire risk. Application of high-resolution climate models at regional scale may provide fire managers, including foresters, farmers, risk disaster managers and nature conservationists with an understanding of physical processes conducive to extreme weather and climate variabilities that cause catastrophic fire events. More research is thus needed to reduce the future impacts and vulnerabilities of the grasslands to high fire risk.

6.4 Conclusion

The study of projecting fire risk over an area that is prone to fire is very important under increasing global warming levels due to climate change. In the present study, future climate change projections for three periods including near future (2021 – 2040), mid future (2041 – 2060), and far future (2080 – 2099) over Limpopo grasslands are presented. An ensemble of six GCMs from CMIP6 dynamically downscaled though RCM CCAM with a high resolution of 8 km was used. Taylor diagram (Taylor, 2001) was used for model verification and statistics showed best performance from models compared with CRU ts4 observation during historical baseline of 1961 – 1980. Model verification increases confidence in using climate model for realistic presentation

of future climate change variabilities. The study a found drier and warmer climate consistent with the recent literature. The projected increasing high fire danger days under RCP8.5 showed high fire risk in the future over Limpopo grasslands. Models' findings agree with future projections from other studies, projecting increasing temperatures and an elongated future drying (Engelbrecht et al, 2015; Archer et al, 2018; Engelbrecht and Monteiro, 2021). This study contributed new knowledge to the understanding of fire risk on the grasslands, via an ensemble of very high-resolution climate models at the regional scale.

References

Abatzoglou, J. T., Smith, C. M., Swain, D. L., Ptak, T. and Kolden, C. A., 2020. Population exposure to pre-emptive de-energization aimed at averting wildfires in Northern California.

Abdel-Lathif, A.Y., Roehrig, R., Beau, I. and Douville, H., 2018. Single-column modeling of convection during the CINDY2011/DYNAMO field campaign with the CNRM Climate Model version 6. *Journal of Advances in Modeling Earth Systems* **10**(3),578-602.

Abrha, H. and Adhana, K., 2019. Desa'a national forest reserve susceptibility to fire under climate change. *Forest Science and Technology* **15**(3), 140 – 146.

Adepoju, K. and Adelabu, S., 2019, July. Assessment of fuel and wind drivers of fire risk in protected mountainous grassland of south africa. In IGARSS 2019-2019 IEEE International Geoscience and Remote Sensing Symposium, 867 – 870. IEEE.

Agovino, M., Cerciello, M., Ferraro, A. and Garofalo, A., 2021. Spatial analysis of wildfire incidence in the USA: the role of climatic spillovers. *Environment, Development and Sustainability* 23(4), 6084-6105.

Ahmed, M., 2020. Introduction to Modern climate Change. Andrew E. Dessler: Cambridge University Press, 2011, 252 pp, ISNB-10: 0521173159

Alexander, M. E. 1990. Computer Calculation of the Keetch-Byram Drought Index-Programmers Beware! Fire Management Notes. 51(4), 23–25.

Ali, M. E and Medhat, T., 2021. Correlation Coefficient Via Statistical and Rough Set Concepts. *Information Sciences Letters* **10**(3), 6. https://digitalcommons.aaru.edu.jo/isl/vol10/iss3/6

Anderson, S.A., 2009. Future options for fire behaviour modelling and fire danger rating in New Zealand. *Proceedings of the Royal Society of The Queensland*, **115,** 119-128.

Archer, E., Du Toit, J., Engelbrecht, C., Hoffman, M.T., Landman, W., Malherbe, J. and Stern, M., 2022. The 2015-19 multi year drought in the Eastern Cape, South Africa: it's evolution and impacts on agriculture. *Journal of Arid Environments* **196**, 104630.

Archer, E.R., Engelbrecht, F.A., Hänsler, A., Landman, W., Tadross, M. and Helmschrot, J., 2018. Seasonal prediction and regional climate projections for southern Africa. Klaus Hess Publishers.

Archibald, S., 2016. Managing human component of fire regimes: lessons from Africa. *Philosophical Transactions of the Royal Society B: Biological Sciences* **371**(1696), 20150346.

Archibald, S., Beckett, H., Bond, W.J., Coetsee, C., Druce, D.J. & Staver, C.A., 2017. Interactions between fire and ecosystem processes in Conserving Africa's megadiversity in the anthropocene: The Hluhluwe-iMfolozi Park story, 233–262, Cambridge University Press, Cambridge.

Archibald, S., Nickless, A., Govender, N., Scholes,R. J., and Lehsten, V., 2010. Climate and the inter-annual variability of fire in southern Africa: a meta-analysis using long-term field data and satellite-derived burnt area data. *Global Ecology and Biogeography* **19**, 794–809.

Bajocco, S., Ferrara, C., Guglietta, D. and Ricotta, C., 2019. Fifteen years of changes in fire ignition frequency in Sardinia (Italy): A rich-get-richer process. *Ecological Indicators* **104**, 543-548.

Baker, J., Bradley, B., and Stafford, P., 2021. Basics of Statistics for Model Calibration. In Seismic Hazard and Risk Analysis, 519-532. Cambridge: Cambridge University Press. doi:10.1017/9781108425056.018

Ballantyne, D., 2019. Case Study of an Effective Fire Protection Association in South Africa. *Biodiversidade Brasileira-BioBrasil* **1**, 29-29.

Barbehenn, R. V., Chen, Z., Karowe, D., and Spickards, A., 2004. C3 grasses have higher nutritional quality than C4 grasses under ambient and elevated atmospheric CO2. *Global Change Biology* **10**, 1565 – 1575, dio:10.1111/j.1365-2486.2004.00833.x

Barbero, R., Abatzoglou, J.T., Pimont, F., Ruffault, J. and Curt, T., 2020. Attributing increases in fire weather to anthropogenic climate change over France. *Frontiers in Earth Science* **8,** 104.

Barik, A. and Baidya Roy, S., 2020, May. Effects of meteorology on forest fires in India: A modeling study. In EGU General Assembly Conference Abstracts, 18317.

Barnes, M.A., Turner, K., Ndarana, T. and Landman, W.A., 2021. Cape storm: A dynamical study of a cut-off low and its impact on South Africa. *Atmospheric Research* **249**, 105290.

Barros, A.M., Day, M.A., Preisler, H.K., Abatzoglou, J.T., Krawchuk, M.A., Houtman, R. and Ager, A.A., 2021. Contrasting the role of human-and lightning-caused wildfires on future fire regimes on a Central Oregon landscape. *Environmental Research Letters* **16**(6), 064081.

Beaumont, L.J., Hughes, L. and Pitman, A.J., 2008. Why is the choice of future climate scenarios for species distribution modelling important? *Ecology letters* **11**(11), 1135-1146.

Bentsen, M., Bethke, I., Debernard, J.B., Iversen, T., Kirkevåg, A., Seland, Ø., Drange, H., Roelandt, C., Seierstad, I.A., Hoose, C. and Kristjánsson, J.E., 2012. The Norwegian earth system model, NorESM1-M–Part 1: Description and basic evaluation. Geosci. Model Dev. Discuss, 5(3), pp.2843-2931.

Berry, R. S and Kulmatiski, A., 2017. Savanna response to precipitation intensity. *PLoS ONE* **12**(4), e01754402. https://dio.0.1371/journal.pone.0175402

Bilgili, E., Coskuner, K.A., Usta, Y., Saglam, B., Kucuk, O., Berber, T. and Goltas, M., 2019. Diurnal surface fuel moisture prediction model for Calabrian pine stands in Turkey. *Forest-Biogeosciences and Forestry* **12(**3), 262.

Biswell, H. H., 2020. Chapter One. Fundamentals of Fire Behavior. *In Prescribed Burning in California Wildlands Vegetation Management* 18-37. University of California Press.

Blackmon, M., Boville, B., Bryan, F., Dickinson, R., Gent, P., Kiehl, J., Moritz, R., Randall, D., Shukla, J., Solomon, S. and Bonan, G., 2001. The community climate system model. *Bulletin of the American Meteorological Society* **82**(11), 2357-2376.

Bond, W.J., 2019, Open ecosystems: Ecology and evolution beyond the forest edge, Oxford University Press, Oxford. https://doi.org/10.1093/oso/9780198812456.001.0001

Bowman, D. M., Kolden, C. A., Abatzoglou, J. T., Johnston, F. H., van der Werf, G. R and Flannigan, M., 2020. Vegetation fires in the Anthropocene. *Nature Reviews Earth & Environment* **1**(10), 500 -515.

Bridgett, J.A., Van Wilgen, B.W., Kruger, F.J., Forsyth, G.G., Jayiya, T.P. and Kruger, L., 2003. A new approach to wildland fire management in South Africa. In rd International Wildland Fire Conference and Exhibition, Sydney, Australia.

Brown, E. K., Wang, J. and Feng, Y., 2021. US wildfire potential: a historical view and future projection using high-resolution climate data. *Environmental Research Letters* **16**(3) 034060.

Burls, N.J., Blamey, R.C., Cash, B.A., Swenson, E.T., al Fahad, A., Bopape, M.J.M., Straus, D.M. and Reason, C.J., 2019. The Cape Town “Day Zero” drought and Hadley cell expansion. *Climate and Atmospheric Science* **2**(1) 1-8.

Byram, G. M., 1959. Combustion of forest fuels. In ‘Forest Fire: Control and Use’. (Ed. KP Davis) 61–89. (McGraw-Hill: New York)

Calheiros, T., Pereira, M. G. and Nunes, J. P., 2021. Assessing impacts of future climate change on extreme fire weather and pyro-regions in Iberian Peninsula. *Science of The Total Environment* **754** 142233.

Calkin, D.E., O'Connor, C. D., Thompson, M. P. and Stratton, R., 2021. Strategic Wildfire Response Decision Support and the Risk Management Assistance Program. *Forests* **12**(10), 1407.

Canadell, J.G., Meyer, C.P., Cook, G.D., Dowdy, A., Briggs, P.R., Knauer, J., Pepler, A. and Haverd, V., 2021. Multi-decadal increase of forest burned area in Australia is linked to climate change. *Nature communications* **12**(1), 1-11.

Cannon, A.J., Piani, C. and Sippel, S., 2020. Bias correction of climate model output for impact models. In Climate Extremes and Their Implications for Impact and Risk Assessment, 77-104. Elsevier.

Cansler, C.A., Kane, V.R., Hessburg, P.F., Kane, J.T., Jeronimo, S.M., Lutz, J.A., Povak, N.A., Churchill, D.J. and Larson, A.J., 2022. Previous wildfires and management treatments moderate subsequent fire severity. *Forest Ecology and Management* **504**, 119764.

Cardil, A., Monedero, S., Schag, G., de-Miguel, S., Tapia, M., Stoof, C.R., Silva, C.A., Mohan, M., Cardil, A. and Ramirez, J., 2021. Fire behavior modeling for operational decision-making. *Current Opinion in Environmental Science & Health* **23**, 100291.

Carlson, K. M., Curran, L. M., Ratnasari, D., Pittman, A.M., Soares-Filho, B. S., Asner, G. P., Trigg, S.N., Gaveau, D.A., Lawrence, D., Rodrigues, H. O., 2012, Committed carbon emissions, deforestation, and community land conversion from oil palm plantation expansion in West Kalimantan, Indonesia. *Proceedings of the National Academy of Science of the United States of America* **109**, 7559–7564.

Carvalho, D., Cardoso Pereira, S. and Rocha, A., 2021. Future surface temperatures over Europe according to CMIP6 climate projections: an analysis with original and bias-corrected data. Climatic Change **167**(1), 1-17.

Castillo, M., Plaza, Á. and Garfias, R., 2020. A recent review of fire behavior and fire effects on native vegetation in Central Chile. *Global Ecology and Conservation* **24**, e01210.

Chartan, E.K., Wright, J. and Landwehr, G., 2018. Comparing the Value of Improved Variable Renewable Energy Forecasting Accuracy in South African and United States Power Systems (No. NREL/CP-5D00-72593). National Renewable Energy Lab (NREL), Golden, CO (United States).

Chen, F., Niu, S., Tong, X., Zhao, J., Sun, Y. and He, T., 2014. The impact of precipitation regimes on forest fires in Yunnan Province, Southwest China. *The Scientific World Journal*, **2014**, 326782. https://doi.org/10.1155/2014/326782

Chen, J., Li, C., Ristovski, Z., Milic, A., Gu, Y., Islam, M.S., Wang, S., Hao, J., Zhang, H., He, C. and Guo, H., 2017. A review of biomass burning: Emissions and impacts on air quality, health and climate in China. *Science of the Total Environment* **579**, 1000-1034.

Chen, Z.Y., Chu, Y.H. and Su, C.L., 2021. Intercomparisons of Tropospheric Wind Velocities Measured by Multi-Frequency Wind Profilers and Rawinsonde. *Atmosphere* **12**(10), 1284.

Chikoore H., and Jury, M., 2021. South African drought, deconstructed. *Weather and Climate Extremes* **33**, 100334, https://doi.org/10.1016/j.wace.2021.100334

Chikoore, H., 2016. Drought in southern Africa. PhD Thesis, University of Zululand, South Africa, Durban.

Chikoore, H., Bopape, M.J.M., Ndarana, T., Muofhe, T.P., Gijben, M., Munyai, R.B., Manyanya, T.C. and Maisha, R., 2021. Synoptic structure of a sub-daily extreme precipitation and flood event in Thohoyandou, north-eastern South Africa. *Weather and Climate Extremes* **33**, 100327.

Christensen, E.G., Hu, Y., Purnomo, D.M. and Rein, G., 2021. Influence of wind and slope on multidimensional smouldering peat fires. *Proceedings of the Combustion Institute* **38**(3), 5033-5041.

Chuvieco, E., Giglio, L. and Justice, C., 2008. Global characterization of fire activity: toward defining fire regimes from Earth observation data. *Global change biology*, **14**(7), 1488-1502.

Cochrane, M. A., and Bowman, D. M., 2021. Manage fire regimes, not fires. Nature Geosciences **14**(7), 455 – 457.

Cordova, C., Kirsten, K., Scott, L., Meadows, M., and Lücke, A. 2019. Multi-proxy evidence of Late-Holocene paleoenvironmental change at Princessvlei, South Africa: The effects of fire, herbivores, and humans. Quaternary Science Reviews. 221. 105896. 10.1016/j.quascirev.2019.105896.

Countryman, C.M., 1972. The Fire Environment Concept. USDA Forest Service, Pacific Southwest Forest and Range Experiment Station, Berkeley. 12.

Crutzen, P. J., Heidt, L. E., Krasnec, J. P., Pollock, W. H., and Seiler, W. 1979. Biomass burning as a source of atmospheric gases CO, H2, N2O, NO, CH3Cl and COS. *Nature* **282**, 253–256, https://doi.org/10.1038/282253a0.

Cruz, M. G., Alexander, M. E., Fernandes, P. M., Kilinc, M. and Sil, Â., 2020. Evaluating the 10% wind speed rule of thumb for estimating a wildfire's forward rate of spread against an extensive independent set of observations. *Environmental Modelling & Software* **133,** 104818.

Curt, T., 2018. Fire Frequency. In: Manzello S. (eds) Encyclopedia of Wildfires and Wildland-Urban Interface (WUI) Fires. Springer, Cham. http://doi.org/10.1007/978-3-319-51727-8_110-1

Dayaram, A., Harris, L.R., Grobler, B.A., Van der Merwe, S., Rebelo, A.G., Ward Powrie, L., Vlok, J.H., Desmet, P.G., Qabaqaba, M., Hlahane, K.M. and Skowno, A.L., 2019. Vegetation map of South Africa, Lesotho and Swaziland 2018: a description of changes since 2006. *Bothalia-African Biodiversity & Conservation* **49**(1), 1 – 11.

de Dios, V. R., 2020. Plant-fire interactions. *Applying ecophysiology to wildfire management* **36**. Springer Nature.

de Groot, W., Goldammer J, Keenan T, Brady M, Lynham T, Justice C, Csiszar I, O'Loughlin K., 2006. Developing a global early warning system for wildland fire. *For Ecol Manag **234***, S10.doi: 10.1016/j.foreco.2006.08.025

De Paor, D. G., Dordevic, M. M., Karabinos, P., Burgin, S., Coba, F., Whitmeyer, J. S. 2017. Exploring the reasons for the seasons using Google Earth, 3D models, and plots, International *Journal of Digital Earth* **10**(6), 582-603, DOI: 10.1080/17538947.2016.1239770

DeConto, R.M., Pollard, D., Alley, R.B., Velicogna, I., Gasson, E., Gomez, N., Sadai, S., Condron, A., Gilford, D.M., Ashe, E.L. and Kopp, R.E., 2021. The Paris Climate Agreement and future sea-level rise from Antarctica. *Nature* **593**(7857), 83 – 89.

Deeming, J.E., 1972. National fire-danger rating system (Vol. 84). Rocky Mountain Forest and Range Experiment Station, Forest Service, US Department of Agriculture.

Deeming, J.E., Burgan, R.E. and Cohen, J.D., 1977. The national fire-danger rating system, 1978 (Vol. 39). Department of Agriculture, Forest Service, Intermountain Forest and Range Experiment Station.

Devine, A. P., McDonald, R. A., Quaife, T., & Maclean, I. M. 2017. Determinants of woody encroachment and cover in African savannas. *Oecologia* **183**(4), 939–951. https://doi.org/10.1007/s00442-017-3807-6

Dmitruk, G., 2020. A Globe-Circling Synoptic-Scale Winter Disturbance in Northern Hemisphere Midlatitudes (Doctoral dissertation, The Florida State University).

Dowdy, A.J. and Pepler, A., 2018. Pyroconvection risk in Australia: Climatological changes in atmospheric stability and surface fire weather conditions. *Geophysical Research Letters* **45**(4), 2005-2013.

Driver, P., and Reason, C. J. C., 2017. Variability in the Botswana High and its relationship with rainfall and temperature characteristics over southern Africa. *International Journal of Climatology* 37(1), 570 – 581.

Droste, A.M., Steeneveld, G.J. and Holtslag, A.A., 2018. Introducing the urban wind island effect. *Environmental Research Letters* **13**(9), 094007.

Duane, A. and Brotons, L., 2018. Synoptic weather conditions and changing fire regimes in a Mediterranean environment. *Agricultural and Forest Meteorology* **253**,190-202, ISSN 0168-1923, https://doi.org/10.1016/j.agrformet.2018.02.014

Dube, K., Nhamo, G. and Chikodzi, D., 2020. Climate change-induced droughts and tourism: Impacts and responses of Western Cape province, South Africa. *Journal of Outdoor Recreation and Tourism*, 100319

Dupuy, J.L., Fargeon, H., Martin-StPaul, N., Pimont, F., Ruffault, J., Guijarro, M., Hernando, C., Madrigal, J. and Fernandes, P., 2020. Climate change impact on future wildfire danger and activity in southern Europe: a review. *Annals of Forest Science* **77(**2), 1-24.

Dyson, L.L., and van Heerden, J. 2002. A model for the identification of tropical weather systems over South Africa. *Water SA* **28**(3), ISSN 0378-4738

Engelbrecht, C. J., & Engelbrecht, F. A. (2016). Shifts in Köppen-Geiger climate zones over southern Africa in relation to key global temperature goals. *Theoretical and Applied Climatology* **123**, 247–261. https://doi.org/10.1007/s00704-014-1354-1

Engelbrecht, F., Adegoke, J., Bopape, M.J., Naidoo, M., Garland, R., Thatcher, M., McGregor, J., Katzfey, J., Werner, M., Ichoku, C. and Gatebe, C., 2015. Projections of rapidly rising surface temperatures over Africa under low mitigation. *Environmental Research Letters* **10**(8), 085004.

Engelbrecht, F.A., Landman, W.A., Engelbrecht, C.J., Landman, S., Bopape, M.M., Roux, B., McGregor, J.L. and Thatcher, M., 2011. Multi-scale climate modelling over Southern Africa using a variable-resolution global model. *Water SA* **37**(5), 647-658.

Engelbrecht, F.A., McGregor, J.L. and Engelbrecht, C.J., 2009. Dynamics of the Conformal-Cubic Atmospheric Model projected climate-change signal over southern Africa. *International Journal of Climatology: A Journal of the Royal Meteorological Society* **29**(7), 1013-1033.

Fann, N., Alman, B., Broome, R.A., Morgan, G.G., Johnston, F.H., Pouliot, G. and Rappold, A.G., 2018. The health impacts and economic value of wildland fire episodes in the US: 2008–2012. *Science of the total environment* **610**, 802-809.

Fawzy, S., Osman, A. I., Doran, J. and Rooney, D. W., 2020. Strategies for mitigation of climate change: a review. *Environmental Chemistry Letters*, 1 – 26.

Fayolle, A., Swaine, M.D., Aleman, J., Azihou, A.F., Bauman, D., Te Beest, M., Chidumayo, E.N., Cromsigt, J.P., Dessard, H., Finckh, M. and Gonçalves, F.M.P., 2019. A sharp floristic discontinuity revealed by the biogeographic regionalization of African savannas. *Journal of biogeography* **46**(2), 454-465.

February, E., Pausch, J. and Higgins, S.I., 2020. Major contribution of grass roots to soil carbon pools and CO 2 fluxes in a mesic savanna. *Plant and Soil* **454**(1), 207-215.

Flannigan, M. D, Krawchuk, M. A, de Groot, W. J, Wotton B. M, and Gowman, L. M. 2009. Implications of changing climate for global wildland fire. *International Journal of Wildland Fire* 1**8,** 483–507.

Flannigan, M. D., Amiro, B. D., Logan, K. A., Stocks, B. J. and Wotton, B. M., 2006. Forest fires and climate change in the 21st century. *Mitigation and adaptation strategies for global change* **11**(4), 847-859.

Flannigan, M., Cantin, A. S., de Groot, W. J., Wotton, M., Newbery, A. and Gowman, L. M., 2013. Global wildland fire season severity in the 21st century. *Forest Ecology and Management* **294**, 54-61.

Forsyth, G.G., Kruger, F.J. and Le Maitre, D.C., 2010. National veldfire risk assessment: Analysis of exposure of social, economic and environmental assets to veldfire hazards in South Africa. National Resources and the Environment CSIR, Fred Kruger Consulting cc.

Friberg, M.D., Wu, D.L., Carr, J.L., Limbacher, J.A., Zou, Y. and O'Neill, S., 2021, March. Diurnal Observations of Wildfires Boundary Layer Dynamics and Aerosol Plume Convection using Stereo-Imaging Techniques. In EGU General Assembly Conference Abstracts, EGU21-16351.

Fried, J. S., Gilless, J. K., Riley, W. J., Moody, T. J., de Blas, C. S., Hayhoe, K., Mortiz, M., Stephens, S., Torn, M., 2008. Predicting the effect of climate change on wildfire behavior and initial attack success. *Climatic Change* **87**, 251-264

Frost, P., 1996. The ecology of miombo woodlands. In: B. Campbell (ed.) The Miombo in Transition: Woodlands and Welfare in Africa, 11-57. Centre for International Forestry Research, Bogor, Indonesia.

Fujioka, F., 2019, December. Temporal Variability of Wildfire Danger: A Multi-dimensional Perspective. In AGU Fall Meeting Abstracts (Vol. 2019, NH52A-01).

Gallagher, R. V., Allen, S., Mackenzie, B. D., Yates, C. J., Gosper, C. R., Keith, D. A., White, M. D., Wenk, E., Maitner, B. S. and He, K., 2021.Hire fire frequency and impact of the 2019 – 2020 megafires on Australian plant diversity. *Diversity and Distributions* **27**(7), 1166 – 1179.

Gandrud, C., 2018. Reproducible research with R and RStudio. Chapman and Hall/CRC.

Gao, C., Wang, G., Santin, C., Doerr, S.H., Cong, J. and Zhao, H., 2021. Response of Calamagrostis angustifolia to burn frequency and seasonality in the Sanjiang Plain wetlands (Northeast China). *Journal of Environmental Management* **300,** 113759.

Gent, P.R., 2006. Preface to special issue on community climate system model (CCSM). *Journal of Climate* **19**(11), 2121-2121.

Gordijn P.J., Everson T.M., and O'Connor T.G. 2018. Resistance of Drakensberg grasslands to compositional change depends on the influence of fire-return interval and grassland structure on richness and spatial turnover. *Perspectives in Plant Ecology, Evolution and Systematics* **34**, 26-36.

Gordon, C.E. and Letnic, M., 2019. Evidence that the functional extinction of small mammals facilitates shrub encroachment following wildfire in arid Australia. *Journal of Arid Environments* **164**, 60-68.

Govender, N., Trollope, W. S. and Van Wilgen, B. W., 2006. The effect of fire season, fire frequency, rainfall and management on fire intensity in savanna vegetation in South Africa. *Journal of Applied Ecology* **43**(4), 748 – 758.

Gowan, T. A. and Horel, J. D., 2020. Evaluation of IMERG-E Precipitation Estimates for Fire Weather Applications in Alaska. *Weather and Forecasting* **35**(5), 1831-1843.

Guo, C., Bentsen, M., Bethke, I., Ilicak, M., Tjiputra, J., Toniazzo, T., Schwinger, J. and Otterå, O.H., 2019. Description and evaluation of NorESM1-F: a fast version of the Norwegian Earth System Model (NorESM). *Geoscientific Model Development* **12**(1), 343-362.

Gutjahr, O., Putrasahan, D., Lohmann, K., Jungclaus, J.H., Storch, J.S.V., Brüggemann, N., Haak, H. and Stössel, A., 2019. Max Planck Institute Earth System Model (MPI-ESM1. 2) for the High-Resolution Model Intercomparison Project (HighResMIP). *Geoscientific Model Development* **12**(7), 3241-3281.

Gütschow, J., Jeffery, M.L., Günther, A. and Meinshausen, M., 2021. Country-resolved combined emission and socio-economic pathways based on the Representative Concentration Pathway (RCP) and Shared Socio-Economic Pathway (SSP) scenarios. *Earth System Science Data* **13**(3), 1005-1040.

Hadisuwito, A.S. and Hassan, F.H., 2021. A Comparative Study of Drought Factors in the Mcarthur Forest Fire Danger Index in Indonesian Forest. *Ecol. Environ. Conserv. Pap* **5**, 202-206.

Harris, I., Osborn, T.J., Jones, P. and Lister, D., 2020. Version 4 of the CRU TS monthly high-resolution gridded multivariate climate dataset. *Scientific data* **7**(1), 1-18.

Harris, L., Grobler, B., der Merwe, V., Vlok, J., Desmet, P., Qabaqaba, M. and Hlahane, K., 2019. Vegetation Map of South Africa, Lesotho and Swaziland 2018: A description of changes since 2006.

Harris, S., Anderson, W., Kilinc, M. and Fogarty, L., 2012. The relationship between fire behaviour measures and community loss: an exploratory analysis for developing a bushfire severity scale. *Natural Hazards* **63**(2), 391-415.

Harrison, D. C., 2015. Improving integrated wildfire management in the Fynbos Biome of South Africa using information on synoptic-scale atmospheric features that promote wildfires (Master's thesis, University of Cape Town).

Harrison, M. S. J., 1984. A generalised classification of South African rain-bearing synoptic systems. *J Climatol* **4**, 547 – 560

Harrison, S. P., Prentice, I. C., Bloomfield, K. J, Dong, N., et al., 2021. Understanding and modelling wildfire regimes: an ecological perspective. *Environ Res Lett* **16**, 125008. https://dio.org/10.1088/1748-9326/ac39be

Hart, N. C. G., Reason, C. J. C. and Fauchereau, N., 2010. Tropical–extratropical interactions over southern Africa: Three cases of heavy summer season rainfall. *Monthly weather review* **138**(7), 2608-2623.

Hart, N. C. G., Reason, C. J. C and Fauchereau, N., 2013. Cloud bands over southern Africa: seasonality, contribution to rainfall variability and modulation by the MJO. *Clim Dyn* **41**, 1199 – 1212. https://doi.org/10.11007/s00382-012-1589-4

Hassan, R. A and Hamdy, R. S. 2021. Overview of Exotic Acacia, Senegalia, Vachelia (Caesalpiniodeae, Mimsoid Clade, Fabaceae) in Egypt. *Plants* **10**, 1344. https://dio.org/10.3390/plants10071344

Hausfather, Z., Drake, H.F., Abbott, T. and Schmidt, G.A., 2020. Evaluating the performance of past climate model projections. *Geophysical Research Letters* **47**(1), e2019GL085378.

Heim, R.J., Hölzel, N., Heinken, T., Kamp, J., Thomas, A., Darman, G.F., Smirenski, S.M. and Heim, W., 2019. Post-burn and long-term fire effects on plants and birds in floodplain wetlands of the Russian Far East. *Biodiversity and Conservation* **28**(6), 1611-1628.

Hoegh-Guldberg, O., Jacob, D., Bindi, M., Brown, S., Camilloni, I., Diedhiou, A., Djalante, R., Ebi, K., Engelbrecht, F., Guiot, J. and Hijioka, Y., 2018. Impacts of 1.5 C global warming on natural and human systems. Global warming of 1.5 C. An IPCC special report.

Hoffmann, W. A., Schroeder, W., and Jackson, R. B., 2002. Positive feedbacks of fire, climate and vegetation and the conversion of tropical savanna. *Geophysical Research Letters* **29**, 22 https://dio.org/10.1029/2002GL01524

Holbrook, N.J., Scannell, H.A., Gupta, A.S., Benthuysen, J.A., Feng, M., Oliver, E.C., Alexander, L.V., Burrows, M.T., Donat, M.G., Hobday, A.J. and Moore, P.J., 2019. A global assessment of marine heatwaves and their drivers. *Nature Communications* **10**(1), 1-13.

Holden, Z.A., Swanson, A., Luce, C.H., Jolly, W.M., Maneta, M., Oyler, J.W., Warren, D.A., Parsons, R. and Affleck, D., 2018. Decreasing fire season precipitation increased recent western US forest wildfire activity. *Proceedings of the National Academy of Sciences* **115**(36), E8349-E8357.

Horowitz, L.W., Naik, V., Paulot, F., Ginoux, P.A., Dunne, J.P., Mao, J., Schnell, J., Chen, X., He, J., John, J.G. and Lin, M., 2020. The GFDL global atmospheric chemistry-climate model AM4. 1: Model description and simulation characteristics. *Journal of Advances in Modeling Earth Systems* **12**(10), e2019MS002032.

Hovenden, M.J., Leuzinger, S., Newton, P.C.D. et al., 2019. Globally consistent influences of seasonal precipitation limit grassland biomass response to elevated CO2. *Nature Plants* **5**, 167–173 https://doi.org/10.1038/s41477-018-0356-x

Hutley, L. B and Setterfield, S. A., 2008. Savanna. Encyclopedia of Ecology, 3143-3154 https://doi.org/10.1016/B978-008045405-4.00358-X

IPCC. 2021. Summary for policymakers. In: Masson-Delmotte V, Zhai P, Pirani A, Connors SL, Péan C, Berger S, et al. editors. Climate change 2021: The physical science basis. Contribution of Working Group I to the Sixth Assessment Report of the Intergovernmental Panel on Climate Change. Cambridge, UK: Cambridge University Press.

Irrgang, C., Boers, N., Sonnewald, M., Barnes, E.A., Kadow, C., Staneva, J. and Saynisch-Wagner, J., 2021. Will Artificial Intelligence supersede Earth System and Climate Models? arXiv preprint arXiv:2101.09126.

Isah, A.D., Abubakar, M.S., Nasiru, A.M., Lawal, U.A., Audu, Y.A.M. and Haliru, M., 2021. Impact of Prescribed Burning on Soil Physico-Chemical Properties in Semi-Arid Environment, Sokoto State, Nigeria. *International Journal of Pure and Applied Science Research* **12**(2), 153-165.

Jain, H., 2020. An approach for forewarning forest fires in Shivalik forest tracts of Uttarakhand by application of fire trends and Keetch Byram Drought Index. In Remote Sensing for Agriculture, Ecosystems, and Hydrology XXII (Vol. 11528, 115280O). International Society for Optics and Photonics.

James, R., and Washington R., 2013. Changes in African temperature and precipitation associated with degrees of global warming. *Clim Chang* **117**(4):859–872

Jatta, E., Jawara, M., Bradley, J., Jeffries, D., Kandeh, B., Knudsen, J.B., Wilson, A.L., Pinder, M., D'Alessandro, U. and Lindsay, S.W., 2018. How house design affects malaria mosquito density, temperature, and relative humidity: an experimental study in rural Gambia. *The Lancet Planetary Health* **2**(11), e498-e508.

Jimoh, M.Y., Bikam, P. and Chikoore, H., 2021. The Influence of Socioeconomic Factors on Households' Vulnerability to Climate Change in Semiarid Towns of Mopani, South Africa. *Climate* **9**(1), 13.

Jobe, T.O., Rahimzadeh Karvansara, P., Zenzen, I. and Kopriva, S., 2020. Ensuring Nutritious Food Under Elevated CO2 Conditions: A Case for Improved C4 Crops. *Frontiers in Plant Science* **11**, 1267.

Johansson, M.U., Abebe, F.B., Nemomissa, S., Bekele, T. and Hylander, K., 2021. Ecosystem restoration in fire-managed savanna woodlands: Effects on biodiversity, local livelihoods and fire intensity. *Ambio* **50**, 190-202.

John, J., Garland, R.M. and Landman, W.A., 2015. Understanding of extreme temperature events by environmental health stakeholders in South Africa. In: 31st Conference of the South African Society for Atmospheric Science, Hennops River Valley, Centurion, South Africa, 21-22 September 2015

Johnson, M.B. and Forthum, G., 2001, November. Spatial mapping of KBDI for the southeast United States. In Proceedings of the 4th Symposium on Fire and Forest Meteorology, 13-15. Nevada: American Meteorological Society, Preprints.

Jones, P.D. and Harris, I., 2008. Climatic Research Unit (CRU) time-series datasets of variations in climate with variations in other phenomena. NCAS British Atmospheric Data Centre, 15.

Jury, M. R., 2021. Spreading of the semi-arid climate across South Africa. *Journal of Water and Climate Change* **12**(8), 3734–3749. https://doi.org/10.2166/wcc.2021.187

Kasischke, E.S., Hoy, E.E., 2012. Controls on carbon consumption during Alaskan wildland fires. *Global Change Biology* **18**, 685–699.

Kaur, P., Stoltzfus, J. and Yellapu, V., 2018. Descriptive statistics. *International Journal of Academic Medicine* **4**(1), 60.

Kavhu, B., and Ndaimani, H., Analysing factors influencing fire frequency in Hangwe National Park. *South African Geographical Journal*, 1 – 16.

Keane, R. E., Burgan, R. E., and van Wagtendonk, J. W., 2001. Mapping wildland fuels for fire management across multiple scales: Integrating remote sensing GIS and biophysical modelling. *Int. J. Wildland Fire* **10**(4), 301-319.

Keeley, J. E, Alexandra D., and Syphard, A. D., 2016. Climate Change and Future Fire Regimes: Examples from California. *Geosciences* **6**, 37 doi:10.3390/geosciences6030037.

Keeley, J. E., 2009. Fire intensity, fire severity and burn severity: a brief review and suggested usage. *Int J Wildl Fire* **18**,116 –126. https://doi.org/10.1071/WF07049

Keetch, J. J. and Byram, G. M., 1968. A drought index for forest fire control. Res. Pap. SE-38, Vol. 35. Asheville (NC): US Department of Agriculture, Forest Service, Southeastern Forest Experiment Station. 38

Kennedy, M. C., Bart, R. R., Tague, C. L. and Choate, J. S., 2021. Does hot and dry equal more wildfire? Contrasting short-and long-term climate effects on fire in the Sierra Nevada, CA. *Ecosphere* **12**(7), e03657.

Kganyago, M., Govender, K., Shikwambana, L. and Sivakumar, V., 2021. Study on blazing wildfires at the outeniqua pass in South Africa during the october/november 2018 period. *Remote Sensing Applications: Society and Environment* **21**, 100464.

Kharuk, V.I., Ponomarev, E.I., Ivanova, G.A., Dvinskaya, M.L., Coogan, S.C. and Flannigan, M.D., 2021. Wildfires in the Siberian taiga. *Ambio,* 1-22.

Khastagir, A. 2018. Fire frequency analysis for different climatic stations, Natural Hazards. *Springer Netherlands* **93**(2), 787–802. doi: 10.1007/s11069-018-3324-x.

Kholoshyn, I., Bondarenko, O., Hanchuk, O. and Shmeltser, E., 2019. Cloud ArcGIS Online as an innovative tool for developing geoinformation competence with future geography teachers. arXiv preprint arXiv:1909.04388.

Kraaij, T., Baard, J.A., Arndt, J., Vhengani, L. and Van Wilgen, B.W., 2018. An assessment of climate, weather, and fuel factors influencing a large, destructive wildfire in the Knysna region, South Africa. *Fire Ecology* **14**(2), 1-12.

Kruger, A. and Shongwe, S., 2004. Temperature trends in South Africa: 1960-2003. *International Journal of Climatology* **15**, 1929-1945.

Kruger, F., Forsyth, G., Kruger, L., Slater, K., Le Maitre, D. C., & Matshate, J., 2006. Classification of veldfire risk in South Africa for the administration of the legislation regarding fire management. http://hdl.handle.net/10204/851

Kumar, A., 2020. Modelling and Analysis of Heat Waves for Excessive Heat Factor (EHF) Over Some Tropical Regions of India. In Recent Trends in Materials and Devices, 101-109. Springer, Singapore.

Kumari, B. and Pandey, A.C., 2020. MODIS based forest fire hotspot analysis and its relationship with climatic variables. *Spatial Information Research* **28**(1), 87-99.

Kumari, R., Mayoor, M., Mahapatra, S., Parhi, P.K. and Singh, H.P., 2019. Estimation of Rainfall-Runoff Relationship and Correlation of Runoff with Infiltration Capacity and Temperature Over East Singhbhum District of Jharkhand. *International Journal of Engineering and Advanced Technology* **9**, 2, 461.

Lall, S. and Mathibela, B., 2016, December. The application of artificial neural networks for wildfire risk prediction. In 2016 International Conference on Robotics and Automation for Humanitarian Applications (RAHA), 1-6. IEEE.

Landman, W.A., Sweijd, N., Masedi, N. and Minakawa, N., 2020. The development and prudent application of climate-based forecasts of seasonal malaria in the Limpopo province in South Africa. Environmental Development, 35, 100522.

Laris, P., Jacobs, R., Kone, M., Dembele, F., and Rodrigue, M. C., 2020. Determinants of fire intensity in working landscapes of an African savanna. *Fire Ecology* **16**, 27 https://doi.org/10.1186/s42408-020-00085-x

Law, M. and Collins, A., 2019. Getting to know ArcGIS PRO. Redlands, CA, USA: Esri press.

Leys, B. A., Marlon, J. R., Umbanhowar, C., and Vannière, B., 2018. Global fire history of grassland biomes. *Ecology and evolution* **8**(17), 8831–8852. https://doi.org/10.1002/ece3.4394

Li, Y., Ruan, S., Zhou, A., Xie, P., Azam, S.R. and Ma, H., 2022. Ultrasonic modification on fermentation characteristics of Bacillus varieties: Impact on protease activity, peptide content and its correlation coefficient. LWT, 154, 112852.

Lindenmayer, D., Taylor, C. and Blanchard, W., 2021. Empirical analyses of the factors influencing fire severity in southeastern Australia. *Ecosphere* **12**(8), e03721.

Lindenmayer, D.B., Kooyman, R.M., Taylor, C., Ward, M. and Watson, J.E., 2020. Recent Australian wildfires made worse by logging and associated forest management. *Nature ecology & evolution* **4**(7), 898-900.

Linder, H. P. 2017.East African Cenozoic vegetation history. Evol. Anthropol. 26, 300–312.

Littell, J.S., 2018. Drought and fire in the western USA: is climate attribution enough? *Current Climate Change Reports* **4**(4), 396-406.

Liu, Z., and Wimberly, M.C., 2016. Direct and indirect effects of climate change on projected future fire regimes in the western United States. Sci. *Total Environ* **542**, 65–75

Lyon, B., 2009. Southern Africa summer drought and heat waves: observations and coupled model behavior. *Journal of Climate* **22**(22), 6033-6046.

Ma, W., Zhai, L., Pivovaroff, A., Shuman, J., Buotte, P., Ding, J., Christoffersen, B.O., Knox, R.G., Moritz, M. and Fisher, R.A., 2021. Assessing climate change impacts on live fuel moisture and wildfire risk using a hydrodynamic vegetation model. *Biogeosciences* **18**, 4005–4020, https://doi.org/10.5194/bg-18-4005-2021, 2021.

Mahdavi, P. and Bergmeier, E., 2018. Distribution of C4 plants in sand habitats of different climatic regions. *Folia Geobotanica* **53**(2), 201-211.

Malherbe, J., Engelbrecht, F.A. and Landman, W.A., 2013. Projected changes in tropical cyclone climatology and landfall in the Southwest Indian Ocean region under enhanced anthropogenic forcing. *Climate dynamics* **40**(11), 2867-2886.

Maposa, D., Seimela, A.M., Sigauke, C. and Cochran, J.J., 2021. Modelling temperature extremes in the Limpopo province: bivariate time-varying threshold excess approach. *Natural Hazards* **107**(3), 2227-2246.

Marques, J.F., Alves, M.B., Silveira, C.F., e Silva, A.A., Silva, T.A., Dos Santos, V.J. and Calijuri, M.L., 2021. Fires dynamics in the Pantanal: Impacts of anthropogenic activities and climate change. *Journal of Environmental Management* **299**, 113586.

Martens, C, Hickler, T, Davis-Reddy, C, et al. 2020. Large uncertainties in future biome changes in Africa call for flexible climate adaptation strategies. *Glob Change Biol.* **27**, 340– 358. https://doi.org/10.1111/gcb.15390

Masemola, M.J., 2021. Assessment of vulnerability of cattle farming to climate variability and change in South Africa (Master's Degree dissertation). University of KwaZulu-Natal.

Matsoukis, A., Kamoutsis, A. and Chronopoulos, K., 2018. Estimation of the meteorological forest fire risk in a mountainous region by using remote air temperature and relative humidity data. International Letters of Natural Sciences, 67.

Maule, C.F., Mendlik, T. and Christensen, O.B., 2017. The effect of the pathway to a two degrees warmer world on the regional temperature change of Europe. *Climate Services* **7**, 3-11.

Maúre, G., Pinto, I., Ndebele-Murisa, M., Muthige, M., Lennard, C., Nikulin, G., Dosio, A. and Meque, A., 2018. The southern African climate under 1.5 C and 2 C of global warming as simulated by CORDEX regional climate models. *Environmental Research Letters* **13**(6), 065002.

Maurin, O., Davies, T. J., Burrows, J. E., Daru, B. H., Yessoufou, K., Muasya, A. M., van der Bank, M., & Bond, W. J., 2014. Savanna fire and the origins of the 'underground forests' of Africa. *The New phytologist* ***204*****(**1), 201–214. https://doi.org/10.1111/nph.12936

Mawlood, Y., Salih, A., Hummadi, R., Hasan, A. and Ibrahim, H., 2021. Comparison of artificial neural network (ANN) and linear regression modeling with residual errors to predict the unconfined compressive strength and compression index for Erbil City soils, Kurdistan-Iraq. *Arabian Journal of Geosciences* **14**(6), 1-14.

Mbokodo, I., Bopape, M.J., Chikoore, H., Engelbrecht, F. and Nethengwe, N., 2020. Heatwaves in the future warmer climate of South Africa. *Atmosphere* **11**(7), 712.

McBride, J.R., 2019. Fuel management and wildfire mitigation proposal for the University of California property in Strawberry and Claremont canyons.

McGregor, J. L., 2005. C-CAM: Geometric aspects and dynamical formulation. CSIRO Atmospheric Research Technical Paper No. 70, 43.

McLauchlan, K. K., Higuera, P. E., Miesel, J., Rogers, B. M., Schweitzer, J., Shuman, J. K., Tepley, A. J., Varner, J. M., Veblen, T. T., Adalsteinsson, S. A. and Balch, J. K., 2020. Fire as a fundamental ecological process: Research advances and frontiers. *Journal of Ecology* **108**(5), 2047-2069.

Meikle, S. and Heine, J., 1987. A fire danger index system for the Transvaal Lowveld and adjoining escarpment areas. *South African Forestry Journal* **143** (1), 55-56.

Mendelsohn, R., 2021. The Extent of Future Damages from Climate Change. In Oxford Research Encyclopedia of Economics and Finance.

Menning, K.M. and Stephens, S.L., 2007. Fire climbing in the forest: a semiqualitative, semiquantitative approach to assessing ladder fuel hazards. *Western Journal of Applied Forestry* **22**(2), 88-93.

Miller, E. A., 2020. A Conceptual Interpretation of the Drought Code of the Canadian Forest Fire Weather Index System. *Fire* **3**(2), 23.

Miller, E.A. and Wilmore, B., 2020. Evaluating the Drought Code Using In Situ Drying Timelags of Feathermoss Duff in Interior Alaska. *Fire* **3**(2), 25.

Mills, A.J., Strydom, T., Allen, J.L. and Baum, J., 2021. The chemistry of the pedoderm–part 1: grasslands and savannas in the central Kruger National Park, South Africa. *African Journal of Range & Forage Science*, 1-6.

Milutin, M., 1941. Canon of Insolation and the Ice Age Problem. Belgrade: Zavod za Udžbenike i Nastavna Sredstva

Ming, A., Rowell, I., Lewin, S., Rouse, R., Aubry, T. and Boland, E., 2021. Key messages from the IPCC AR6 climate science report.

Mishra, N.B. and Young, K.R., 2020. Savannas and grasslands. In Terrestrial Ecosystems and Biodiversity, 235-247. CRC Press.

Montgomery, R.B., 1950. The Taylor diagram (temperature against vapor pressure) for air mixtures. *Archiv für Meteorologie, Geophysik und Bioklimatologie, Serie A* **2**(2), 163-183.

Mosase, E. and Ahiablame, L., 2018. Rainfall and temperature in the Limpopo River basin, Southern Africa: means, variations, and trends from 1979 to 2013. *Water* **10**(4), 364.

Moshobane, M.C., Olowoyo, J.O. and Middleton, L., 2021. Alien plant species of Haenertsburg Village, Limpopo Province, South Africa.

Moyo, T., Musakwa, W., Nyathi, N.A., Mpofu, E. and Gumbo, T., 2020. Modelling of Natural Fire Occurrences: a Case of South Africa. *The International Archives of Photogrammetry, Remote Sensing and Spatial Information Sciences* **43**, 1477-1482.

Mpandeli, S., Nesamvuni, E. and Maponya, P., 2015. Adapting to the impacts of drought by smallholder farmers in Sekhukhune District in Limpopo Province, South Africa. *Journal of Agricultural Science* **7**(2), 115.

Munday, C., Washington, R. and Hart, N., 2021. African low-level jets and their importance for water vapor transport and rainfall. *Geophysical Research Letters* **48**(1), e2020GL090999.

Munyai, R. B., Nethengwe, N. S. and Musyoki, A., 2019. An assessment of flood vulnerability and adaptation: A case study of Hamutsha-Muungamunwe village, Makhado municipality. *Jàmbá: Journal of Disaster Risk Studies* **11**(2)1-8.

Muofhe, T. P., Chikoore, H, Bopape, M. M., Nethengwe, N. S., Ndarana, T., Rambuwani, G. T., 2020. Forecasting Intense Cut-Off Lows in South Africa Using the 4.4 km Unified Model. *Climate* **8**, 129, doi:10.3390/cli8110129

Muvengwi, J., Chisango, T., Mpakairi, K., Mbiba, M. and Witkowski, E.T.F., 2020. Structure, composition and regeneration of miombo woodlands within harvested and unharvested areas. *Forest Ecology and Management* **458**, 117792.

Nampak, H., Love, P., Fox-Hughes, P., Watson, C., Aryal, J. and Harris, R., 2021. Characterizing Spatial and Temporal Variability of Lightning Activity Associated with Wildfire over Tasmania, Australia. *Fire* **4**(1), 10.

Ndarana, T., Rammopo, T. S., Reason, C.J.C., Bopape M., Engelbrecht, F., and Chikoore, H., 2022. Two types of ridging South Atlantic Ocean anticyclones over South Africa and the associated dynamical processes. *Atmospheric Research* **265**, 105897. https://doi.org/10.1016/j.atmosres.2021.105897

Nembilwi, N., Chikoore, H., Kori, E., Munyai, R.B. and Manyanya, T.C., 2021. The Occurrence of Drought in Mopani District Municipality, South Africa: Impacts, Vulnerability and Adaptation. *Climate* **9**(4), 61.

Nguyen, A.T., Rockwood, D., Doan, M.K. and Le, T.K.D., 2021. Performance assessment of contemporary energy-optimized office buildings under the impact of climate change. *Journal of Building Engineering* **35**, 102089.

Nicholson, S. E. 2018. The ICTZ and Seasonal Cycle over Equatorial Africa. *Bulletin of the American Meteorological Society* **99**(2), 337-348.

Nordgren, A., 2021. Pessimism and optimism in the debate on climate change: a critical analysis. *Journal of Agricultural and Environmental Ethics* **34**(4), 1-23.

Nyoni, N., Grab, S., Archer, E. and Malherbe, J., 2021. Temperature and relative humidity trends in the northernmost region of South Africa, 1950-2016. *South African Journal of Science* **117**(11-12),1-11.

Ogwang, B.A., Ongoma, V., Shilenje, Z.W., Ramotubei, T.S., Letuma, M. and Ngaina, J.N., 2020. Influence of Indian Ocean dipole on rainfall variability and extremes over southern Africa. *Mausam* **71**(4), 637-648.

Osborne, C. P., Charles-Dominique, T., Stevens, N., Bond, W. J., Midgley, G., & Lehmann, C. 2018. Human impacts in African savannas are mediated by plant functional traits. The New phytologist, 220, 1, 10–24. https://doi.org/10.1111/nph.15236

Oyewole, O., Beauregard, P. and Bradley, R., 2019, January. High soil charcoal production temperature greatly reduces nitrification in the boreal forest soils. *In Geophysical Research Abstracts*, **21**, 1.

Pardo, J. and VanBuren, R., 2021. Evolutionary innovations driving abiotic stress tolerance in C4 grasses and cereals. *The Plant Cell* **33**(11), 3391-3401.

Pausas, J.G. and Parr, C.L., 2018. Towards an understanding of the evolutionary role of fire in animals. *Evolutionary Ecology* **32**(2), 113-125.

Perry, A., 1987. Middle latitude climates. In: Climatology. Encyclopedia of Earth Science. Springer, Boston, MA. https://doi.org/10.1007/0-387-30749-4_116

Petermann, J. S. and Buzhdygan, O. Y., 2021. Grassland biodiversity. *Current Biology* **31**(19), R1195-R1201.

Pickell, P. D., Coops, N. C. Ferster, C. J. Bater C. W., Blouin, K. D. Flannigan, M. D. and Zhang, J., 2017: An early warning system to forecast the close of the spring burning window from satellite-observed greenness. *Sci. Rep* **7**, 14190, https://doi.org/10.1038/s41598-017-14730-0

Pierre-Louis, K. and Schwartz, J., 2018. Why does California have so many wildfires. The New York Times, November, 9, 2018.

Piñol, J., Terradas, J., Lloret, F., 1998. Climate warming, wildfire hazard and wildfire occurrence in coastal eastern Spain. *Clim. Change* **38**, 345–357.

Platt, W. J, Orzell, S. L and Slocum, M. G., 2015. Seasonality of Fire Weather Strongly Influences Fire Regimes in South Florida Savanna-Grassland Landscapes. *PloS ONE* 10(1), e0116952. dio:10.1371/journal.pone.0116952

Popp, A., Calvin, K., Fujimori, S., Havlik, P., Humpenöder, F., Stehfest, E., Bodirsky, B.L., Dietrich, J.P., Doelmann, J.C., Gusti, M. and Hasegawa, T., 2017. Land-use futures in the shared socio-economic pathways. *Global Environmental Change* **42**, 331-345.

Potter, B. E., and McEvoy, D., 2021. Weather Factors Associated with Extremely Large Fires and Fire Growth Days. *Earth Interactions* ***25***(1), 160-176.

Preston-Whyte, R. A. and Tyson, P. D., 2000. The Weather and Climate of Southern Africa. (2nd ed.). Oxford University Press, South Africa.

Price, M. H., 2019. Switching To ArcGIS Pro from ArcMap. *Photogrammetric Engineering & Remote Sensing* **85**(12), 861.

Price, O.H., Nolan, R.H. and Samson, S.A., 2022. Fuel consumption rates in resprouting eucalypt forest during hazard reduction burns, cultural burns and wildfires. *Forest Ecology and Management* **505**, 119894.

Prichard, S.J., Povak, N.A., Kennedy, M.C. and Peterson, D.W., 2020. Fuel treatment effectiveness in the context of landform, vegetation, and large, wind-driven wildfires. *Ecological Applications,* **30**(5), e02104.

Prior, L.D., Murphy, B.P. and Bowman, D.M., 2018. Conceptualizing ecological flammability: an experimental test of three frameworks using various types and loads of surface fuels. *Fire* **1**(1), 14.

Pyke, D.A., Brooks, M.L. and D'Antonio, C., 2010. Fire as a restoration tool: a decision framework for predicting the control or enhancement of plants using fire. *Restoration ecology* **18**(3), 274-284.

Pyne, S., Andrews, P., Laven, R., 1996a. Introduction to wildland fire, 2nd Ed. Wiley, New York, 769

Quirk, J., Bellasio, C., Johnson, D.A., Osborne, C.P. and Beerling, D.J., 2019. C4 savanna grasses fail to maintain assimilation in drying soil under low CO2 compared with C3 trees despite lower leaf water demand. *Functional Ecology* **33**(3), 388-398.

Ramafoko, E.M., Lekunze, J.N. and Luvhengo, U., 2021. Revising the National Framework for the Management of Drought (NFMD) to Enhance Vegetable Farmers' Vulnerability to Drought in the Northern Cape Province of South Africa.

Rani, R., 2021. Wildfire Risk Prediction for a Smart City. Master's Projects. 1014. https://scholarworks.sjsu.edu/etd_projects/1014

Rapolaki, R.S., Blamey, R.C., Hermes, J.C. and Reason, C.J., 2019. A classification of synoptic weather patterns linked to extreme rainfall over the Limpopo River Basin in southern Africa. *Climate Dynamics* **53**(3), 2265-2279.

Rapolaki, R.S., Blamey, R.C., Hermes, J.C. and Reason, C.J.C., 2021. Moisture sources and transport during an extreme rainfall event over the Limpopo River Basin, southern Africa. *Atmospheric Research,* **264,** 105849.

Ratajczak, Z., Nippert, J. B, Briggs, J. M and Blair, J. M., 2014. Fire dynamics distinguish grasslands, shrublands and woodlands as alternative attractors in the Central Great Plains of North America. *Journal of Ecology,* **102(**6), 1374-1385

Reason, C. J. C., Rouault, M., Mélice, J. L. & Jagadheesha, D., 2002. Interannual winter rainfall variability in SW South Africa and large scale ocean–atmosphere interactions. *Meteorol. Atmos. Phys.* **80**, 19–29.

Reason, C.J.C., Landman, W. and Tennant, W., 2006. Seasonal to decadal prediction of southern African climate and its links with variability of the Atlantic Ocean. *Bulletin of the American Meteorological Society* **87**(7), 941-956.

Reddy, P.J., Sriram, D., Gunthe, S.S. and Balaji, C., 2021. Impact of climate change on intense Bay of Bengal tropical cyclones of the post-monsoon season: a pseudo global warming approach. *Climate Dynamics* **56**(9), 2855-2879.

Reichler, T., 2016. Chapter 6 - Poleward Expansion of the Atmospheric Circulation. Climate Change (2nd Ed). Observed Impacts on Planet Earth, 79-104.

Restaino, C.M. and Safford, H.D., 2018. Chapter Twenty-Six. Fire and Climate Change. In Fire in California's Ecosystems, 493-506. University of California Press.

Retallack, G. J. 1992. Middle Miocene fossil plants from Fort Ternan (Kenya) and evolution of African grasslands. *Paleobiology* **18**, 383–400.

Rodrigues, C.A., Zirondi, H.L. and Fidelis, A., 2021. Fire frequency affects fire behavior in open savannas of the Cerrado. *Forest Ecology and Management* **482**, 118850.

Rodrigues, M., Trigo, R.M., Vega-García, C. and Cardil, A., 2020. Identifying large fire weather typologies in the Iberian Peninsula. *Agricultural and Forest Meteorology* **280**, 107789.

Rodrigues, V. B., and Torres, F.T.P., 2020. Fire Behavior Prediction Using Machine Learning Algorithms. *Revista Brasileira De Biometria* **38**(3), 343-352.

Roffe, S.J., Fitchett, J.M. and Curtis, C.J., 2021. Investigating changes in rainfall seasonality across South Africa: 1987–2016. *International Journal of Climatology* **41**, E2031-E2050.

Rogers, B.M., Balch, J.K., Goetz, S.J., Lehmann, C.E. and Turetsky, M., 2020. Focus on changing fire regimes: interactions with climate, ecosystems, and society. *Environmental Research Letters* **15**(3), 030201.

Rossi, J. L., Chatelon F. J., and Marcelli T., 2019. Fire Intensity. In: Manzello S. (eds) Encyclopedia of Wildfires and Wildland-Urban Interface (WUI) Fires. Springer, Cham. https://doi.org/10.1007/978-3-319-51727-8_51-1

Ruecker, G., Leimbach, D. and Tiemann, J., 2021. Estimation of Byram's Fire Intensity and Rate of Spread from Spaceborne Remote Sensing Data in a Savanna Landscape. Fire, 4, 4, 65.

Ruffault, J., Martin-StPaul, N., Pimont, F. and Dupuy, J.L., 2018. How well do meteorological drought indices predict live fuel moisture content (LFMC)? An assessment for wildfire research and operations in Mediterranean ecosystems. *Agricultural and Forest Meteorology* **262**, 391-401.

Sankaram, M., 2019. Drought and ecological future of tropical savanna vegetation. *Journal of Ecology,* **10**(4), 1531 – 1549.

Santos, F. L., Nogueira, J., de Souza, R. A., Falleiro, R. M., Schmidt, I. B. and Libonati, R., 2021. Prescribed burning reduces large, high-intensity wildfires and emissions in the Brazilian savanna. *Fire* **4**(3), 56.

Sato, Y., Goto, D., Michibata, T., Suzuki, K., Takemura, T., Tomita, H. and Nakajima, T., 2018. Aerosol effects on cloud water amounts were successfully simulated by a global cloud-system resolving model. *Nature Communications* **9**(1), 1-7.

Schmidt, I. B. and Eloy, L., 2020. Fire regime in the Brazilian Savanna: Recent changes, policy and management. Flora, 268, 151613.

Schober, P., Boer, C. and Schwarte, L.A., 2018. Correlation coefficients: appropriate use and interpretation. *Anesthesia & Analgesia* **126**(5), 1763-1768.

Scott, A. C., 2000. The pre-quaternary history of fire. *Paleogeography, Paleoclimatology, Paleoecology* **164**, 281-329

Séférian, R., Delire, C., Decharme, B., Voldoire, A., Salas y Melia, D., Chevallier, M., Saint-Martin, D., Aumont, O., Calvet, J.C., Carrer, D. and Douville, H., 2016. Development and evaluation of CNRM Earth system model–CNRM-ESM1. Geoscientific Model Development, 9(4), pp.1423-1453.

Seland, Ø., Bentsen, M., Olivié, D., Toniazzo, T., Gjermundsen, A., Graff, L.S., Debernard, J.B., Gupta, A.K., He, Y.C., Kirkevåg, A. and Schwinger, J., 2020. Overview of the Norwegian Earth System Model (NorESM2) and key climate response of CMIP6 DECK, historical, and scenario simulations. Geoscientific Model Development, 13, 12, 6165-6200.

Sharples, J.J. and Manzello, S.L., 2018. Foehn Winds. In Encyclopedia of Wildfires and Wildland-Urban Interface (WUI) Fires. 1-7. Cham: Springer International Publishing

Sharratt, B., and Auvermann, B., 2014. Dust Pollution from Agriculture. *Encyclopedia of Agriculture and Food Systems*, 487-504. https://doi.org/10.1016/B978-0-444-52512-3.00089-9

Shi, G., Yan, H., Zhang, W., Dodson, J., Heijnis, H. and Burrows, M., 2021. Rapid warming has resulted in more wildfires in northeastern Australia. *Science of the total environment* **771**, 144888.

Sikuzani, Y.U., Muteya, H.K. and Bogaert, J., 2020. Miombo woodland, an ecosystem at risk of disappearance in the Lufira Biosphere Reserve (Upper Katanga, DR Congo)? A 39-years analysis based on Landsat images. *Global Ecology and Conservation* **24**, e01333.

Sinclair, R., 2002. Ecophysiology of grasses in Flora of Australia. *Introduction and Atlas* **43**(1), 133 – 137.Australian Biological Resources Study/CSIRO, Camberra.

Sinha, P., Hobbs, P. V., Yokelson, R. J., Blake, D. R., Gao, S., and Kirchstetter, T. W. 2003. Emissions From Miombo Woodland and Dambo Grassland Savanna Fires in Southern Africa. NASA (ADS). https://ui.adsabs.harvard.edu/abs/2003AGUFM.A22B1061S

Smit, I. P., & Prins, H. H. 2015. Predicting the Effects of Woody Encroachment on Mammal Communities, Grazing Biomass and Fire Frequency in African Savannas. *PloS one* **10**(9), e0137857. https://doi.org/10.1371/journal.pone.0137857

Smith, E. T., and Sheridan, S. C., 2020. Where do cold air breaks occur and how have they changes over time? *American Geophysical Union,* **47**, e2020GL086983.

Spranger, R., Ringelman, A. and Sinervo, B., 2020, December. Assessing Wildfire Impacts on Canopy Density and the Extinction Risk of Amphibians. In AGU Fall Meeting Abstracts, 2020, H087-0003.

Srinivasan, R. and Narasimhan, B., 1998. Estimation of KBDI (Drought Index) in Real-Time Using GIS and Remote Sensing Technologies. In 2001 ASAE Annual Meeting, 1. American Society of Agricultural and Biological Engineers

Stephenson, A. G., 2015. Estimating Spatially Varying Severity Thresholds of a Forest Fire Danger Rating System Using Max-Stable Extreme-Event Modeling, American Meteorological Society. 54, 395–407. doi:10.1175/JAMC-D-14-0041.1

Storey, M.A., Price, O.F., Sharples, J.J. and Bradstock, R.A., 2020. Drivers of long-distance spotting during wildfires in south-eastern Australia. *International journal of wildland fire* **29**(6), 459-472.

Su, P., Zhang, A., Wang, R., Wang, J.A., Gao, Y. and Liu, F., 2021. Prediction of future natural suitable areas for rice under Representative Concentration Pathways (RCPs). *Sustainability*, **13**(3), 1580.

Sullivan, A.L., Surawski, N.C., Crawford, D., Hurley, R.J., Volkova, L., Weston, C.J. and Meyer, C.P., 2018. Effect of woody debris on the rate of spread of surface fires in forest fuels in a combustion wind tunnel. *Forest ecology and management* **424**, 236-245.

Sun, P., Rodriguez, A., Kim, W.I., Huang, X. and Fernandez-Pello, C., 2021. Effect of external and internal heating on the flame spread and phase change of thin polyethylene tubes. *International Journal of Thermal Sciences* **168**, 107054.

Synodinos, A. D., Tietjen, B., Lohmann, D., and Jeltsch, F. 2018. The impact of inter-annual rainfall variability on African savannas changes with mean rainfall. *Journal of theoretical biology* **437**, 92–100. https://doi.org/10.1016/j.jtbi.2017.10.019

Tang, R., Mao, J., Jin, M., Chen, A., Yu, Y., Shi, X., Zhang, Y., Hoffman, F.M., Xu, M. and Wang, Y., 2021. Interannual variability and climatic sensitivity of global wildfire activity. *Advances in Climate Change Research* **12**(5), 686-695.

Tavra, M., Racetin, I., and Peroš J., 2021. The role of crowdsourcing and social media in crisis mapping: a case study of a wildfire reaching Croatian City of Split. *Geoenvironmental Disasters* **8**, 10.

Taylor, C., 2020. Definition of a Percentile in Statistics and How to Calculate It. Available at: https://www.thoughtco.com/what-is-a-percentile-3126238 (Accessed 31 December 2021)

Taylor, K. E., 2001. Summarizing multiple aspects of model performance in a single diagram. *J. Geophys. Res.***106**, 7183-7192.

Taylor, K.E., 2005. Taylor diagram primer. Work. Pap, 1-4.

Thatcher, M., McGregor, J., Dix, M. and Katzfey, J., 2015, March. A new approach for coupled regional climate modeling using more than 10,000 cores. *In International Symposium on Environmental Software Systems*, 599-607. Springer, Cham.

Thevakaran, A., McGregor, J. L., Katzfey, J., Hoffmann, P., Suppiah, R., and Sonnadara, D. U. J., 2015. An assessment of CSIRO Conformal Cubic Atmospheric Model simulations over Sri Lanka, Clim Dyn, 46, 1861 – 1875, dio:10.1007/s00382-015-2680-4

Torres, F.T.P., Romeiro, J.M.N., de Albuquerque Santos, A.C., de Oliveira Neto, R.R., Lima, G.S. and Zanuncio, J.C., 2018. Fire danger index efficiency as a function of fuel moisture and fire behavior. *Science of the total environment* **631**, 1304-1310.

Turco, M., Jerez, S., Augusto, S., Tarín-Carrasco, P., Ratola, N., Jiménez-Guerrero, P. and Trigo, R.M., 2019. Climate drivers of the 2017 devastating fires in Portugal. *Scientific reports,* **9**(1), 1-8.

Tymstra, C., Jain, P. and Flannigan, M.D., 2021. Characterisation of initial fire weather conditions for large spring wildfires in Alberta, Canada. *International Journal of Wildland Fire* **30**(11), 823-835.

Uno, K. T. et al. 2011. Late Miocene to Pliocene carbon isotope record of differential diet change among East African herbivores. *Proc. Natl. Acad. Sci*. *USA* **108**, 6509–6514.

Utaile, Y.U., Honnay, O., Muys, B., Cheche, S.S. and Helsen, K., 2021. Effect of Dichrostachys cinerea encroachment on plant species diversity, functional traits and litter decomposition in an East-African savannah ecosystem. *Journal of Vegetation Science,* **32**(1), e12949.

Val, A., de la Peña, P., Duval, M., Bansal, S., Colino, F., Culey, J., Hodgskiss, T., Morrissey, P., Murray, A., Murungi, M. and Neumann, F.H., 2021. The place beyond the trees: renewed

excavations of the Middle Stone Age deposits at Olieboomspoort in the Waterberg Mountains of the South African Savanna Biome. *Archaeological and Anthropological Sciences* **13**(7), 1-32.

van Breda Weaver, A., 1991. The distribution of soil erosion as a function of slope aspect and parent material in Ciskei, Southern Africa. *GeoJournal* **23**(1), 29-34.

van Der Walt, A.J. and Fitchett, J.M., 2021. Extreme Temperature Events (ETEs) in South Africa: a review. *South African Geographical Journal*, 1-20.

Van Wagner, C. E., 1974. Structure of the Canadian forest fire weather index (Vol. 1333). Ontario: Environment Canada, Forestry Service.

Vancil, J., Jirak, I.L. and Elliott, M., 2020. Evaluation of the Down-slope Wind Component in the High-Resolution Ensemble Forecast System for the Prediction of Large Wildfires. In AGU Fall Meeting Abstracts, 2020, A143-0010.

Vaughan, M. C., Hagan, D. L., Bridges, W. C., Dickinson, M. B. and Coates, T. A., 2021. How do fire behavior and fuel consumption vary between dormant and early growing season prescribed burns in the southern Appalachian Mountains*? Fire Ecology* **17**(1), 1-16.

Verhoeven, E. M., Murray, B. R., Dickman, C. R., Wardle, G. M. and Greenville, A. C., 2020. Fire and rain are one: extreme rainfall events predict wildfire extent in an arid grassland. *International Journal of Wildland fire* **29**(8), 702 – 711.

Viedma, O., Urbieta, I. R., and Moreno, J. M., 2018. Wildfires and the role of their drivers are changing over time in a large rural area of west-central Spain. *Sci Rep* **8**, 17797 https://doi.org/10.1038/s41598-018-36134-4

Voelker, S.L., Merschel, A.G., Meinzer, F.C., Ulrich, D.E., Spies, T.A. and Still, C.J., 2019. Fire deficits have increased drought sensitivity in dry conifer forests: Fire frequency and tree-ring carbon isotope evidence from Central Oregon. *Global Change Biology* **25**(4), 1247-1262.

Vose, J. M., Peterson, D. L., Fettig, C. J., Halofsky, J. E., Hiers, J.K., Keane, R. E., Loehman, R. and Stambaugh, M. C., 2021. Fire and Forests in the 21st Century: Managing Resilience Under Changing Climates and Fire Regimes in USA Forests. *In Fire Ecology and Management: Past, Present, and Future of US Forested Ecosystems*, 465-502. Springer, Cham.

Wachsmann, F., 2020, May. CDOs for CMIP6 and Climate Extremes Indices. In EGU General Assembly Conference Abstracts, 8543.

Wainwright, C. M., Black, E., and Allan, R. P., 2021. Future changes in wet and Dry Season characteristics in CMIP5 and CMP6 Simulations. *Journal of Hydrometeology* **22**(9), 2339 – 2357.

Wang, G., 2004: A conceptual modeling study on biosphere–atmosphere interactions for physically based climate modeling. *J. Climate* **17**, 2572–2583.

Wang, X., Studens, K., Parisien, M. A., Taylor, S. W., Candau, J.N., Boulanger, Y. and Flannigan, M.D., 2020. Projected changes in fire size from daily spread potential in Canada over the 21st century. *Environmental Research Letters,* **15**(10), 104048.

Wang, Y.Q., 2019. An Open-Source Software Suite for Multi-Dimensional Meteorological Data Computation and Visualisation. *Journal of Open Research Software* **7**(1), 21.

Ward, D. S., Kloster, S., Mahowald, N. M., Rogers, B. M., Randerson, J. T. and Hess, P. G., 2012. The changing radiative forcing of fires: global model estimates for past, present and future. Atmospheric Chemistry and Physics, **12**(22), 10857-10886.

Watson-Parris, D., 2021. Machine learning for weather and climate are worlds apart. *Philosophical Transactions of the Royal Society A* **379**(2194), 20200098.

Wei, W., Pang, S., Wang, X., Zhou, L., Xie, B., Zhou, J. and Li, C., 2020. Temperature vegetation precipitation dryness index (TVPDI)-based dryness-wetness monitoring in China. *Remote Sensing of Environment*, **248**, 111957.

Weiss, S.L. and Brower, R.M., 2021. Wildfire as a natural stressor and its effect on female phenotype and ornament development. *Ecology and Evolution*.

Willis, C., van Wilgen, B., Tolhurst, K., Everson, C., D'Abreton, P., Pero, L. and Fleming, G. 2001. The development of a national fire danger rating system for South Africa. Department of Water Affairs and Forestry, Pretoria, South Africa

Wilson, M., 2021. Temperature measurement. *Anaesthesia & Intensive Care Medicine* **22**(3), 202 – 207. https://doi.org/10.1016/j.mpaic.2021.01.015

Winter, B., 2019. Statistics for linguists: An introduction using R. Routledge.

Wotton, B. M. and Flannigan, M. D., 1993. Length of the fire season in a changing climate. *The Forestry Chronicle* **69**(2), 187-192.

Wotton, B. M., 2009. Interpreting and using outputs from the Canadian Forest Fire Danger Rating System in research applications. *Environmental and Ecological Statistics* **16**(2), 107-131.

Wu, J., Kong, S., Wu, F., Cheng, Y., Zheng, S., Yan, Q., Zheng, H., Yang, G., Zheng, M., Liu, D. and Zhao, D., 2018. Estimating the open biomass burning emissions in central and eastern China from 2003 to 2015 based on satellite observation. *Atmospheric Chemistry and Physics,* **18**(16), 11623-11646.

Xanthopoulos, G., Maheras, G., Gouma, V. and Gouvas, M., 2006. Is the Keetch-Byram drought index (KBDI) directly related to plant water stress? *Forest Ecology and Management,* **234**(1), S27.

Xi, D. D., Dean, C. B. and Taylor, S. W., 2021. Modeling the duration and size of wildfires using joint mixture models. *Environmetrics*, e2685.

Yadav, I and Devi, N. 2019. Biomass burning, regional air quality, and climate change. *Encyclopedia of Environmental Health,* 386-391, doi:10.1016/B978-0-12-409548-9.11022-X.

Yahia, E. M., 2019. Postharvest technology of perishable horticultural commodities. Woodhead Publishing.

Yan, L., Feng, J., Hang, T. and Zhu, Y., 2021. Flow interval prediction based on deep residual network and lower and upper boundary estimation method. *Applied Soft Computing* **104**,107228.

Yan, Y. Y., 2005. Intertropical Convergence Zone (ITCZ). In: Oliver J. E (eds) Enclopedia of the World Climatology, Encyclopedia of Earth Sciences Series. Springer, Dordrcht. https://dio.org/10.1007/1-4020-3266-8_110

Yuan, J. and Kopp, R.E., 2021. Emulating Ocean Dynamic Sea Level by Two-Layer Pattern Scaling. *Journal of Advances in Modeling Earth Systems* **13**(3), e2020MS002323.

Zhang, F., Kong, R. and Peng, J., 2018. Effects of heating on compositional, structural, and physicochemical properties of loess under laboratory conditions. *Applied Clay Science* **152**, 259-266.

Zhao, F., Liu, Y. and Shu, L., 2020. Change in the fire season pattern from bimodal to unimodal under climate change: The case of Daxing'anling in Northeast China. *Agricultural and Forest Meteorology* **291**, 108075.

Ziel, R. H., Wolken, J., St. Clair, T., and Henderson, M., 2015. Modeling fire growth potential by emphasizing significant growth events: Characterizing a climatology of fire growth days in Alaska's boreal forest. 11th Symp. on Fire and Forest Meteorology, Minneapolis, MN, Amer. Meteor. Soc.,1.2, https://ams.confex.com/ams/11FIRE/webprogram/Paper272864.html.

Zigner, K., Carvalho, L., Peterson, S., Fujioka, F., Duine, G.J., Jones, C., Roberts, D. and Moritz, M., 2020. Evaluating the ability of FARSITE to simulate wildfires influenced by extreme, downslope winds in Santa Barbara, California. *Fire,* **3**(3), 29.

Ziter, C.D., Pedersen, E.J., Kucharik, C.J. and Turner, M.G., 2019. Scale-dependent interactions between tree canopy cover and impervious surfaces reduce daytime urban heat during summer. *Proceedings of the National Academy of Sciences,* **116**(15), 7575-7580.